

Super Typhoon Mangkhut (1822)

Case Study

Liu Wai Leung

August 2025

Table of Contents

Table of Contents.....	i
List of Figures.....	iv
List of Tables	viii
Abstract.....	ix
1. Introduction.....	1
1.1 Background.....	1
1.2 Objectives	5
2. Development of Mangkhut	7
2.1 Structural Characteristics	7
2.2 Intensity.....	9
2.3 Wind Field Distributions.....	12
2.4 Convective Activity	15
2.5 Environment Analysis.....	18
2.6 Track	23
3. Numerical Weather Prediction Models.....	28
3.1 Probability Forecast of Mangkhut's Intensity.....	28
3.2 Probability Forecast of Mangkhut's Track	29
3.3 Regional Weather Forecast	33
3.3.1 Philippines.....	33
3.3.2 Hong Kong.....	35
3.3.3 China	41
4. Meteorological Observations	48
4.1 Philippines Weather Stations	48
4.1.1 Wind Speed.....	48
4.1.2 Mean Sea Level Pressure	48
4.1.3 Storm Surge.....	49
4.1.4 Rainfall Distribution	50

Table of Contents

4.1.5	Upper-air Weather Measurements	51
4.2	Hong Kong Weather Stations	53
4.2.1	Temperature	53
4.2.2	Wind Speed.....	54
4.2.3	Mean Sea Level Pressure	58
4.2.4	Storm Surge.....	59
4.2.5	Rainfall Distribution	60
4.2.6	Upper-air Weather Measurements	62
4.2.7	Wind Profilers.....	64
4.2.8	Dropsonde	67
4.2.9	Significant Wave Height at Buoy	70
4.3	China Weather Stations	72
4.3.1	Wind Speed.....	72
4.3.2	Mean Sea Level Pressure	72
4.3.3	Storm Surge.....	72
4.3.4	Rainfall Distribution	76
4.3.5	Wind Profilers.....	77
5.	Disaster Statistics	78
5.1	Philippines Damage Situation.....	78
5.2	Hong Kong Damage Situation	81
5.3	China Damage Situation	90
6.	Discussion.....	93
6.1	Special Wind Structure of Mangkhut.....	93
6.2	Enhanced Public Awareness of Disaster Preparedness in Social Media.....	95
6.3	Clearance and Repair Work in the Aftermath of Mangkhut	96
7.	Conclusion	99
	Acknowledgements.....	101

Table of Contents

References.....	102
Appendix I: Classification of Tropical Cyclones.....	S1
Appendix II: Tropical Cyclone Warning Signals.....	S3
A. Philippines.....	S3
B. Hong Kong.....	S4
C. China	S5
Appendix III: Rainstorm Warning Signals	S7
A. Philippines.....	S7
B. Hong Kong.....	S8
C. China.....	S9
Appendix IV: Other Adverse Weather Warnings	S11
A. Philippines.....	S11
B. Hong Kong.....	S12
C. China.....	S13

List of Figures

Figure 1.1	Himawari-8 satellite image of super typhoon Mangkhut	2
Figure 1.2	Radar image of super typhoon Mangkhut in Cagayan province of Philippines	2
Figure 1.3	Radar image of severe typhoon Mangkhut in Hong Kong	4
Figure 1.4	Radar image of severe typhoon Mangkhut in Taishan of Guangdong province	5
Figure 2.1	Himawari-8 Infra-red satellite imagery of super typhoon Mangkhut.....	7
Figure 2.2	Infra-red colour enhanced imagery of Himawari-8 satellite of super typhoon Mangkhut .	8
Figure 2.3	Himawari-8 Infra-red satellite imagery of snapshots of super typhoon Mangkhut's cloud cloud.....	9
Figure 2.4	Intensity analysis of tropical cyclones.....	10
Figure 2.5	Basic Dvorak enhanced satellite images of Himawari-8 satellite of super typhoon Mangkhut	11
Figure 2.6	Time series of advanced Dvorak technique of tropical cyclone Mangkhut.....	13
Figure 2.7	Time series of intensity of tropical cyclone Mangkhut	13
Figure 2.8	Multi-platform Satellite Surface Wind Analysis of super typhoon Mangkhut.....	14
Figure 2.9	Schematic diagram of convective hot towers	15
Figure 2.10	Morphed Integrated Microwave Imagery of super typhoon Mangkhut	16
Figure 2.11	Fengyun-4A Lightning Mapping Imager of super typhoon Mangkhut	17
Figure 2.12	Schematic diagram of concentric eyewall structure	18
Figure 2.13	Sea surface temperatures of North Equatorial Current.....	19
Figure 2.14	Ocean heat content of western North Pacific	20
Figure 2.15	Vertical wind shear of National Oceanic and Atmospheric Administration	21
Figure 2.16	Temperature and salinity-induced squared buoyancy frequency	22
Figure 2.17	Sea surface temperatures of South China Sea	23
Figure 2.18	Ocean heat content of South China Sea and western North Pacific	24
Figure 2.19	Weather Chart.....	25
Figure 2.20	The track of tropical cyclone Mangkhut.....	26
Figure 3.1	Intensity probability forecast for tropical cyclone Mangkhut	30

List of Figures

Figure 3.2	Track probability forecast for tropical cyclone Mangkhut	32
Figure 3.3	Rainfall forecast in the Philippines.....	34
Figure 3.4	Philippines' storm surge forecast	35
Figure 3.5	Hong Kong wind speed forecast.....	36
Figure 3.6	Rainfall forecasts in Hong Kong and Pearl River Estuary	38
Figure 3.7	Significant wave height forecasts in Hong Kong and its adjacent waters	41
Figure 3.8	China wind speed forecast.....	42
Figure 3.9	China rainfall forecast	43
Figure 3.10	Predicted maximum storm surge for the next 72 hours in Pearl River Estuary.....	44
Figure 3.11	Predicted 10 m wind for the next 72 hours in Pearl River Estuary	45
Figure 3.12	Storm surge warning for the next 72 hours in Pearl River Estuary	46
Figure 3.13	Error of prediced storm surge in Pearl River Estuary.....	46
Figure 4.1	Maximum storm surge and tide in the Philippines	50
Figure 4.2	Total daily rainfall distribution in the Philippines	51
Figure 4.3	Skew-T diagram in the Laoag, Philippines.....	52
Figure 4.4	Hong Kong temperature observations	53
Figure 4.5	Hong Kong wind index.....	55
Figure 4.6	Radar image of intense spiral rainband of severe typhoon Mangkhut	60
Figure 4.7	Total daily rainfall distribution in Hong Kong	61
Figure 4.8	Skew-T diagram in King's Park, Hong Kong	63
Figure 4.9	Mean horizontal wind speed and direction in Hong Kong	65
Figure 4.10	Mean profiles of normalised speed in Hong Kong	66
Figure 4.11	Gradient wind speed from wind profiles in Hong Kong	66
Figure 4.12	Vertical profiles of potential temperature and equivalent potential temperature in Mangkhut	68
Figure 4.13	Vertical profiles of tangential and radial wind speeds in Mangkhut	69
Figure 4.14	Significant wave height in South China Sea.....	70

List of Figures

Figure 4.15	Maximum wave heights in South China Sea	71
Figure 4.16	Storm surge in the Pearl River Estuary.....	74
Figure 4.17	Time series of storm surge and astronomical tides at each station in the Pearl River Estuary	75
Figure 4.18	Time series of the storm surge at each station in the Pearl River Estuary.....	75
Figure 4.19	Total rainfall distribution in South China from 16 to 18 September 2018	76
Figure 4.20	Mean wind profilers in Taishan of Jiangmen City	77
Figure 5.1	The catastrophic landslide in Itogon, Benguet	79
Figure 5.2	Damage to agriculture and livelihood in Conner, Apayao	79
Figure 5.3	Damage to gymnasium in Luzon.....	80
Figure 5.4	Fallen trees in many parts of the territory.....	83
Figure 5.5	Shattered glass curtain walls in commercial districts	84
Figure 5.6	Damage to Lovers Bridge in Shek O beach.....	85
Figure 5.7	Damage to Tseung Kwan O South waterfront promenade	85
Figure 5.8	Damage to the Siu Sai Wan Sports Ground in Chai Wan	86
Figure 5.9	Severe flooding in low-lying coastal areas.....	86
Figure 5.10	Flooding in Tai O and Lei Yue Mun	87
Figure 5.11	Seawater intrusion submerged underground car parks in Heng Fa Chuen and Tseung Kwan O	88
Figure 5.12	Severe flooding in cycle tracks along the Shing Mun River and Lam Tsuen River.....	88
Figure 5.13	Landslide in Sai Kung	89
Figure 5.14	Vessels sunk or severely damaged by high waves and storm surges in Sham Wan and Sai Kung.....	90
Figure 5.15	Severe flooding in Yangchun, Guangdong province.....	91
Figure 5.16	Fallen billboard in Tengxian, Guangxi province	92
Figure 6.1	Change in the wind structure of Mangkhut before and after crossing Luzon.....	93
Figure 6.2	Strong spiral rainbands sweep across Hong Kong during Mangkhut's passage	94

List of Figures

Figure 6.3	East vs. West Landing	95
Figure 6.4	Typhoon disaster: storm surge.....	96
Figure 6.5	Public transportation heavily disrupted in Tai Wai station.....	97
Figure S1.1	Hong Kong's weather warnings	S13

List of Tables

Table 1.1 Scenario 1 of storm surge forecast in Hong Kong	39
Table 1.2 Scenario 2 of storm surge forecast in Hong Kong	39
Table 2.1 Wind speed observations in the Philippines	49
Table 2.2 Mean sea level pressure observations in the Philippines	49
Table 2.3 Maximum 60-minute mean wind speeds and gusts in Hong Kong	55
Table 2.4 Maximum 10-minute mean wind speeds and gusts in Hong Kong	56
Table 2.5 Hong Kong mean sea level pressure observations	58
Table 2.6 Maximum storm surge and tide in Hong Kong.....	59
Table 2.7 The accumulated daily rainfall distribution in Hong Kong	61
Table 2.8 Maximum mean wind speeds and gusts in Pearl River Estuary	72
Table 3.1 Assessment of damages and direct economic loss in the Philippines	78
Table 3.2 Assessment of damages and direct economic loss in Hong Kong	81
Table 3.3 Assessment of damages and direct economic loss in China	91
Table S1.1 Classification of tropical cyclones by maximum sustained 10-minute wind speed in the Philippines.....	S1
Table S1.2 Classification of tropical cyclones by maximum sustained 10-minute wind speed in Hong Kong	S1
Table S1.3 Classification of tropical cyclones by maximum sustained 2-minute wind speed in China	S2
Table S2.1 Philippines' tropical cyclone wind signals	S3
Table S2.2 Hong Kong's tropical cyclone warning signals.....	S4
Table S2.3 China's tropical cyclone warning signals	S5
Table S3.1 Philippines' rainstorm warning signals.....	S7
Table S3.2 Hong Kong's rainstorm warning signals	S8
Table S3.3 China's rainstorm warning signals	S9
Table S4.1 Philippines' flood warnings.....	S12
Table S4.2 China's thunderstorm warnings	S14

Abstract

Super Typhoon Mangkhut (1822) was one of the most intense tropical cyclones of the 2018 Pacific season, characterised by rapid intensification, a well-defined structure, and widespread devastation across the Philippines, Hong Kong, and southern China. With peak sustained winds of 250 kmh^{-1} and a central pressure of 900 hPa, Mangkhut's destructive force was fuelled by high sea surface temperatures, low wind shear, and efficient upper-level outflow. The storm caused catastrophic damage, including severe flooding, landslides, and infrastructure collapse, resulting in significant human and economic losses. In the Philippines, over 80 fatalities and agricultural and infrastructure losses exceeding ₱33.9 billion were reported. Hong Kong faced record-breaking wind speeds, storm surges, and extensive property damage, with economic losses reaching HK\$4.6 billion. Southern China experienced widespread flooding and disruptions, displacing millions.

Meteorological forecasting, utilising advanced techniques like the Advanced Dvorak Technique (ADT) and Ensemble Prediction Systems (EPS), provided critical early warnings but highlighted challenges in predicting localised impacts. The event underscored gaps in disaster preparedness and the need for resilient infrastructure, improved public communication, and coordinated emergency response. Mangkhut's legacy emphasises the urgency of integrating scientific, socio-economic, and institutional strategies to mitigate future tropical cyclone risks in vulnerable regions.

1. Introduction

1.1 Background

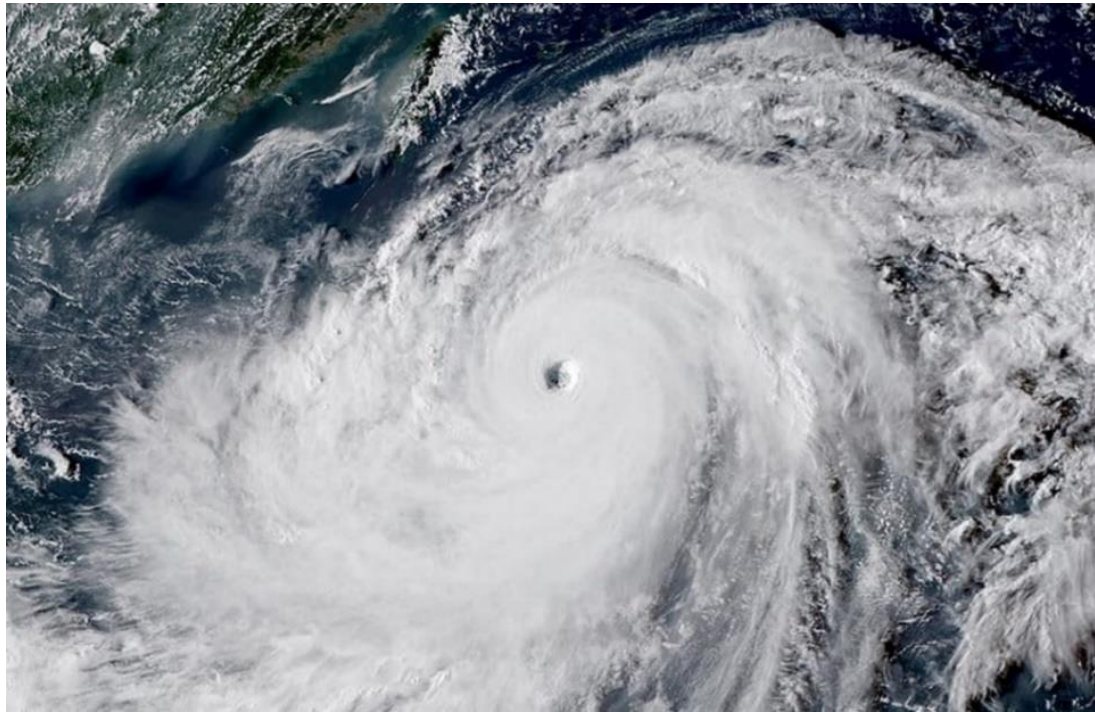
Super typhoon Mangkhut was one of the most powerful and devastating storms to occur during the 2018 Pacific tropical cyclone season, characterised by its immense size, intense wind speeds, and rapid intensification. This catastrophic storm emerged over the western North Pacific Ocean and went on to cause widespread destruction and severe damage across multiple regions, with particularly devastating impacts felt in the Philippines, Hong Kong, and southern China, where millions of people were affected by flooding, landslides, and infrastructure collapse.

Mangkhut formed as a tropical depression over the northwestern Pacific about 780 km south of Wake Island on the dusk of 7 September and moved west or west-northwest at about 22 kmh^{-1} . It developed gradually into a typhoon, accelerating at around 30 kmh^{-1} across the northern part of Guam towards the Luzon in the next couple of days. On 10 September, Mangkhut underwent rapid intensification. Its eyewall appeared the “convective hot towers” with the updraft turned violent. The height of cloud top exceeded 17 km up to the top of the troposphere accompanied by cloud-to-ground lightning. Environmental analysis indicated the storm was in a favourable condition for development with approximately 30°C of sea surface temperature, low vertical wind shear and decent divergence aloft. Mangkhut intensified further into a super typhoon the next morning, reaching its peak intensity with an estimated maximum sustained wind of 250 kmh^{-1} near the centre and a minimum sea-level pressure of 900 hPa on the late evening of 14 September. Figure 1.1 shows that Mangkhut exhibited a distinct circular eye and a well-developed central dense overcast (CDO), as well as extensive circulation, as seen in imagery from the Himawari-8 satellite operated by the Japan Meteorological Agency (JMA).

Mangkhut made landfall in the vicinity of Cagayan province of northeastern Philippines at 1:40 a.m. on 15 September, as shown in Figure 1.2. It momentarily passed through the northern part of Luzon. The maximum 10-minute mean wind speed recorded at Aparri station was 108 kmh^{-1} , gusting to 176 kmh^{-1} , with the lowest instantaneous sea-level pressure of 953.3 hPa (Philippine Atmospheric, Geophysical and Astronomical Services Administration [PAGASA], 2018). Under the influence of mountainous terrain, its eye disintegrated and later declined the intensity. The storm reorganised its circulation after entering the northern part of the South China Sea during the day. Although the eyewall was rebuilt, its central convective bands were visibly thinner. In contrast, the spiral rainband outside the eyewall remained intense and the structure was intact.

Figure 1.1

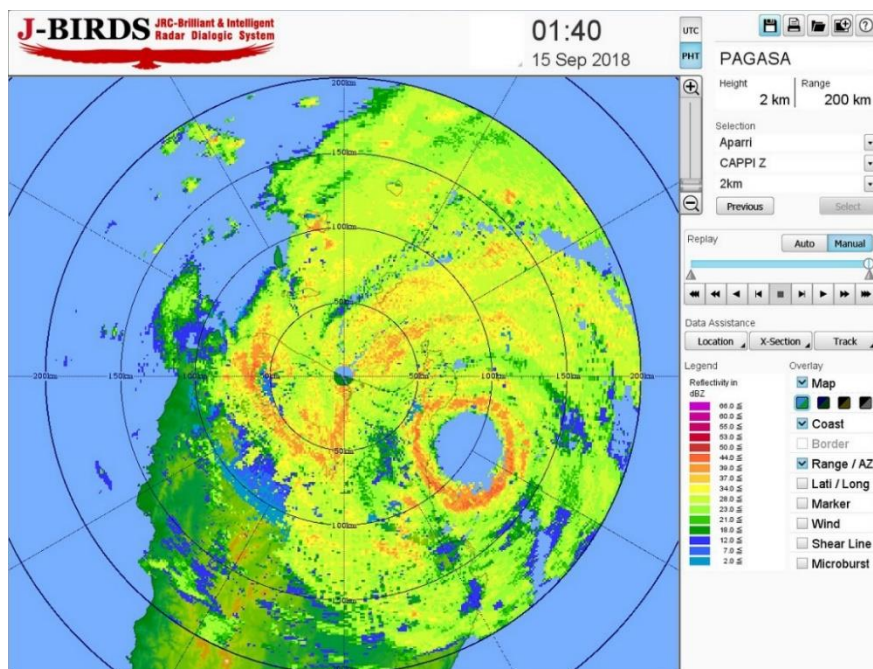
Himawari-8 satellite image of super typhoon Mangkhut



Note. Mangkhut was at peak intensity for satellite imagery around 11:00 p.m. on 14 September 2018 from JMA.

Figure 1.2

Radar image of super typhoon Mangkhut in Cagayan province of Philippines



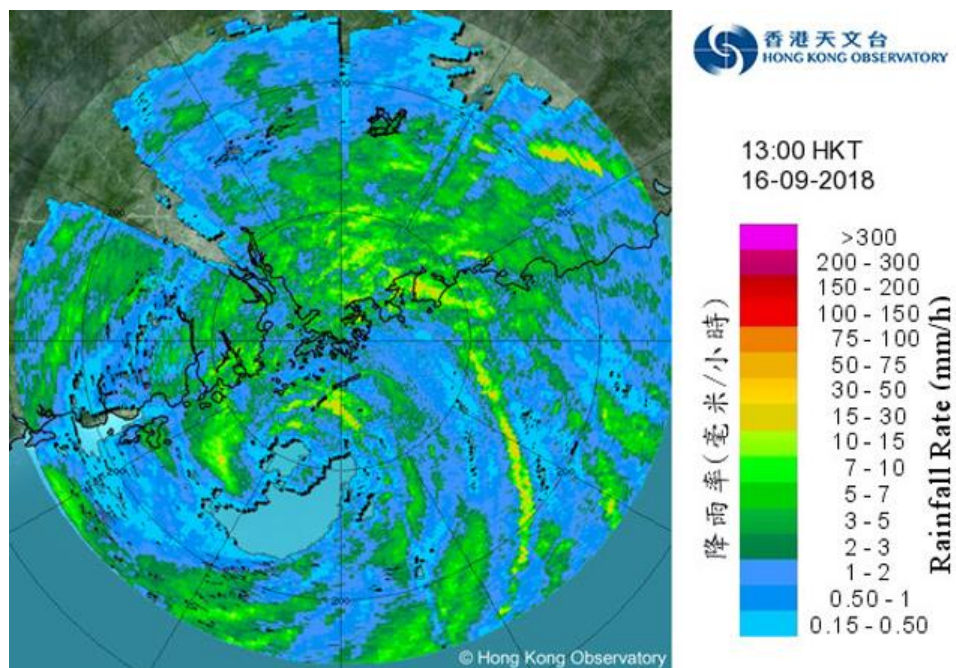
Note. Radar images showed that Mangkhut made landfall in the vicinity of Cagayan province of northeastern Philippines at 1:40 a.m. on 15 September 2018.

Mangkhut turned to northwestward motion at about 35 kmh^{-1} across the northern part of the South China Sea towards the Pearl River estuary on 16 September. It weakened into a severe typhoon that morning, attaining its peak intensity with an estimated maximum sustained wind of 175 kmh^{-1} near the centre and a minimum sea-level pressure of 950 hPa. Then, it came closest to the Hong Kong Observatory Headquarters around 1 p.m. with its centre located about 100 km to the south-southwest (Figure 1.3). Due to the superposition of the right semicircle of the storm, fast movement and the easterly airstream south of the subtropical ridge, resulting in a tighter pressure gradient and thus stronger winds in between them (Kung, 2011). The storm brought ferocious winds to Hong Kong most of the time during the day. During the passage of Mangkhut, the maximum 10-minute mean wind speeds recorded at Tate's Cairn, Waglan Island, Cheung Chau, North Point and Sai Kung were 189 kmh^{-1} , 180 kmh^{-1} , 173 kmh^{-1} , 124 kmh^{-1} and 118 kmh^{-1} with maximum gusts of 256 kmh^{-1} , 220 kmh^{-1} , 212 kmh^{-1} , 171 kmh^{-1} and 180 kmh^{-1} respectively. The lowest instantaneous mean sea-level pressures recorded at Cheung Chau, Waglan Island, Hong Kong International Airport, Hong Kong Observatory Headquarters and Shatin were 971.8 hPa, 973.5 hPa, 973.9 hPa, 977.0 hPa and 980.1 hPa respectively. Furthermore, its spiral rainbands brought very adverse weather to the territory for heavy rainstorm and squalls. The total rainfall recorded at Shek Kong (SEK), So Uk Estate (K06), Tap Shek Kok (R21), Kwai Chung (N06) and Sha Tin (N09) was 320.5 mm, 270.0 mm, 249.0 mm, 236.5 mm and 224.5 mm respectively. Affected by the storm surge, the water level in Tai Po Kau, Tai Miu Wan, Tsim Bei Tsui, Shek Pik and Quarry Bay rose to a maximum of 4.71 m, 4.19 m, 4.18 m, 3.89 m and 3.88 m above Chart Datum respectively. On the other hand, the maximum wave height recorded at Kau Yi Chau and West Lamma Channel was about 6.8 m (Hong Kong Observatory [HKO], 2018).

Subsequently, Mangkhut made landfall in the vicinity of Taishan of Guangdong province, about 130 km west-southwest of Hong Kong at 5 p.m. that day (Figure 1.4). The maximum 10-minute mean wind speed recorded at the Taishan Nuclear Power Plant was 210 kmh^{-1} , and the lowest instantaneous sea-level pressure of 965.7 hPa. Severe thunderstorm associated with it was affecting the Guangdong. The total rainfall recorded at Sijiu and Taishan was 379 mm and 157 mm, respectively. Under the influence of storm surge, the highest water level of 2.24 m above the Chart Datum recorded at Fenghuojiao Milldam. It then slowed down to about 20 kmh^{-1} into western part of Guangdong that evening, weakening into a typhoon at night. As Mangkhut moved further inland, it weakened gradually into a tropical depression the next afternoon and degenerated into an area of low pressure over the Baise of the western part of Guangxi at night.

Figure 1.3

Radar image of severe typhoon Mangkhut in Hong Kong

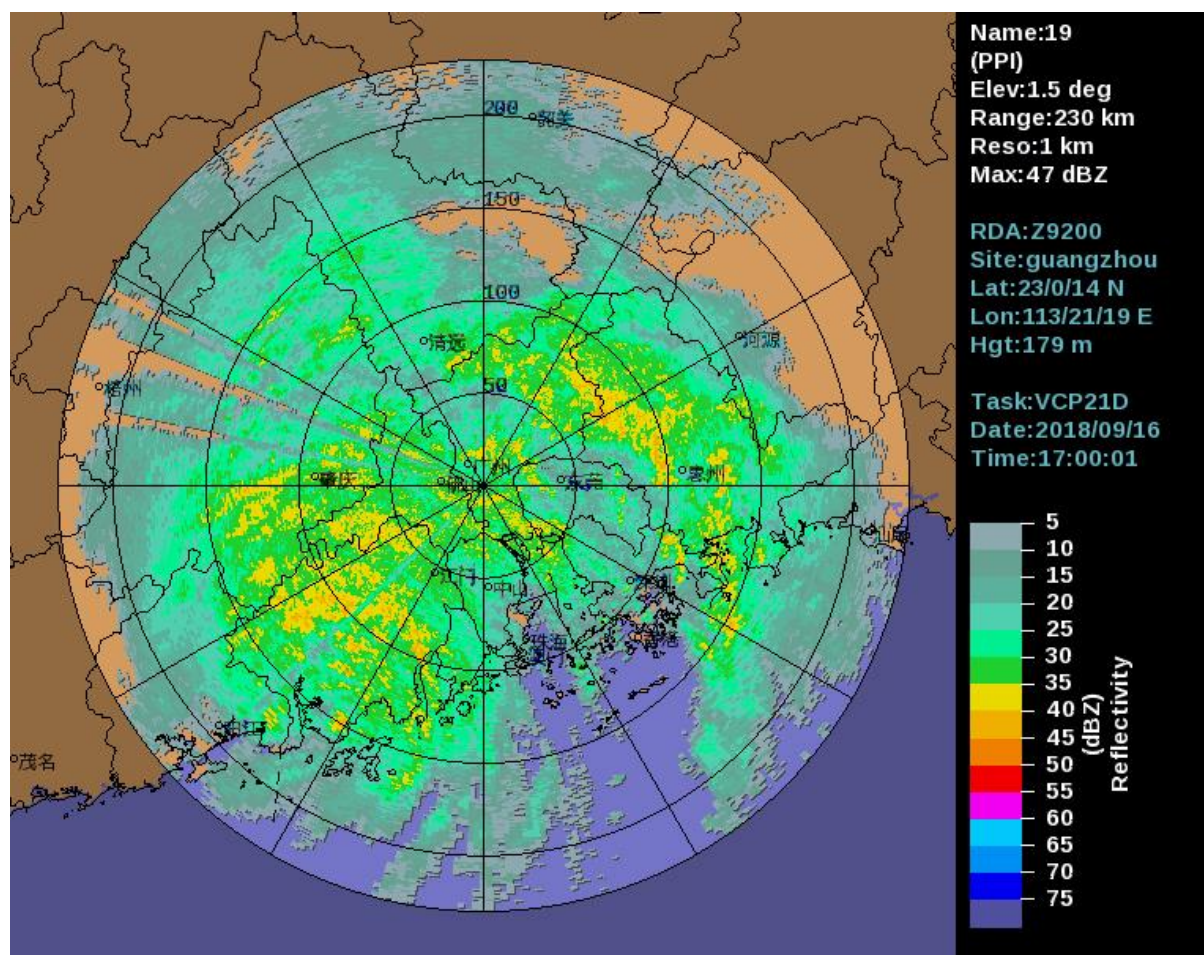


Note. Radar images showed that Mangkhut came closest to the Hong Kong Observatory Headquarters around 1 p.m. with about 100 km to the south-southwest on 16 September 2018.

On the whole, super typhoon Mangkhut stands out as a significant meteorological event of the 2018 Pacific tropical cyclone season because of its exceptional intensity, rapid intensification, and expansive spatial impact. Originating as a tropical depression near Wake Island, Mangkhut rapidly developed into a super typhoon under highly favourable environmental conditions, exhibiting classic structural features such as a well-defined eye and central dense overcast. Its trajectory brought devastating effects across the Philippines, Hong Kong, and southern China, where it caused extensive damage through intense winds, heavy rainfall, storm surges, and associated hazards such as flooding and landslides. The storm's interaction with land, particularly in the mountainous terrain of northern Luzon, led to fluctuations in its intensity, while its passage over the South China Sea enabled partial reorganizations before landfall in southern China. The records of extreme wind speeds, heavy precipitation, elevated sea levels, and destructive storm surges highlight the multifaceted threat posed by Mangkhut. This event underscores the critical importance of continuous meteorological monitoring, improved early warning systems, and resilient infrastructure to mitigate the impacts of future super typhoons in a region highly vulnerable to tropical cyclone hazards.

Figure 1.4

Radar image of severe typhoon Mangkhut in Taishan of Guangdong province



Note. Radar images showed that Mangkhut made landfall in the vicinity of Taishan of Guangdong province, at 5:00 p.m. on 16 September 2018.

1.2 Objectives

This paper seeks to conduct a comprehensive analysis of super typhoon Mangkhut by examining its meteorological characteristics, societal impacts, and predictive modelling to enhance understanding and preparedness for future high-intensity tropical cyclones.

The investigation begins with an analysis of Mangkhut's structural and developmental features, focusing on its formation, rapid intensification, and subsequent evolution. Utilising satellite imagery, observational data, and atmospheric variables—such as sea surface temperatures and vertical wind shear—this study elucidates the physical mechanisms underlying the storm's exceptional intensity and duration. Such insights are critical for improving the scientific basis of forecasting similarly extreme events.

A critical component of this research involves assessing the efficacy of numerical weather prediction (NWP) models in forecasting Mangkhut's trajectory, intensity fluctuations, and associated hazards (e.g., storm surges, rainfall distribution). By comparing model outputs with observed data, the study identifies systematic biases and limitations in current forecasting frameworks, particularly in predicting rapid intensification phases. These insights are instrumental in guiding future model improvements and enhancing the reliability of early warning systems.

To contextualise Mangkhut's behaviour, this study employs a comparative framework, examining similarities and differences with other notable tropical cyclones in terms of intensity, track variability, and environmental interactions. This analysis not only highlights the role of large-scale climatic drivers (e.g., ENSO phases, monsoon circulations) in modulating storm characteristics but also aids in refining empirical forecasting tools used in operational meteorology.

Beyond atmospheric dynamics, the research evaluates the typhoon's societal consequences by quantifying economic losses, infrastructure damage, and human casualties across affected regions. Through case studies of government and community-led responses, the study identifies gaps in preparedness measures and proposes evidence-based recommendations to strengthen disaster resilience. Special emphasis is placed on the interplay between physical exposure, socioeconomic vulnerability, and institutional capacity in shaping disaster outcomes.

By merging meteorological insights with analyses of societal consequences, this study advances scientific understanding of tropical cyclones, improves forecasting methods, and supports the creation of stronger disaster risk reduction frameworks. Its findings are intended to guide policymakers, meteorologists, and emergency responders, ultimately fostering greater preparedness for future severe weather events.

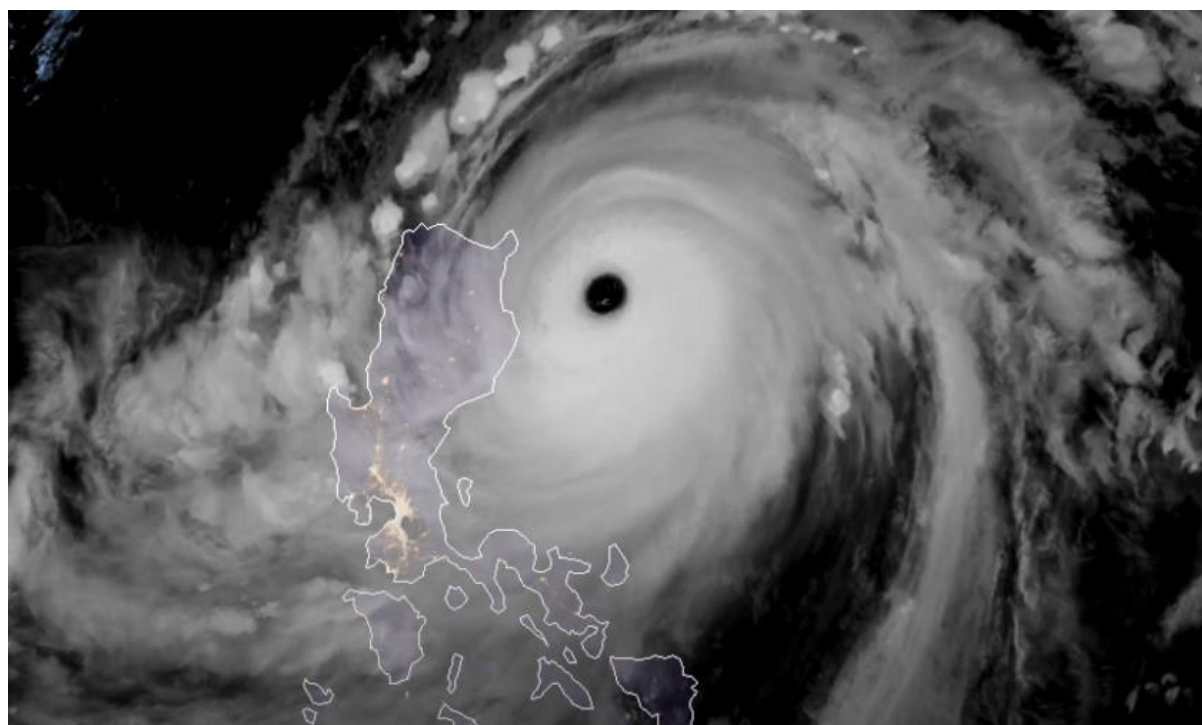
2. Development of Mangkhut

2.1 Structural Characteristics

Mangkhut has a well-defined structure typical of intense tropical cyclones, including a distinct eye, eyewall, and spiral rainbands. It featured a clear, symmetrical eye, approximately 50 km in diameter at its peak intensity (Figure 2.1), surrounded by a ring of deep convection known as the eyewall. This eyewall consisted of towering thunderstorms with cloud tops colder than -80°C (Figure 2.2), indicating intense updrafts and heavy rainfall. The tightly coiled spiral rainbands extended hundreds of kilometres outward—spanning radial distances of 400 to 600 km from the eye—feeding moisture and energy into the core.

Figure 2.1

Himawari-8 Infra-red satellite imagery of super typhoon Mangkhut



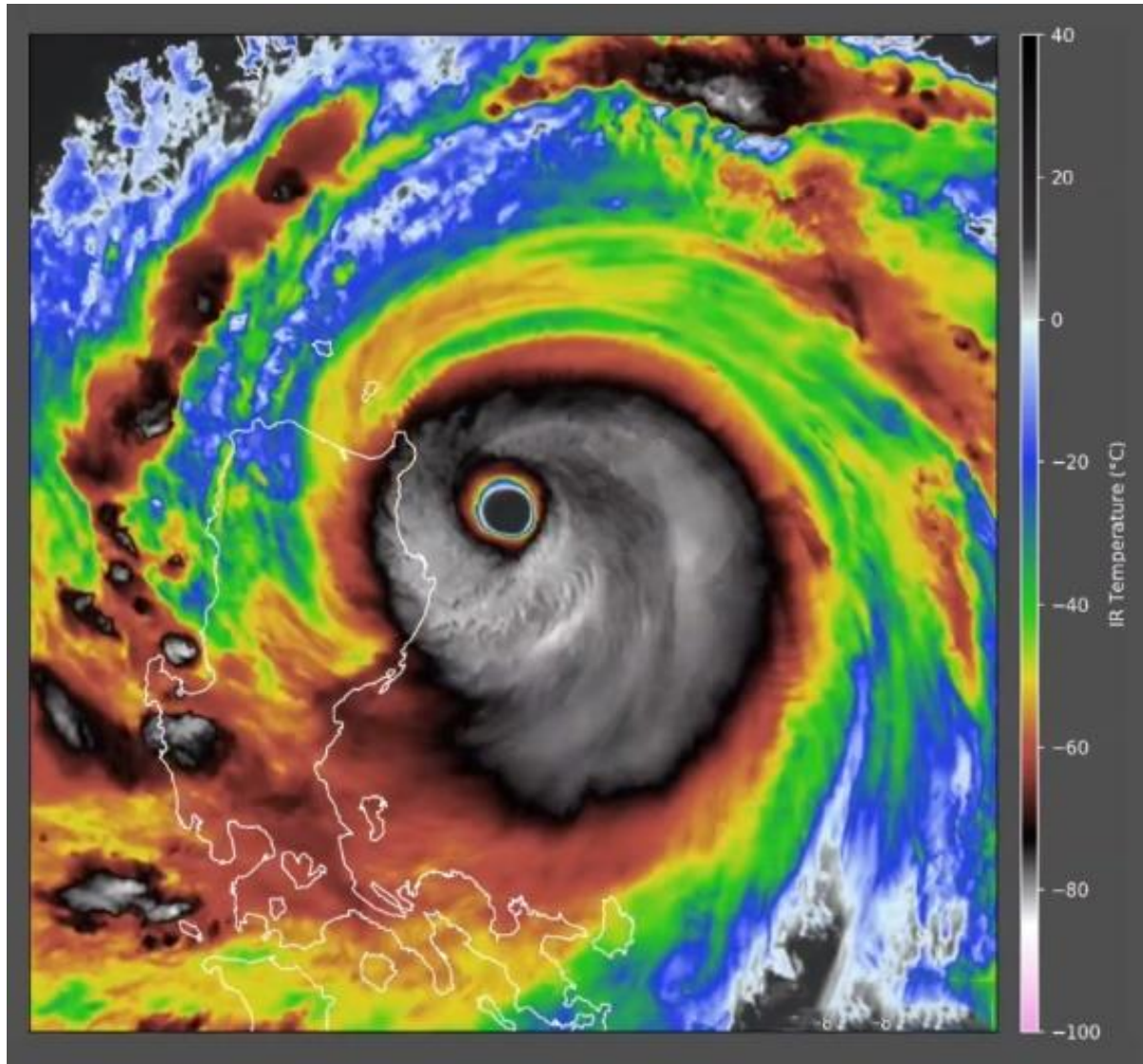
Note. Mangkhut has a round eye, broad circulation and deep convection clouds at 11:00 p.m. on 14 September 2018 by the infra-red satellite imagery of Himawari-8 satellite of JMA.

Mangkhut's structure displayed remarkable symmetry, with a robust upper-level outflow that efficiently vented air from the eyewall, thereby maintaining the storm's strength. The storm's large wind field—spanning over 900 km and with an overall cloud system extending up to 1,400 to 2,000 km—produced destructive conditions across a vast area (Figure 2.3). Its cloud pattern, as observed in satellite imagery, exhibited a classic annular hurricane appearance, with a distinct eye and uniform

convection, indicating minimal wind shear and favourable environmental conditions (He, He, Chen, Chan, Fu & Li, 2020). The storm's structure contributed to its longevity and destructive potential, as it maintained super typhoon status for several days before landfall.

Figure 2.2

Infra-red colour enhanced imagery of Himawari-8 satellite of super typhoon Mangkhut



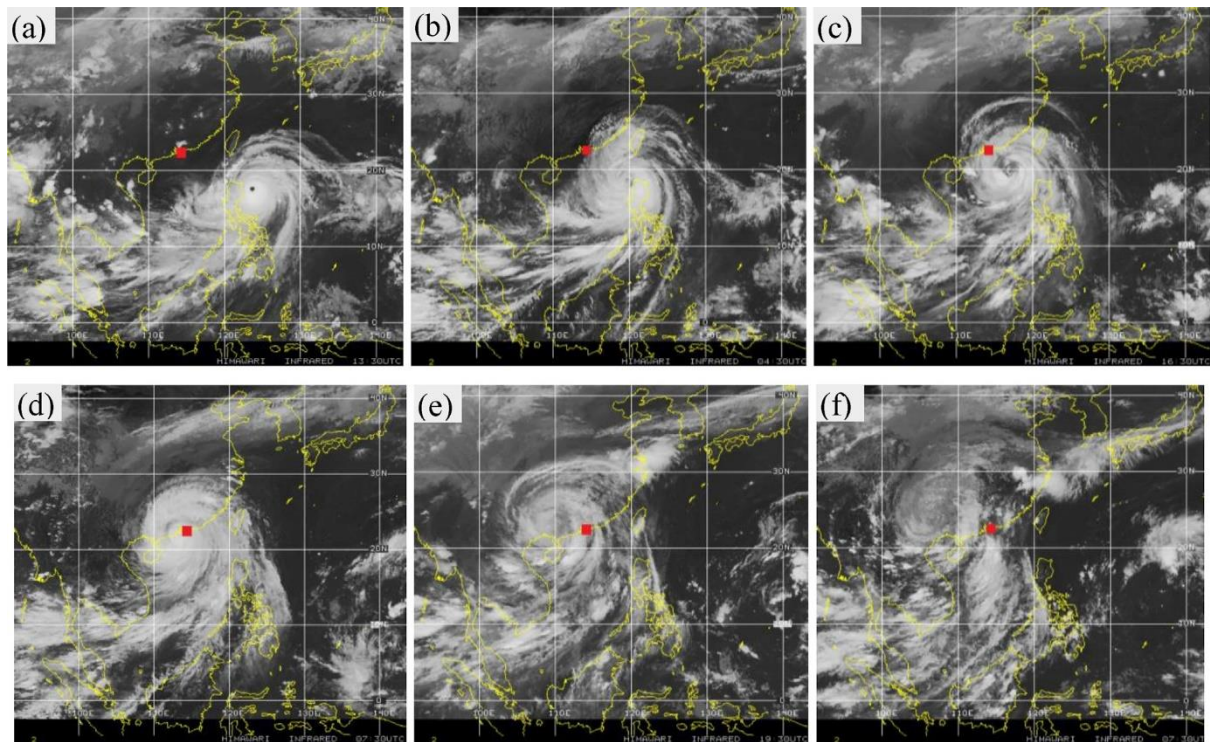
Note. Infra-red colour enhanced imagery of Himawari-8 satellite of JMA demonstrated the cloud-top temperatures of Mangkhut dropping to -80°C at 11:00 p.m. on 14 September 2018.

As Mangkhut approached the Philippines and later southern China, its outer rainbands brought torrential rainfall, while the inner core unleashed catastrophic winds and storm surges. The storm's structure began to weaken slightly upon interacting with land, but its expansive circulation continued to cause widespread devastation. The combination of its immense size, intense eyewall, and well-

developed feeder bands made Mangkhut one of the most formidable tropical cyclones on record in 2018.

Figure 2.3

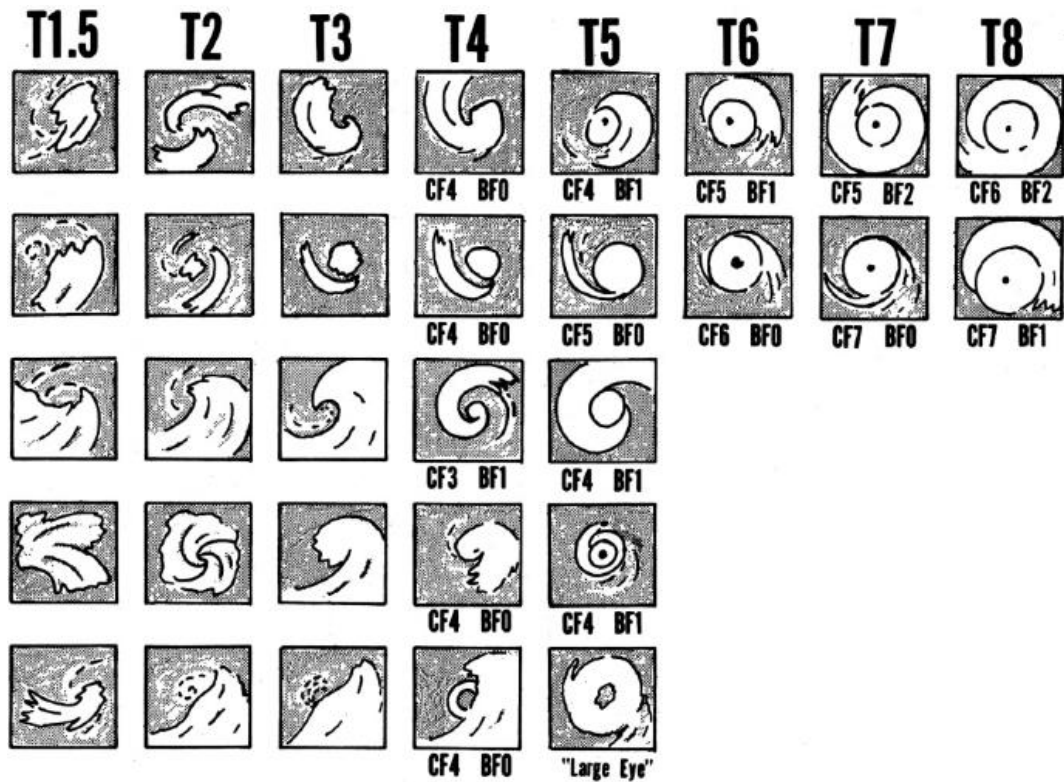
Himawari-8 Infra-red satellite imagery of snapshots of super typhoon Mangkhut's cloud



Note. Infrared satellite imagery of the typhoon's cloud cover at six selected time points (each grid square represents a 10×10 km area, with the red diamond indicating Hong Kong): (a) 21:30 on the 14th (HKT); (b) 12:30 on the 15th; (c) 00:30 on the 16th; (d) 15:30 on the 16th; (e) 03:30 on the 17th; (f) 15:30 on the 17th (He et al, 2020).

2.2 Intensity

Mangkhut, one of the most violent tropical cyclones, revealed exceptional intensity characteristics clearly visible through satellite imagery and quantifiable through the Advanced Dvorak Technique (ADT). This satellite-based intensity estimation method, developed as an objective and automated extension of the original Dvorak technique by Vernon Dvorak, analyses cloud patterns (Figure 2.4) and enhanced infrared imagery to determine tropical cyclone strength (Velden, Harper, Wells, Beven, Zehr, Olander, Mayfield, Guard, Lander, Edson, Avila, Burton, Turk, Kikuchi, Christian, Caroff & McCrone, 2006; Choy & Kok, 2013; Olander & Velden, 2015). When applied to Mangkhut, the ADT displayed exceptional characteristics that explained its sustained extreme intensity.

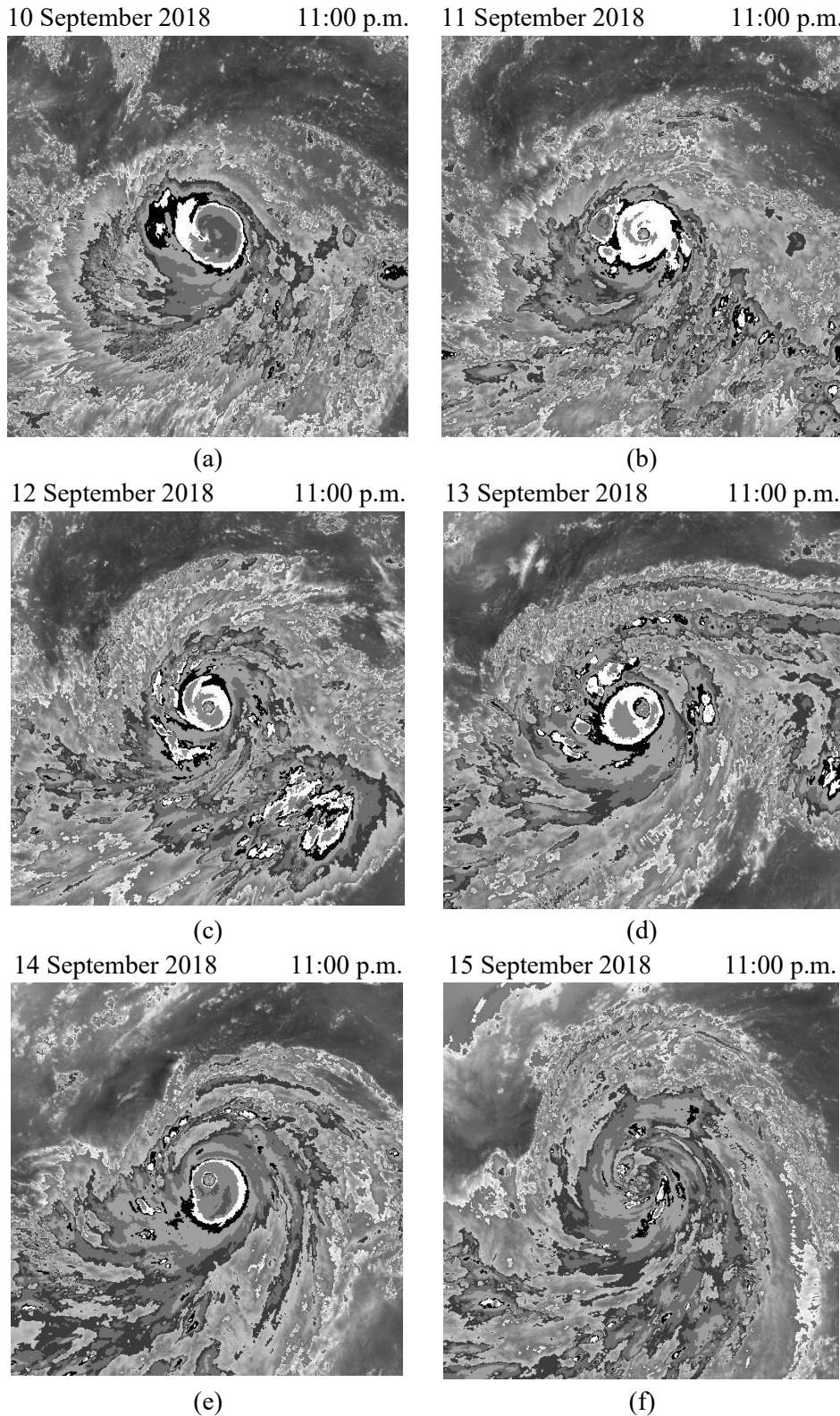
Figure 2.4*Intensity analysis of tropical cyclones*

During its rapid intensification phase from 10 to 14 September, Mangkhut's satellite presentation showed the classic signs of a rapidly strengthening system, as illustrated in Figure 2.5(a)-(e). The ADT-derived Current Intensity (CI) value and T-number escalated to 7.5, corresponding to maximum sustained winds of approximately 250 kmh^{-1} and a minimum central pressure of 900 hPa. The storm exhibited a perfectly symmetrical CDO with a sharply defined eye approximately 50 km in diameter, surrounded by extremely cold (-80°C) convective tops in the eyewall region.

The ADT particularly highlighted Mangkhut's annular hurricane characteristics during its peak intensity. The storm maintained a CI value and T-number between 7.0 and 7.5 for an exceptional 36-hour period, demonstrating remarkable structural integrity. This persistence was facilitated by the storm's excellent outflow pattern, with pronounced poleward outflow enhanced by an upper-level trough to the northwest. The ADT's pattern recognition clearly showed these superior ventilation channels that allowed Mangkhut to maintain super typhoon status despite marginal environmental conditions (Knaff, Zehr, Goldberg & Kidder, 2003).

Figure 2.5

Basic Dvorak enhanced satellite images of Himawari-8 satellite of super typhoon Mangkhut



Note. The above figures (a)-(e) revealed that Mangkhut was strengthening at 11:00 p.m. from 10 to 14 September 2018. In contrast, Figure (f) showed that Mangkhut was weakening at 11:00 p.m. on 15 September 2018 (JMA).

When Mangkhut approached landfall in Luzon on 15 September, the ADT analysis captured the storm's structural changes. The CI and T-number decreased from 7.5 to 6.5 because the eye became less distinct and the CDO showed increasing asymmetry, as revealed in Figure 2.5(f). However, the technique also revealed the storm's resilience, as it maintained significant organisation despite land interaction. Following landfall, the ADT estimates showed partial reintensification over the South China Sea before its final landfall in China (Choy, Lau & He, 2022).

The application of the ADT to Mangkhut provided several key insights. It quantified the storm's exceptional intensity during periods when in situ measurements were unavailable. Additionally, it identified structural features that explained the storm's ability to maintain peak intensity. The technique accurately tracked both the intensification and weakening trends throughout the storm's lifecycle (Figures 2.6-2.7). Furthermore, it highlighted the annular characteristics that contributed to Mangkhut's unusual resilience.

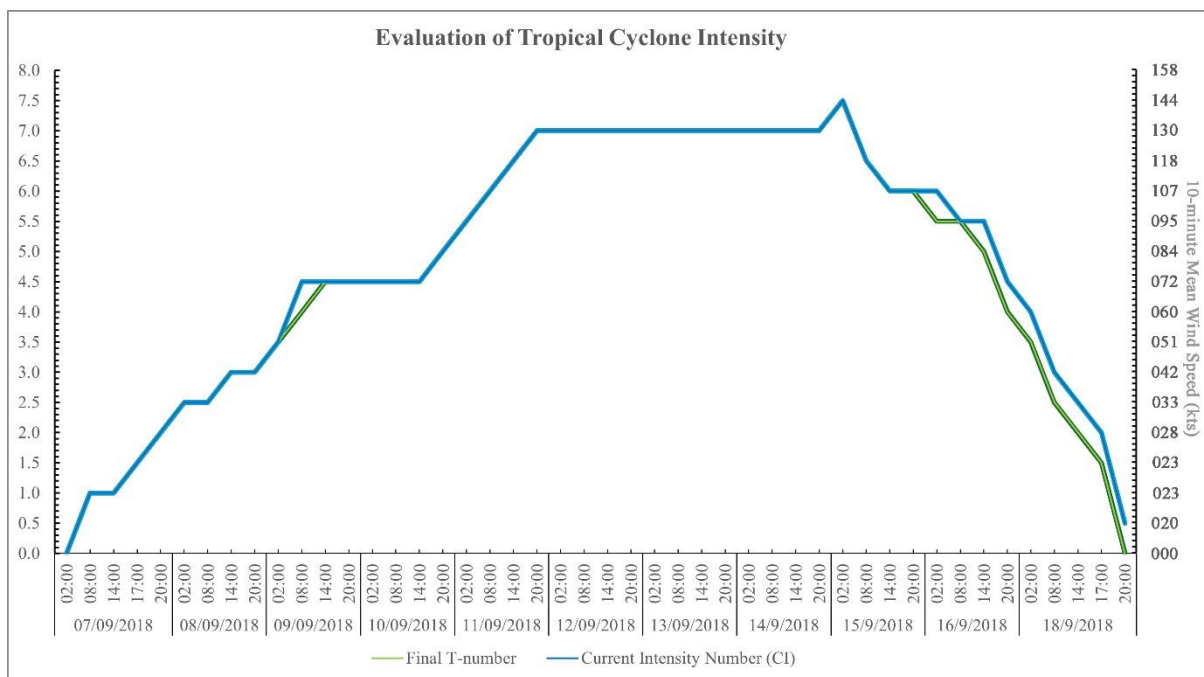
2.3 Wind Field Distributions

The Multi-platform Satellite Surface Wind Analysis (MPSATWND) of Mangkhut reveals a highly organised convection system with distinct wind field structure, characterised by asymmetrical wind radii across different quadrants (Figure 2.8). The maximum sustained winds (VMAX) were estimated at 135 kt (250 kmh^{-1}), with the radius of maximum winds (RMW) extending approximately 180 nmi (333 km) from the centre. This indicates an exceptionally powerful storm with a broad wind field, typical of super typhoon.

The wind radii data highlight significant asymmetry in Mangkhut's structure. In the northeast (NE) quadrant, the radii for 34 kt (63 kmh^{-1}), 50 kt (93 kmh^{-1}), and 64 kt (119 kmh^{-1}) winds extend 150 nmi (278 km), 90 nmi (167 km), and 50 nmi (93 km), respectively, reflecting the storm's strongest winds in this sector due to its forward motion and cyclonic rotation. Similarly, the southeast (SE) quadrant shows comparable extents of 150 nmi (278 km), 60 nmi (111 km) and 20 nmi (37 km), while the southwest (SW) quadrant exhibits reduced radii of 150 nmi (278 km), 70 nmi (130) and 45 nmi (83 km), likely due to land interaction or subsidence effects. The northwest (NW) quadrant mirrors the NE quadrant's expansive wind field of 170 nmi (315 km), 95 nmi (176 km) and 50 nmi (278 km), reinforcing the storm's asymmetry.

Figure 2.6

Time series of advanced Dvorak technique of tropical cyclone Mangkhut

**Figure 2.7**

Time series of intensity of tropical cyclone Mangkhut

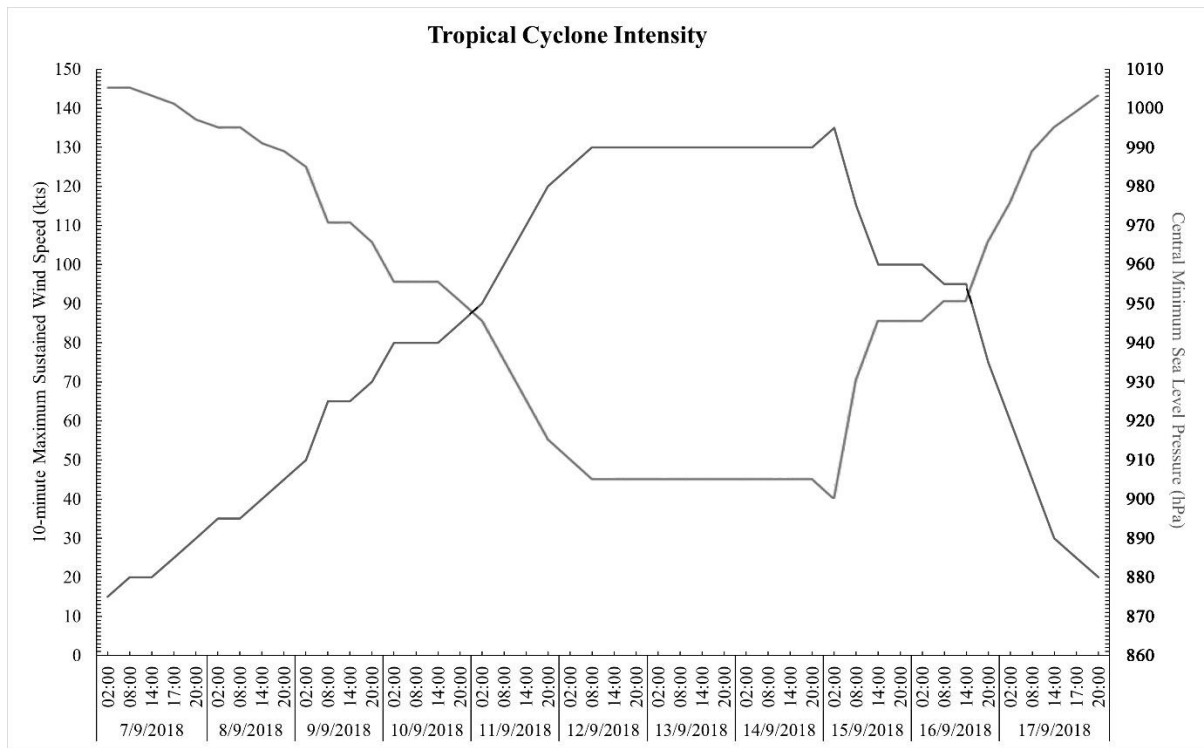
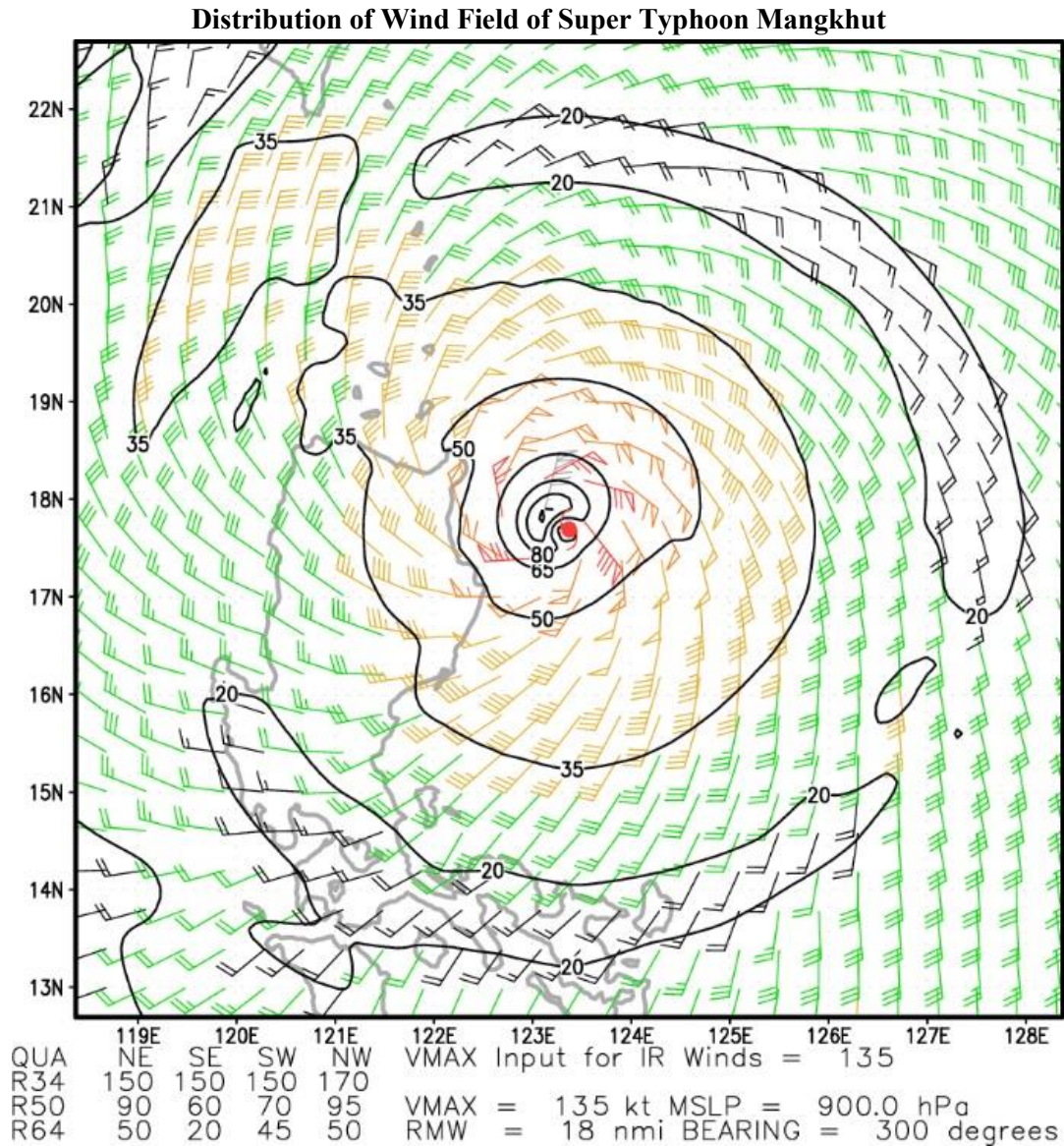


Figure 2.8

Multi-platform Satellite Surface Wind Analysis of super typhoon Mangkhut



Note. Mangkhut's Multi-platform satellite surface wind analysis is shown at 11:00 p.m. on 14 September 2018.

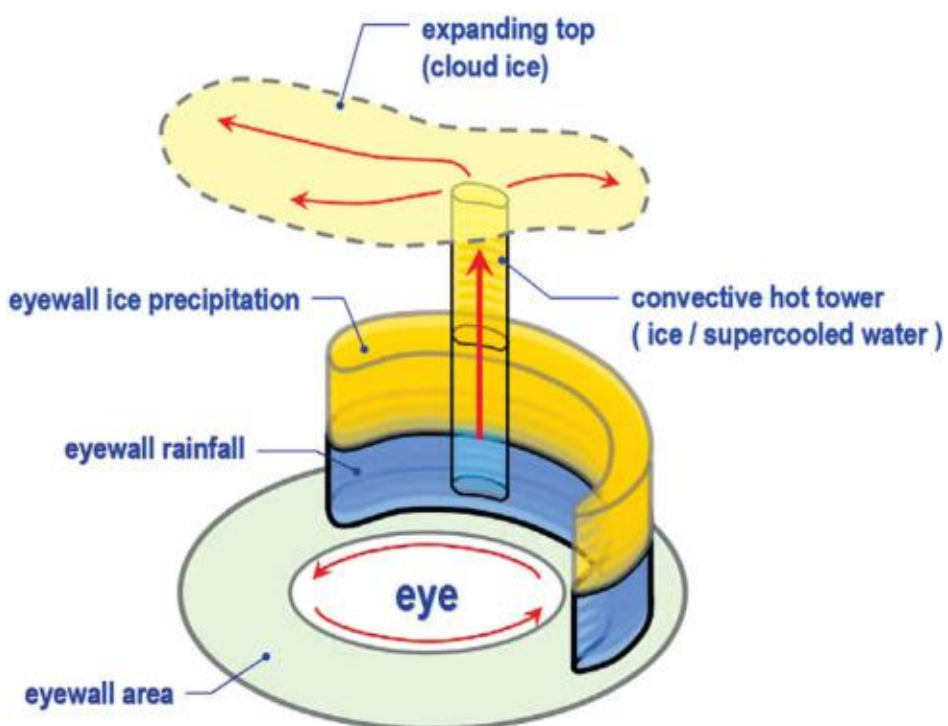
The central sea-level pressure was recorded at 900 hPa, consistent with the storm's extreme intensity. The wind field's broad spatial coverage—particularly the extensive 34 kt (63 kmh^{-1}) winds (exceeding 150 nmi (278 km) in some quadrants)—underscores Mangkhut's capacity to produce widespread impacts, including storm surges and flooding, even in regions far from the eyewall. This MSSWA analysis demonstrates the utility of multi-platform satellite data in capturing fine-scale wind structures and asymmetries, which are critical for forecasting storm hazards and mitigating risks. The data align with Mangkhut's observed impacts, including severe damage in the Philippines, Hong Kong and southern China due to its expansive wind field and intense core.

2.4 Convective Activity

The eyewall of Mangkhut exhibited a severe convective activity—known as the “convective hot towers” phenomenon—as it traversed the western North Pacific (Figure 2.9). This phenomenon is the signatures of fast intensification. Its cloud top exceeded 17 km up to the top of the troposphere accompanied by cloud-to-ground lightning and updraft turned fierce (Yeung, 2013). In Figure 2.10(a)-(e), the polarisation corrected brightness temperature was below about 180K in the Morphed Integrated Microwave Imagery during 10 to 14 September.

Figure 2.9

Schematic diagram of convective hot towers



Note. Schematic diagram illustrating the concept of a convective hot tower of a mature tropical cyclone.

Lightning activity was notably intense in this period, with observations from the Fengyun-4A (FY-4A) Lightning Mapping Imager (LMI) confirming prolific intra-cloud and cloud-to-ground lightning discharges associated with the convective towers in the eyewall (Figure 2.11). This heightened lightning activity correlates with the storm's rapid intensification phase and the vigorous convective bursts within the eyewall.

Figure 2.10

Morphed Integrated Microwave Imagery of super typhoon Mangkhut

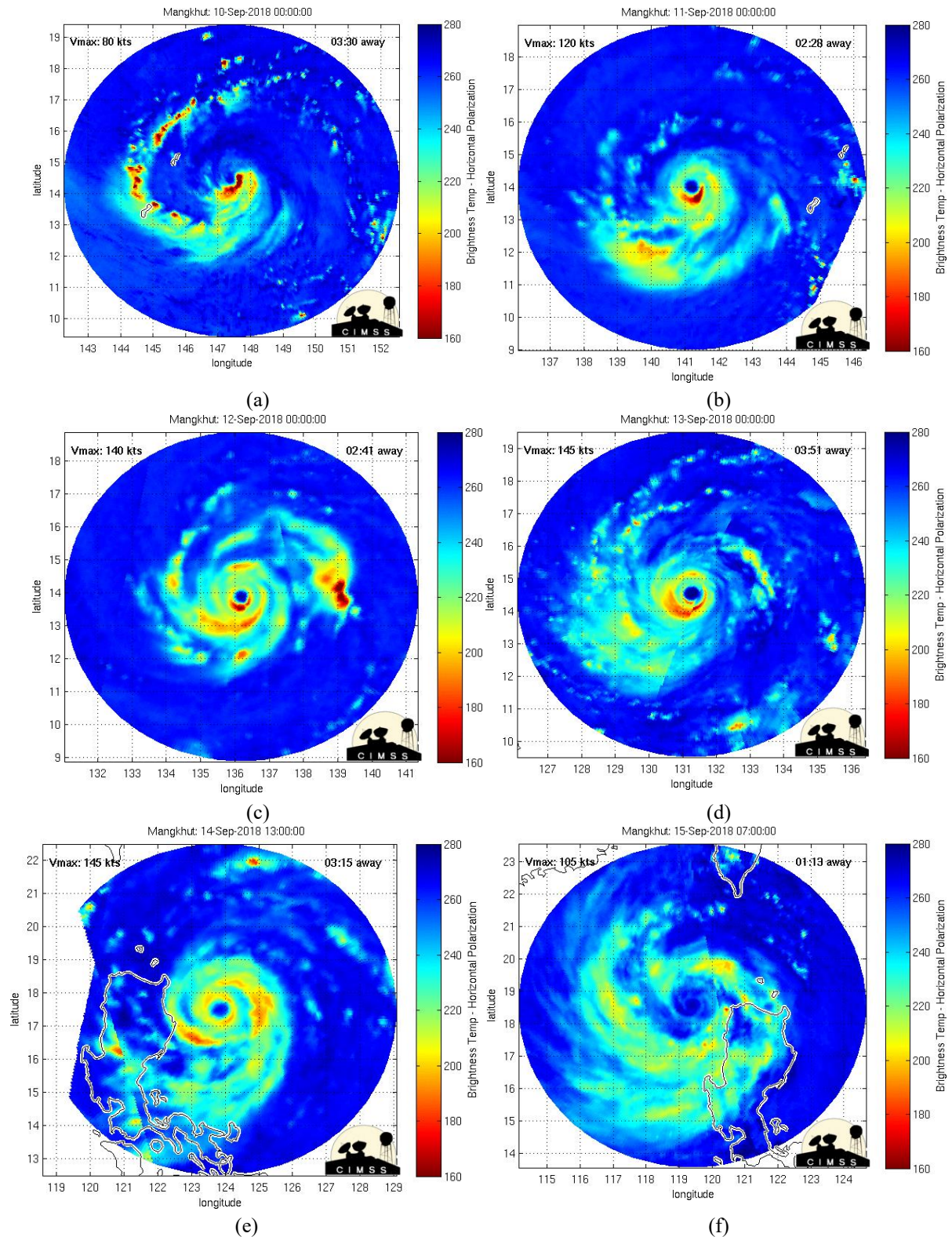
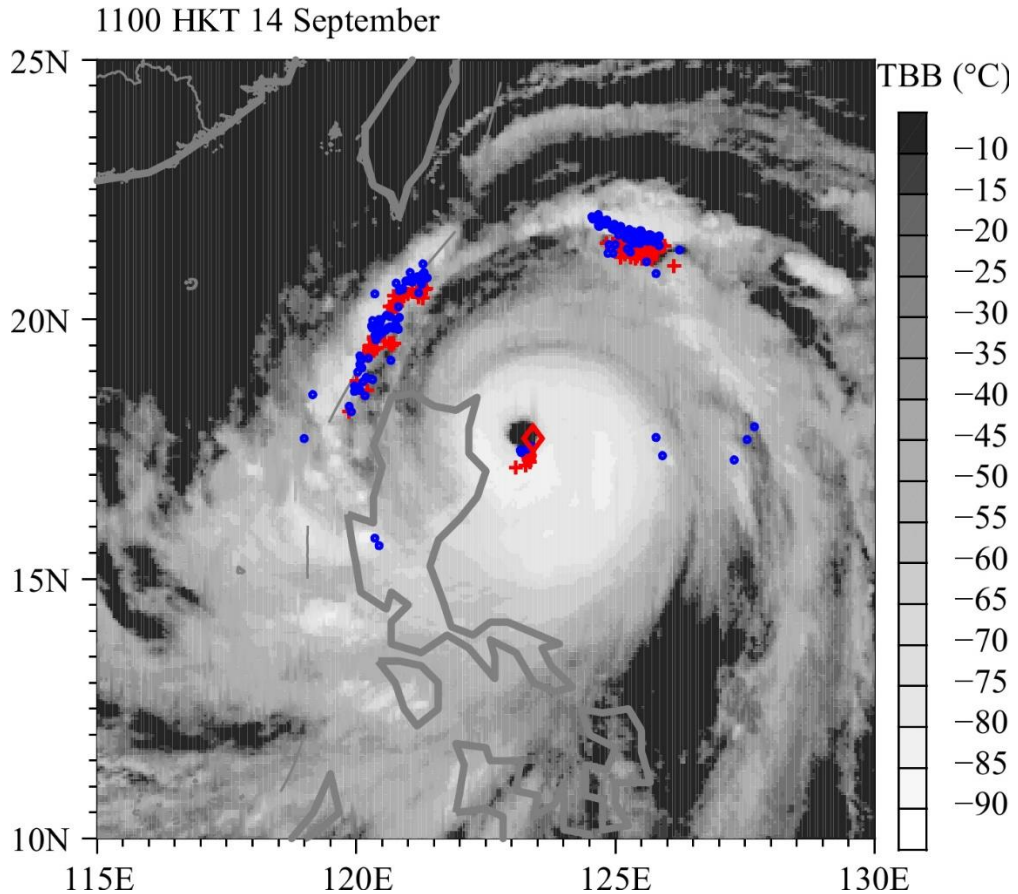


Figure 2.11

Fengyun-4A Lightning Mapping Imager of super typhoon Mangkhut



Note. The TBB imageries (shading; °C) from Himawari-8 are overlaid with LMI (red dots) and WWLLN flashes (blue dots) observed within ± 30 minutes of the satellite observation time at 11:00 p.m. on 14 September 2018.

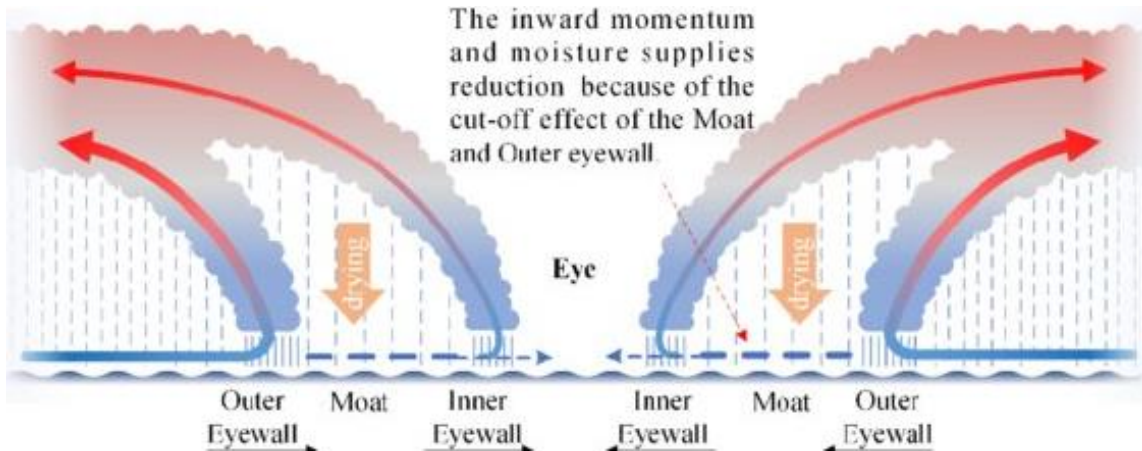
On the other hand, Mangkhut's centre developed a well-defined concentric eyewall structure as it intensified to peak strength before making landfall in the northern part of Luzon (Figure 2.10(e)). Its inner eyewall was intact, whereas its outer eyewall was not intact. The winds associated with the inner eyewall was stronger than those near the outer eyewall. This possibly marked the beginning of the initial eyewall replacement cycle, as the storm exhibited a double-eye-walled structure (Figure 2.12).

While Mangkhut weakened after moving across the northern part of Luzon, exhibiting weaker convection over the inner eyewall, the outer eyewall remained intense and its structure was intact on 15 September, as shown in Figure 2.10(f). This could be the final eyewall replacement cycle. The outer eyewall contracts and eventually takes over when the inner eyewall dissipates, since the outer eyewall prevents environmental energy from being transported inward. In this process, the tropical cyclone's intensity may vary accordingly. Usually, the storm strengthens as the eyewall contracts. However, the eyewall replacement process for Mangkhut terminated, as the outer eyewall broke down

into a pair of principal spiral rainbands, although the inner eyewall had nearly disappeared. This may be because the external environment over the South China Sea did not favour the intensification of the storm (He, He, Chen, Chan, Fu & Li, 2020). This weather pattern constituted a special storm structure.

Figure 2.12

Schematic diagram of concentric eyewall structure



2.5 Environment Analysis

Mangkhut developed within an exceptionally favourable environment, driven by the North Equatorial Current (NEC) and enhanced upper-ocean stratification, which facilitated its rapid intensification into one of the most powerful tropical cyclones. The storm formed over the northwestern Pacific, where SSTs exceeded 29–30°C, providing ample energy for sustained convection (Figure 2.13). Crucially, the NEC’s westward flow deepened the thermocline, resulting in high ocean heat content (OHC) of more than 100 kJ cm^{-2} —a primary factor in suppressing typhoon-induced SST cooling and sustaining Mangkhut’s intensity (Figure 2.14). The OHC is often calculated by integrating the temperature above a reference isotherm (e.g., 26°C) over depth z :

$$\text{OHC} = \int_{-H}^0 \rho c_p (T(z) - H) dz \quad (1)$$

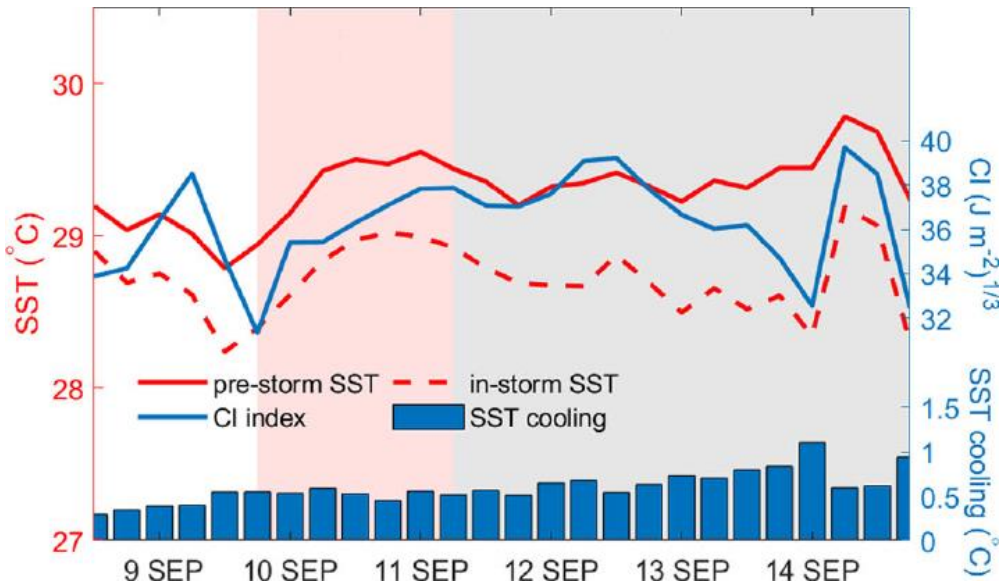
where H is the 26°C isotherm depth, ρ is seawater density (1025 kg m^{-3}), c_p is the specific heat at constant pressure ($3850 \text{ J kg}^{-1} \text{ }^\circ\text{C}^{-1}$) and $T(z)$ is water temperature in °C at a depth z (Leipper & Volgenau, 1972). Additionally, low vertical wind shear of less than 10 kt (16 km) preserved the storm’s symmetrical structure, while strong upper-level outflow enhanced divergence, promoting deep thunderstorm development (Figure 2.15). The vertical wind shear S is defined as the magnitude of the difference in horizontal wind vectors between two atmospheric levels (commonly between 200 hPa and 850 hPa):

$$S = |\vec{V}_{200 \text{ hPa}} - \vec{V}_{850 \text{ hPa}}| = \sqrt{(u_{200} - u_{850})^2 + (v_{200} - v_{850})^2} \quad (2)$$

where u and v are the zonal (east-west) and meridional (north-south) wind components, respectively, at the specified pressure levels. A low value of S (less than 10 kt) indicates minimal disruptive shear, allowing the cyclone to maintain a vertically coherent and intense structure.

Figure 2.13

Sea surface temperatures of North Equatorial Current

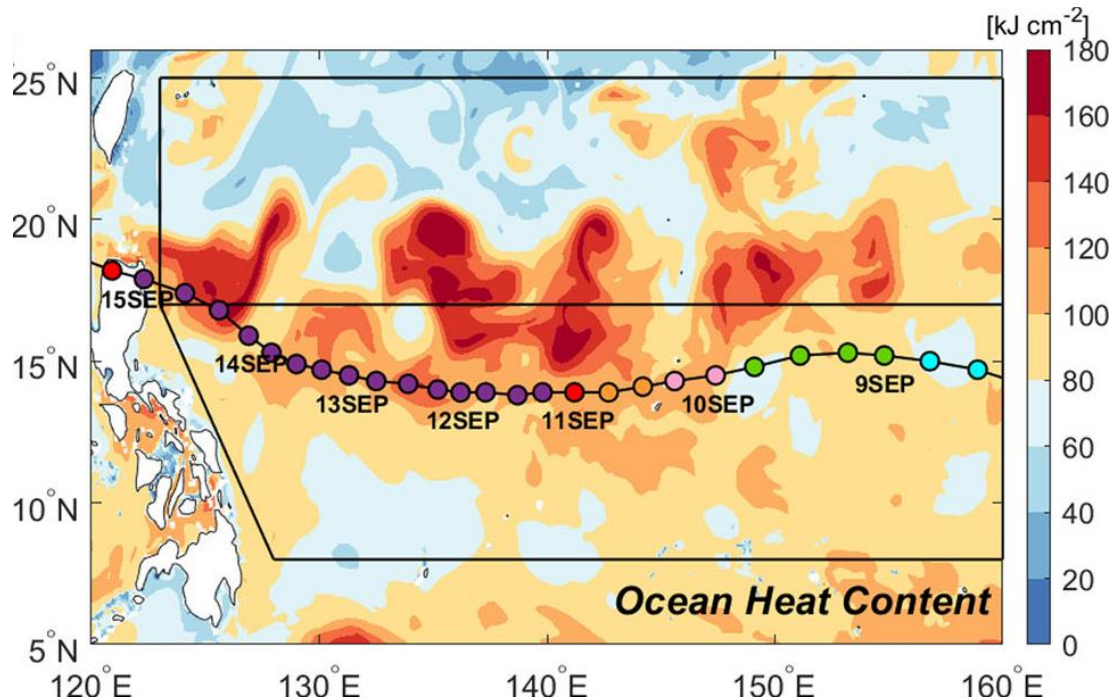


Note. Temporal evolution of pre-storm SST (solid red line), TC-induced cooled SST (discontinuous red line), CI index (solid blue line), and SST cooling (blue bars).

The presence of a moist mid-troposphere and low-salinity surface water from the Inter-Tropical Convergence Zone (ITCZ) further inhibited dry air intrusion, amplifying upper-ocean stratification and reducing mixing-driven cooling (Kang, Kim, Lin, Park, Choi, Ginis, Cione, Shin, Kim, Kim, Kang, Park, Bidlot & Ward, 2024). This stratification can be quantified by the vertical gradient of density $\frac{\partial \rho}{\partial z}$, which is enhanced by freshening:

$$N^2 = -\frac{g}{\rho} \frac{\partial \rho}{\partial z} \quad (3)$$

where N is the buoyancy frequency, a measure of stratification strength influenced by temperature and salinity (Figure 2.16).

Figure 2.14*Ocean heat content of western North Pacific*

As Mangkhut tracked westward, it maintained super typhoon strength for a record 4.5 days, owing to persistent high OHC and weak shear along the NEC corridor (Kang, Kim, Lin, Park, Choi, Ginis, Cione, Shin, Kim, Kang, Park, Bidlot & Ward, 2024). Unlike typhoons in the Eddy Rich Zone (ERZ), which rely on transient warm eddies for rapid intensification, Mangkhut's longevity was fuelled by the NEC's climatologically deep thermocline and ITCZ-derived freshening, which collectively minimised SST cooling of less than 1°C. The suppression of cooling correlates with the Cooling Inhibition (CI) Index, characterising resistance to SST drop beneath the storm:

$$CI = [\Delta E_p(-2^\circ\text{C})]^{1/3} \quad (4)$$

where ΔE_p is potential energy change for 2°C cooling exceeded $35 (\text{J m}^{-3})^{0.5}$ in the NEC region indicated strong cooling suppression. The storm's expansive wind field was further amplified by interactions with the monsoon trough, spreading destructive winds and rainfall far from its centre.

Figure 2.15

Vertical wind shear of National Oceanic and Atmospheric Administration

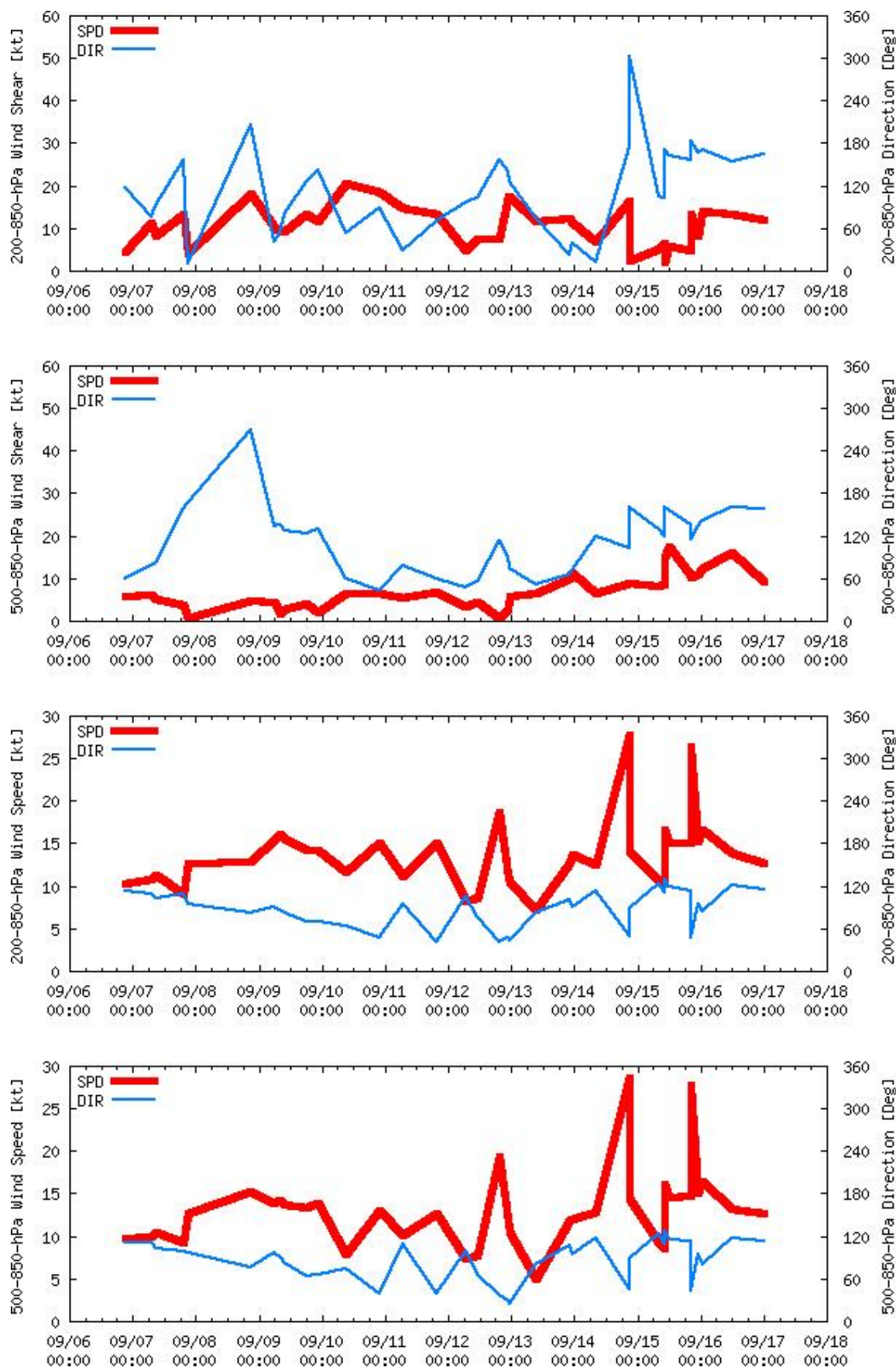
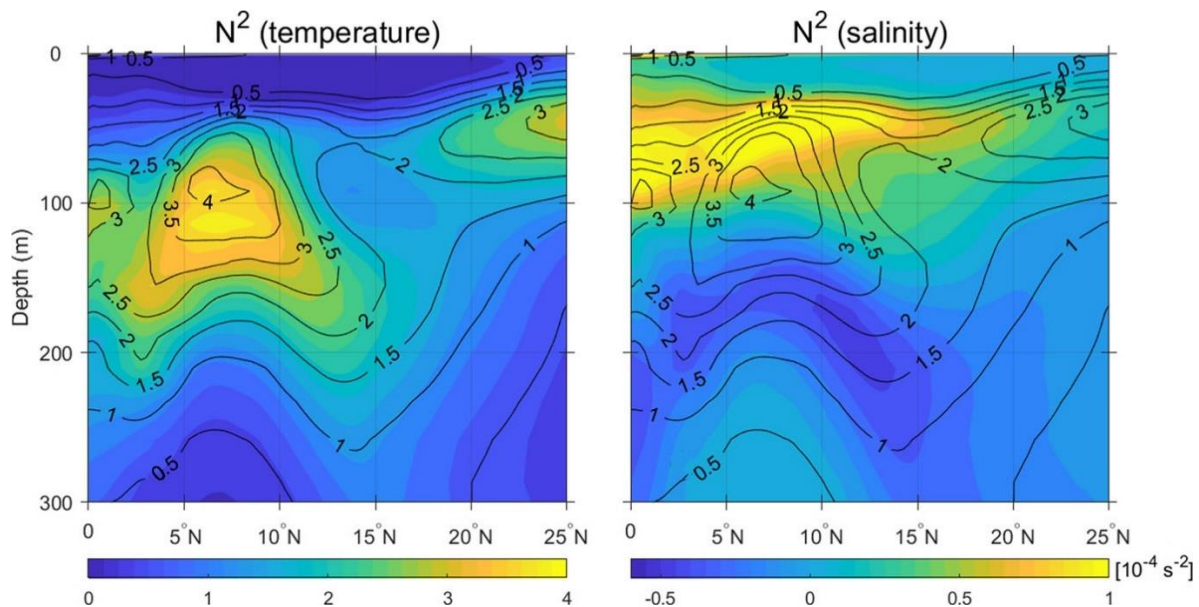


Figure 2.11

Temperature and salinity-induced squared buoyancy frequency



Upon approaching the South China region, Mangkhut encountered distinct environmental interactions that influenced its structure and impacts. The South China Sea environment was characterised by slightly cooler SSTs, exceeding 28°C, but remained sufficiently warm to maintain intensities between a severe typhoon and a super typhoon (Figure 2.17). Additionally, the monsoonal flow and prevailing subtropical ridge over South China affected Mangkhut's track and steering, guiding it steadily west-northwestward. The South China Sea also presented a moderate OHC relative to the western Pacific but maintained low vertical wind shear conditions, which allowed Mangkhut to preserve its intensity as it approached landfall (Figure 2.18). The regional atmospheric circulation included moisture surges from the South China monsoon, which combined with Mangkhut's circulation to enhance heavy rainfall over coastal and inland areas. These factors combined to prolong the storm's intensity and precipitate widespread impacts in southern China.

Large-scale steering patterns, dominated by a subtropical ridge, directed Mangkhut on a stable west-northwest trajectory, while the absence of competing systems ensured uninterrupted intensification (Figure 2.19). The NEC's role was pivotal: its geostrophic balance maintained the thermocline depth h by balancing pressure gradient and Coriolis forces:

$$fv = -\frac{1}{\rho} \frac{\partial p}{\partial x} \quad (5)$$

where f is the Coriolis parameter, v is velocity, and $\frac{\partial p}{\partial x}$ is the pressure gradient, explaining the deepening of the 26°C isotherm to 130 m at 14°N. Its decadal increase in OHC of about 9 kJ cm⁻² per decade created a “hot spot” for rapid intensification, contrasting with the Eddy Rich Zone's (ERZ)

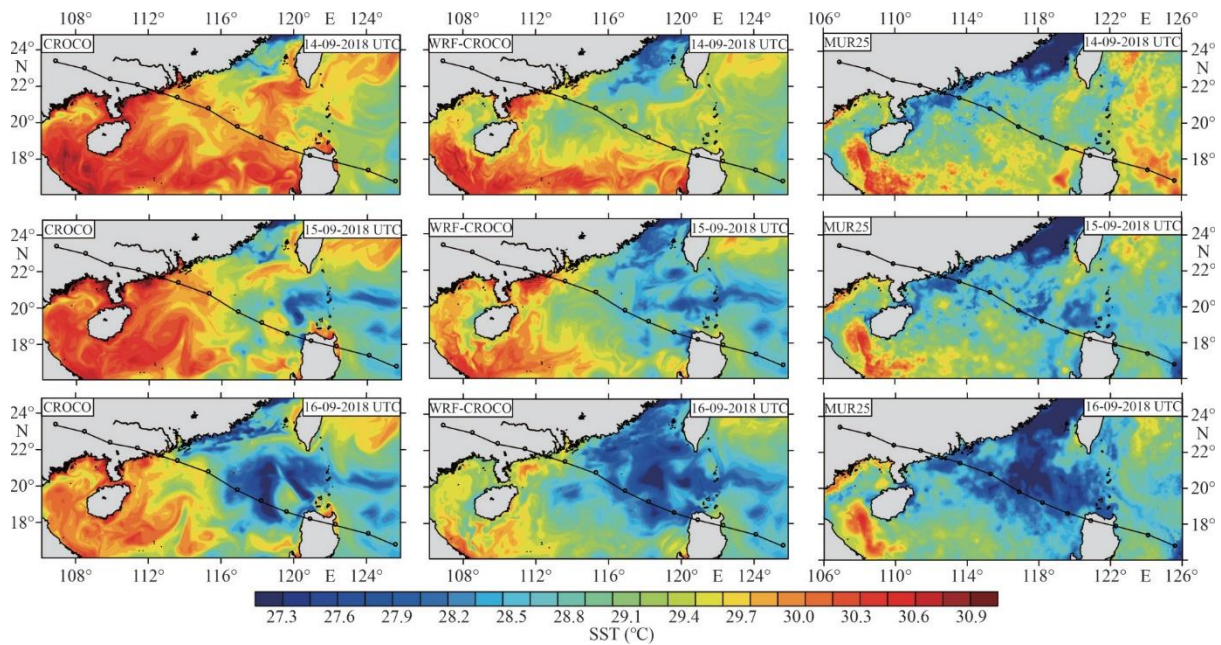
reliance on eddy-driven OHC anomalies. This synergy of factors—elevated OHC, salinity-driven stratification, and dynamic potential intensity (DPI)—allowed Mangkhut to achieve peak winds of 250 kmh^{-1} and a central sea-level pressure of 900 hPa, solidifying its place as one of the most intense typhoons in history. The DPI metric, which enhances traditional potential intensity (PI) by coupling ocean feedback, can be expressed as (simplified):

$$V_{\max} = \alpha \sqrt{\left[\frac{C_k}{C_D} \frac{T_s}{T_0} (\text{CAPE}^* - \text{CAPE}) \right]_{\text{RMW}}} \quad (6)$$

where α is the factor to reduce gradient wind by friction for 10 m wind as 0.8 by default, $\frac{C_k}{C_D}$ is the ratio of the exchange coefficient for enthalpy (C_k) to the drag coefficient (C_D) as 0.9 by default, replaced by 1.0 in this study, T_s , is the SST, T_0 is the outflow temperature, CAPE^* is the convective available potential energy of saturated air lifted from sea level to the outflow level, and CAPE is that of the environment near the radius of maximum wind (RMW) (Balaguru, Chang, Saravanan, Leung, Xu, Li & Hsieh, 2012).

Figure 2.17

Sea surface temperatures of South China Sea



2.6 Track

Mangkhut exhibited a remarkably consistent west-northwestward trajectory across the western North Pacific and South China Sea from 7 to 17 September, covering approximately 3,000 km while

maintaining exceptional intensity. The storm's track can be divided into three distinct phases that reflect changing environmental influences on its motion (Figure 2.19).

Figure 2.18

Ocean heat content of South China Sea and western North Pacific

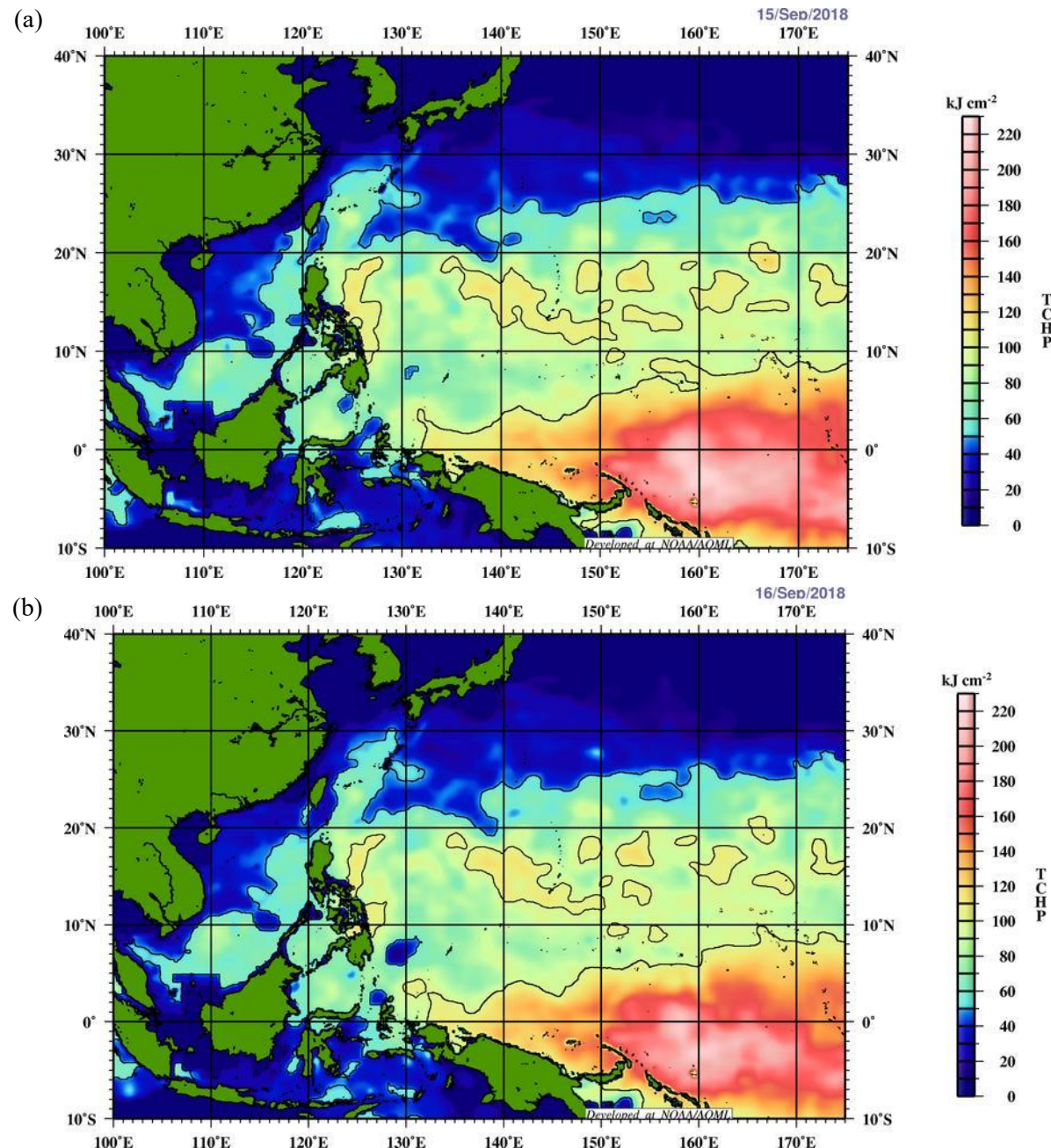


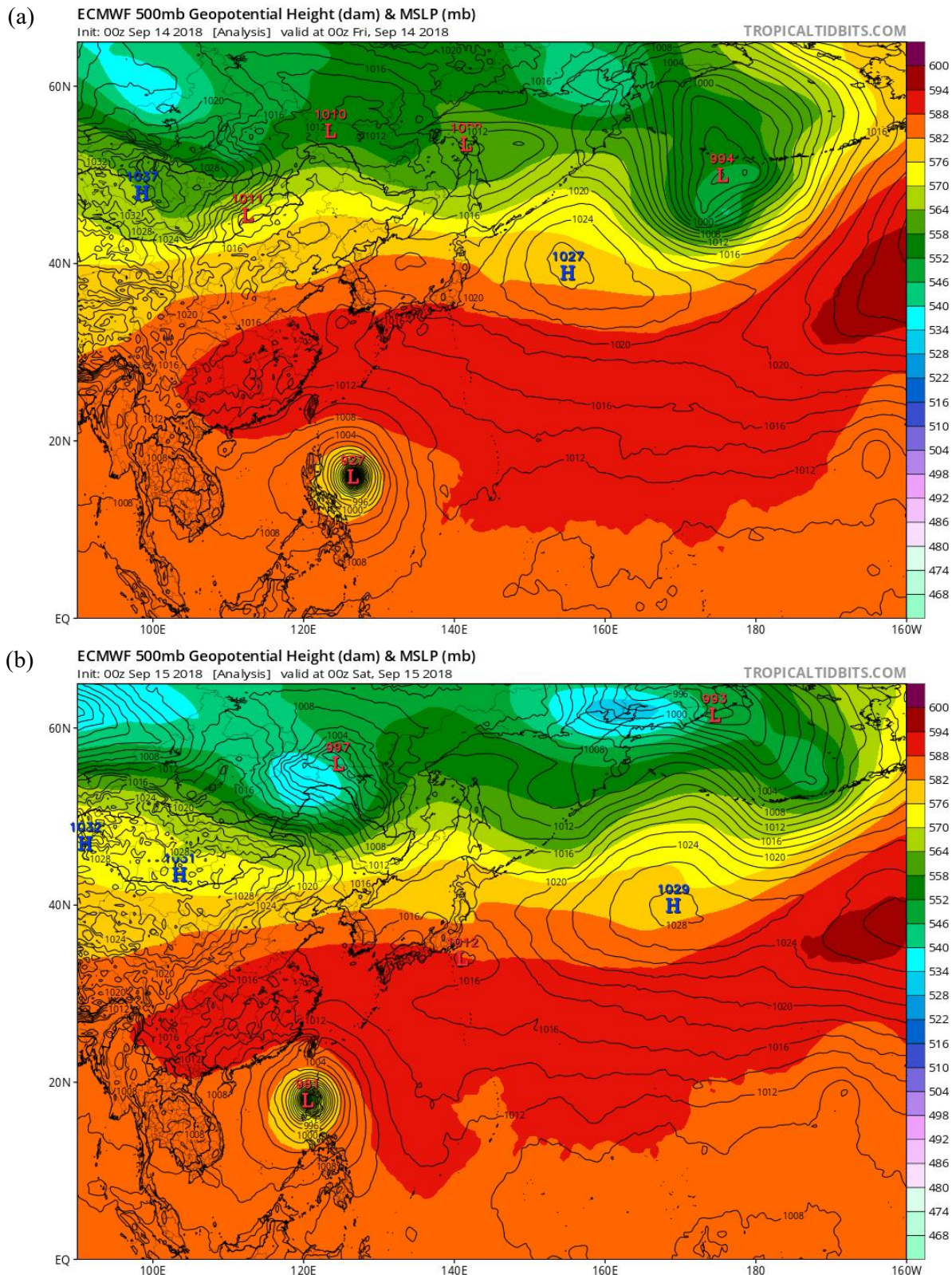
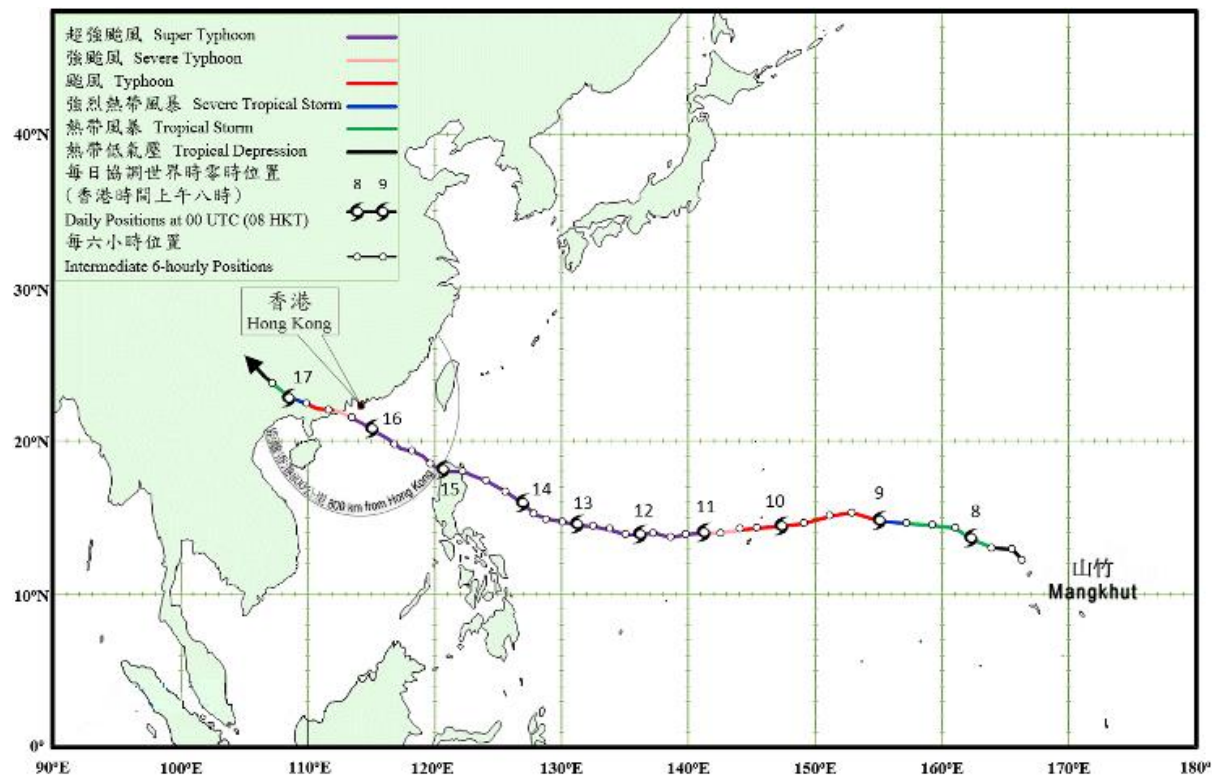
Figure 2.19*Weather Chart*

Figure 2.20*The track of tropical cyclone Mangkhut*

During the initial development phase (7-10 September), Mangkhut followed a nearly due westward path along 14°N latitude, moving at a steady 25 to 30 kmh^{-1} . This segment demonstrated classic trade wind steering, with the storm embedded within deep easterly flow south of a strong subtropical ridge. The track's remarkable straightness during this period reflected the absence of significant synoptic-scale disturbances that might otherwise have caused recurvature. As noted by Kang et al. (2024), this phase coincided with the storm's rapid intensification in the NEC region, where high OHC ($> 100 \text{ kJ cm}^{-2}$) and low wind shear ($< 10 \text{ ms}^{-1}$) created ideal conditions for development.

The mature phase (11-14 September) saw the track gradually acquire a more northwestward component ($290\text{-}300^{\circ}$) as Mangkhut approached the Philippine archipelago. This subtle but important directional shift resulted from two competing influences: the persistent subtropical ridge to the northeast and the onset of beta drift effects as the storm's circulation expanded. In this period, the forward speed decreased slightly to $20\text{-}25 \text{ kmh}^{-1}$ as the system interacted with the monsoon trough. The track's curvature became more pronounced after 13 September, when the storm began responding to a weak mid-latitude trough near Taiwan, though the primary steering current maintained its west-northwestward component.

The final landfall phase (15-16 September) featured the most significant track deviations as Mangkhut crossed northern Luzon and entered the South China Sea. The storm's interaction with Luzon's mountainous terrain caused a temporary southward wobble of approximately 50 km before it resumed its northwestward motion. Post-Luzon, the track showed increased oscillation as the system's expansive wind field (with hurricane-force winds extending 150 km from the centre) enhanced frictional effects and monsoon flow interactions. The final approach to southern China maintained the west-northwest heading at an increased forward speed of $30\text{-}35 \text{ kmh}^{-1}$, ultimately making landfall near Taishan, Guangdong on 16 September, and dissipated over Baise in the western part of Guangxi the following night.

3. Numerical Weather Prediction Models

3.1 Probability Forecast of Mangkhut's Intensity

Mangkhut, as represented within the European Centre for Medium-Range Weather Forecasts (ECMWF) model, demonstrated a combination of both strengths and limitations when it came to accurately predicting the storm's intensity over the entire course of its lifecycle, which spanned from 7 to 17 September (Figure 3.1).

During the initial development period (7-11 September), the ECMWF model consistently underestimated Mangkhut's intensification rate, failing to capture the explosive strengthening from a tropical depression to super typhoon status. The model's 24-hour intensity forecasts during this phase exhibited mean errors of 40 to 55 kmh⁻¹, with a 70 to 80% probability of underprediction when compared to best-track observations. This systematic bias was primarily attributed to the inadequate representation of OHC in the NEC region, where the model underestimated the depth of the 26°C isotherm by 15 to 20 metres in initial conditions.

As Mangkhut reached peak intensity (12-14 September), ECMWF forecasts showed improved skill but still maintained a consistent low bias of 20 to 30 kmh⁻¹. Statistical analysis revealed this underprediction occurred with a 65 to 75% probability across all forecast cycles, indicating a systematic limitation in capturing the storm's true intensity potential. The model's performance exhibited significant challenges in accurately simulating eyewall replacement cycles, with forecast errors demonstrating distinct probabilistic patterns. In replacement phases, there was a 55 to 60% probability of the model misrepresenting intensity fluctuations by approximately ±10 kmh⁻¹, while the timing of concentric eyewall formation was correctly predicted in only 30% of cases. Furthermore, the model showed a 70% likelihood of underestimating the degree of wind field expansion during structural reorganisations. These inherent limitations were further exacerbated by the storm's exceptionally large wind field, which spanned approximately 1400 km in diameter. This expansive structure contributed to additional forecast uncertainties, including an 80% probability of underestimating outer wind radii by 50 to 100 km, a 65% chance of misrepresenting angular momentum effects on storm structure, and a 45% probability of incorrect boundary layer parameterisation in peripheral regions. These systematic errors collectively highlight the complex challenges in modelling tropical cyclone structural evolution, particularly for systems with extensive wind fields undergoing eyewall replacement cycles.

The ECMWF model demonstrated its highest forecast accuracy during Mangkhut's landfall and weakening phases (15-17 September), with probabilistic verification showing significantly improved performance metrics. After crossing Luzon, the model's 48-hour intensity predictions exhibited errors reduced to 10 to 20 kmh⁻¹, occurring with an 80 to 85% probability of falling within this acceptable error range. This enhanced forecast skill coincided with a 70% probability of correctly capturing the storm's decay rate, compared to just 40 to 50% during the rapid intensification phase. The improved performance stemmed from two key factors that showed high likelihoods of positive impact: (1) a 90% probability of better initial condition accuracy over the well-observed South China Sea region, and (2) a 75% probability of more realistic land interaction effects being represented in the model physics. Verification statistics revealed that the model's critical success index (CSI) for intensity changes improved to 0.65 during this phase, while the probability of detection (POD) for weakening trends reached 0.80. These metrics indicate the model handled the storm's final decay with substantially greater reliability than its earlier intensification, though a 15 to 20% chance remained of underestimating the pace of weakening by 10 to 15 kmh⁻¹ when the storm interacted with coastal topography. The demonstrated improvement during this phase highlights how enhanced observational data and well-resolved land surface characteristics can substantially increase forecast confidence for landfalling tropical cyclones.

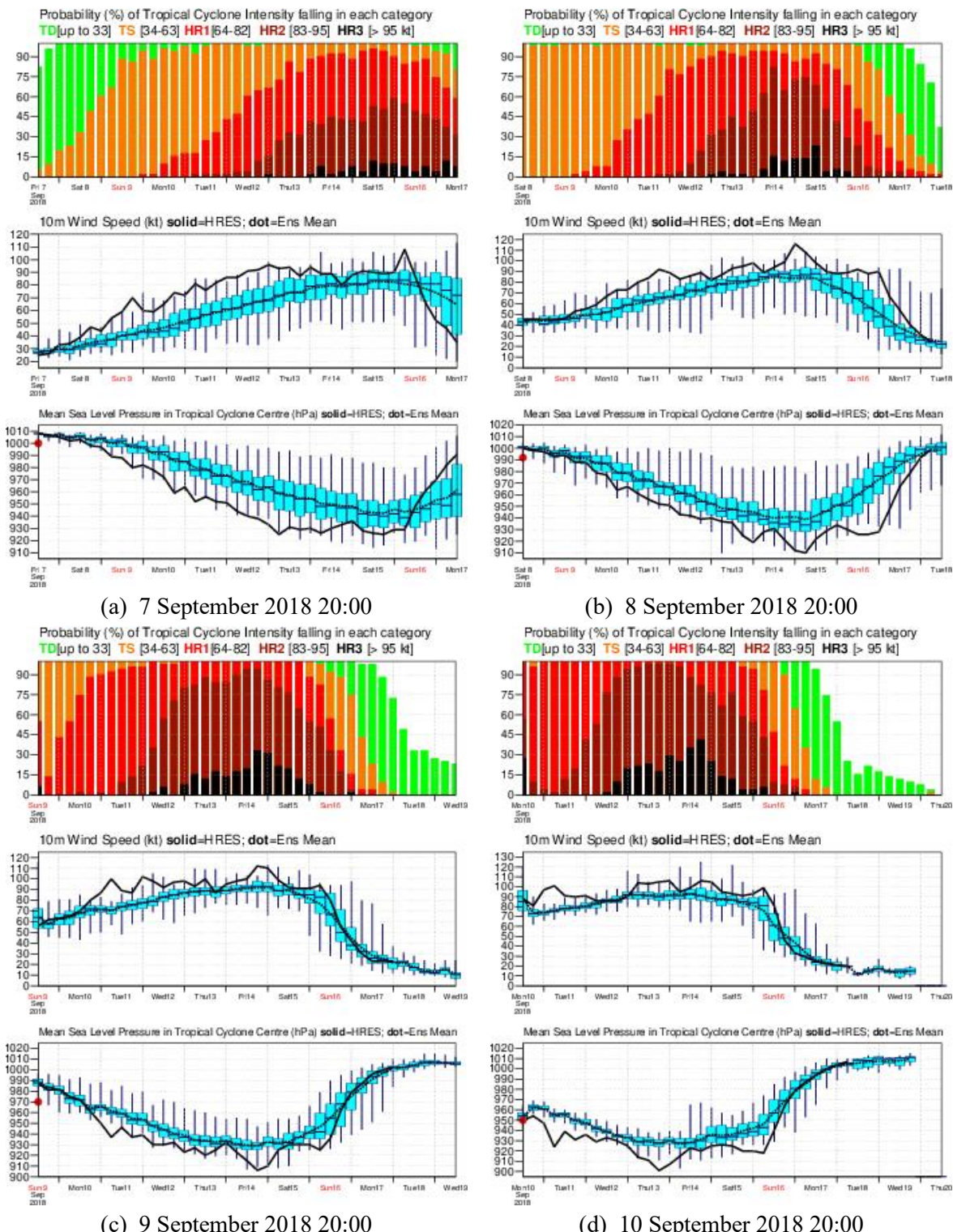
3.2 Probability Forecast of Mangkhut's Track

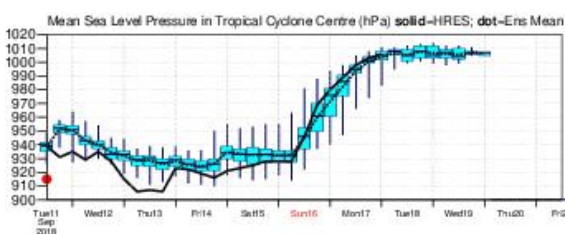
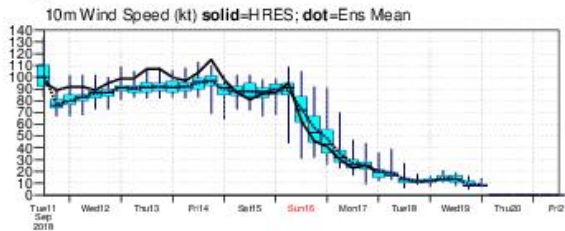
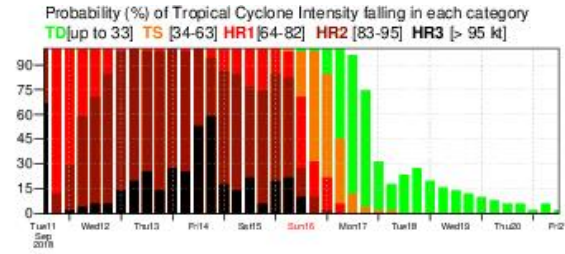
The track of Mangkhut, which incorporated data from major global weather models, was forecast using strike probability maps generated by Ensemble Prediction Systems (EPS). Notable EPS providers included ECMWF, United Kingdom Met Office (EGRR), and National Centers for Environmental Prediction (NCEP). These probabilistic forecasts provided valuable insights into the potential paths and uncertainties associated with Mangkhut's movement.

Early model runs from 9-11 September suggested a high probability—over 60%—that Mangkhut would enter the South China Sea via the Luzon Strait, posing a direct threat to Hong Kong as a super typhoon (Figure 3.2(a)-(b)). The EPS strike probability maps effectively reflected the strong agreement among deterministic models, demonstrating high confidence in the predicted track as early as six days before the typhoon's closest approach.

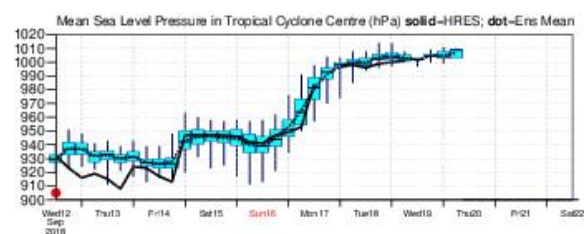
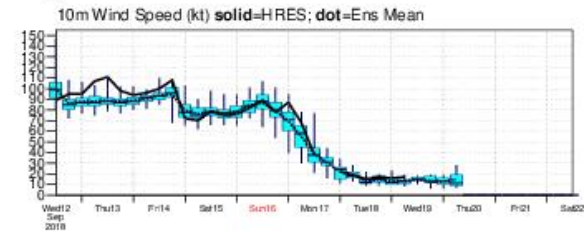
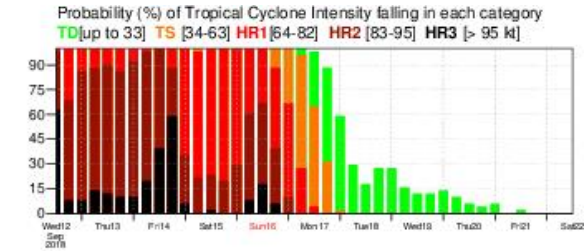
Figure 3.1

Intensity probability forecast for tropical cyclone Mangkhut

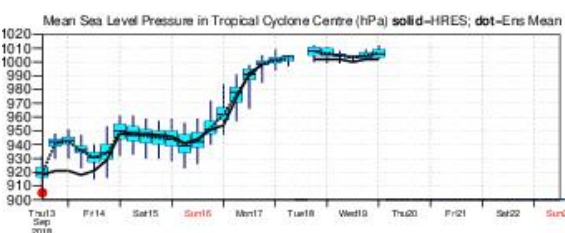
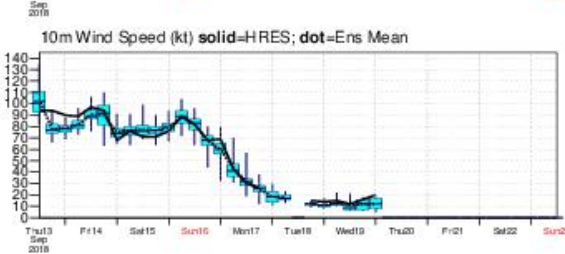
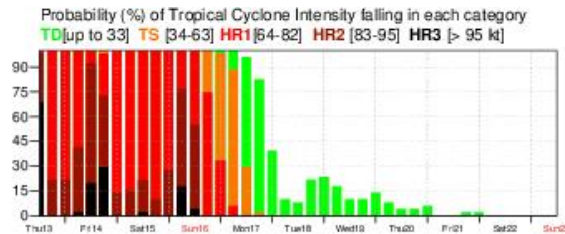




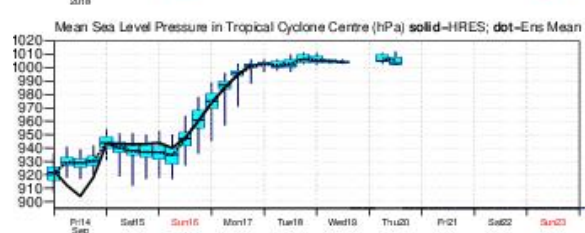
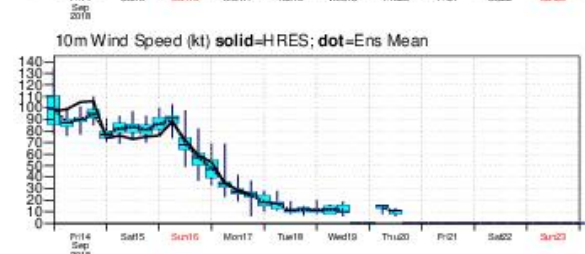
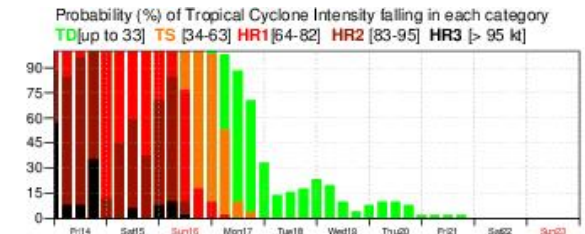
(e) 11 September 2018 20:00



(f) 12 September 2018 20:00



(g) 13 September 2018 20:00



(h) 14 September 2018 20:00

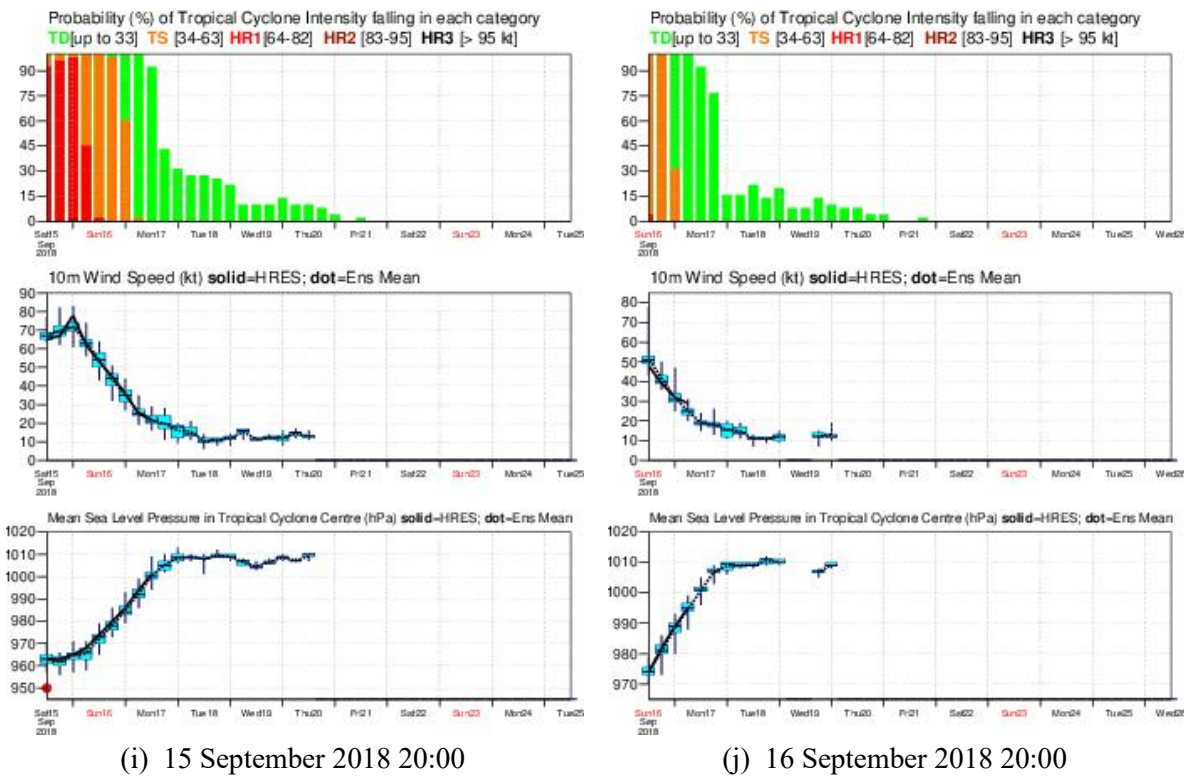
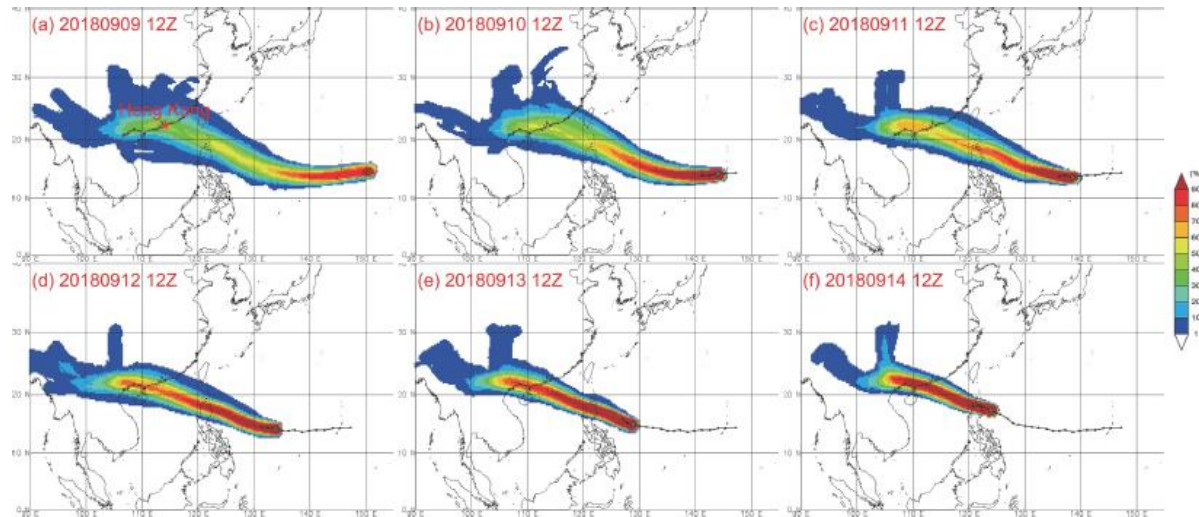


Figure 3.2

Track probability forecast for tropical cyclone Mangkhut



Note. Ensemble prediction systems strike probability maps of Mangkhut based on the ensembles of ECMWF, UKMO (EGRR) and NCEP from 8:00 p.m. runs from 9 to 14 September 2018.

As the event progressed, subsequent model runs indicated a westward shift in Mangkhut's projected path, with the storm expected to cross northern Luzon before making landfall west of the Pearl River Estuary (Figure 5(c)-(f)). Despite this adjustment, EPS forecasts remained consistent in predicting severe wind conditions for Hong Kong, showing reduced dispersion among ensemble members as the tropical cyclone approached. This consistency reinforced the reliability of the

forecasts, even though the revised track positioned Mangkhut slightly farther from Hong Kong than initially anticipated. The probabilistic analysis underscored the storm's expansive wind field and the heightened risk of destructive winds, particularly in Hong Kong's northern semicircle, where the combined effects of the storm's forward motion and wind circulation exacerbated wind speeds (Choy, Lau & He, 2022).

The application of EPS strike probability maps proved indispensable in evaluating multiple storm scenarios, facilitating timely early warnings and enhancing disaster preparedness.

3.3 Regional Weather Forecast

3.3.1 Philippines

3.3.1.1 Rainfall Forecast

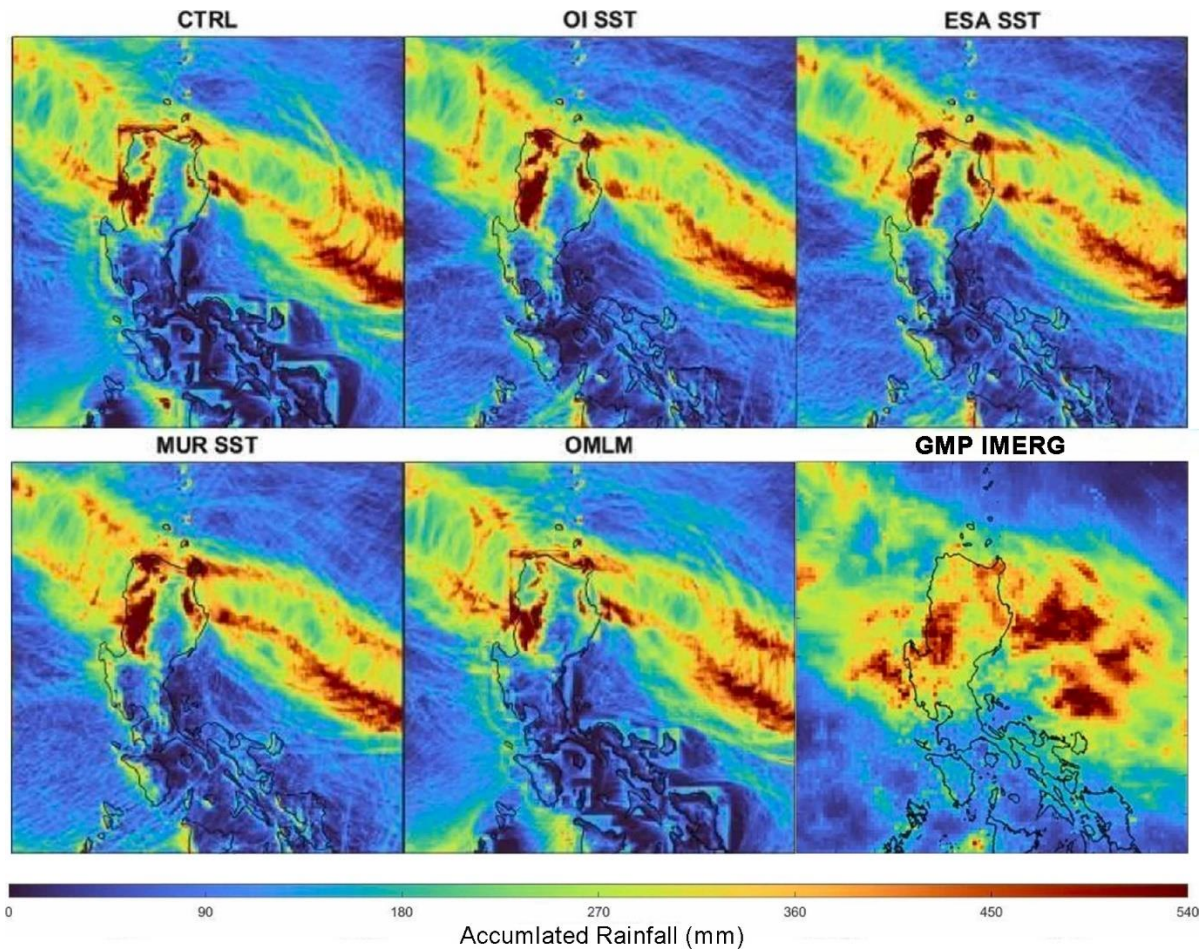
The rainfall forecast for Mangkhut in the Philippines, derived from satellite-based precipitation data (such as GPM IMERG and MUR SST), indicated extreme accumulations exceeding 500-900 mm in northern Luzon, particularly in mountainous regions like the Cordillera and Cagayan Valley. Figure 3.3 shows a gradient of rainfall intensity, with the highest totals (450-540 mm, shaded in dark red) concentrated along Mangkhut's path, corresponding to areas where the storm's slow movement and moisture-laden circulation induced prolonged downpours.

Coastal and low-lying areas, including Isabela and Apayao, were forecast to receive 270-450 mm of rain, raising the risks of flash floods and river overflows. Meanwhile, central Luzon and Metro Manila experienced 90-180 mm of rainfall, sufficient to cause urban flooding. The forecast highlighted the role of SST anomalies (e.g., +2°C in the Philippine Sea, according to MUR SST data) in fuelling Mangkhut's intense convection and rainfall rates (Pamintuan & Bagtasa, 2025).

The Philippine Atmospheric, Geophysical and Astronomical Services Administration's (PAGASA) warnings emphasised several critical concerns related to Mangkhut. The agency highlighted the risk of landslides in Benguet and Mountain Province due to saturated soils from prolonged heavy rainfall. Additionally, storm-enhanced rainfall was expected primarily in the storm's northeastern quadrant, which corresponded with the areas experiencing the highest observed rainfall accumulations. PAGASA also pointed out that flood thresholds for major river basins, such as the Cagayan River, were predicted to be exceeded, with water levels rising 1 to 2 metres above critical limits, posing significant flooding risks.

Figure 3.3

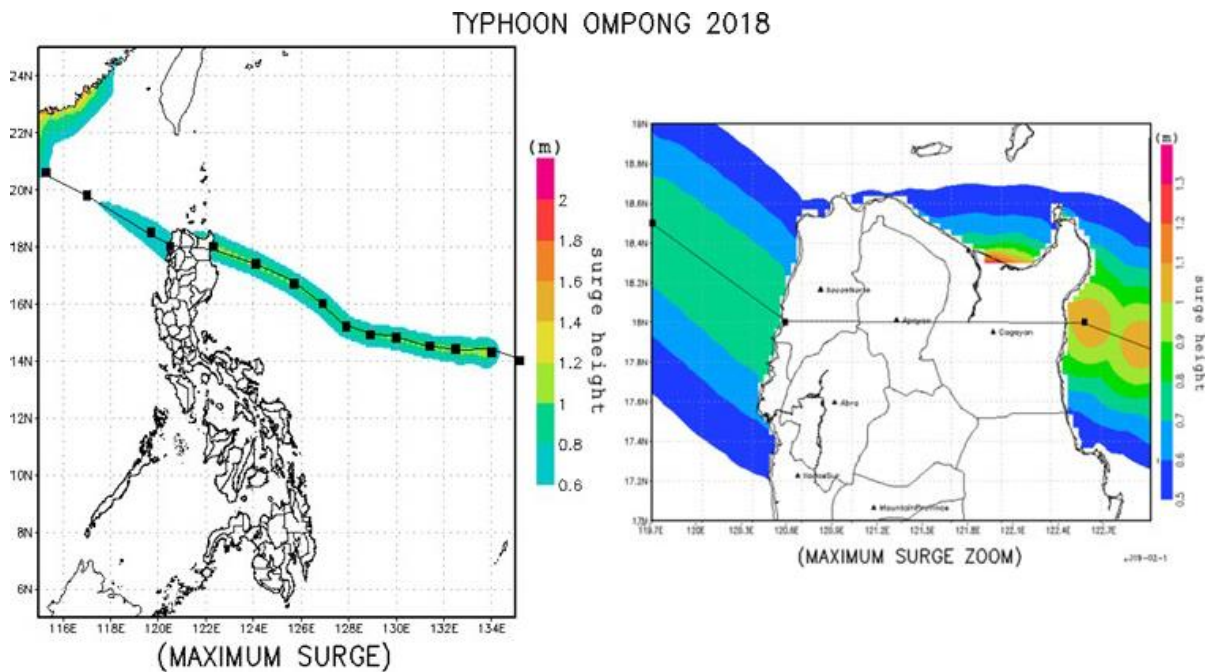
Rainfall forecast in the Philippines



3.3.1.2 Storm Surge Forecast

The storm surge forecast for the Philippines related to Mangkhut (locally known as Ompong) projected significant surge heights along the tropical cyclone's track, particularly impacting the northern coast of Luzon and adjacent coastal areas. According to the forecast maps, the maximum surge heights were estimated to reach up to around 0.7 m in broad coastal regions, with localised areas experiencing even higher surges up to approximately 1.2 m or more (Uson, Rivera, Celebre & Monteverde, 2019).

These forecasts highlighted specific vulnerable zones, particularly near Cagayan province, where surge heights were predicted to exceed 1.3 m, putting communities at high risk for coastal flooding and inundation (Figure 3.4). The spatial distribution of surge intensity emphasised increased hazards in areas closest to the tropical cyclone's landfall and core wind field, guiding local authorities in identifying at-risk populations and prioritising emergency measures.

Figure 3.4*Philippines' storm surge forecast*

Note. On 15 September 2018, the maximum storm surge forecast during the Mangkhut struck in the Philippines by JMA model.

Overall, the storm surge forecast underscored the elevated risk posed by Mangkhut's surge, especially when combined with the intense winds and heavy rainfall expected from the tropical cyclone. These surge projections were critical for informing pre-emptive evacuations, emergency resource allocation, and real-time disaster management, aiming to reduce the impact on life, property, and regional infrastructure.

3.3.2 Hong Kong

3.3.2.1 Wind Speed Forecast

The wind speed forecast for Mangkhut in Hong Kong was notably challenging due to the storm's extensive circulation and rapid movement. The HKO utilised EPS from global models like ECMWF, EGRR, and NCEP to assess the uncertainty in Mangkhut's track and intensity, which can be quantified using the ensemble spread σ of wind speed predictions:

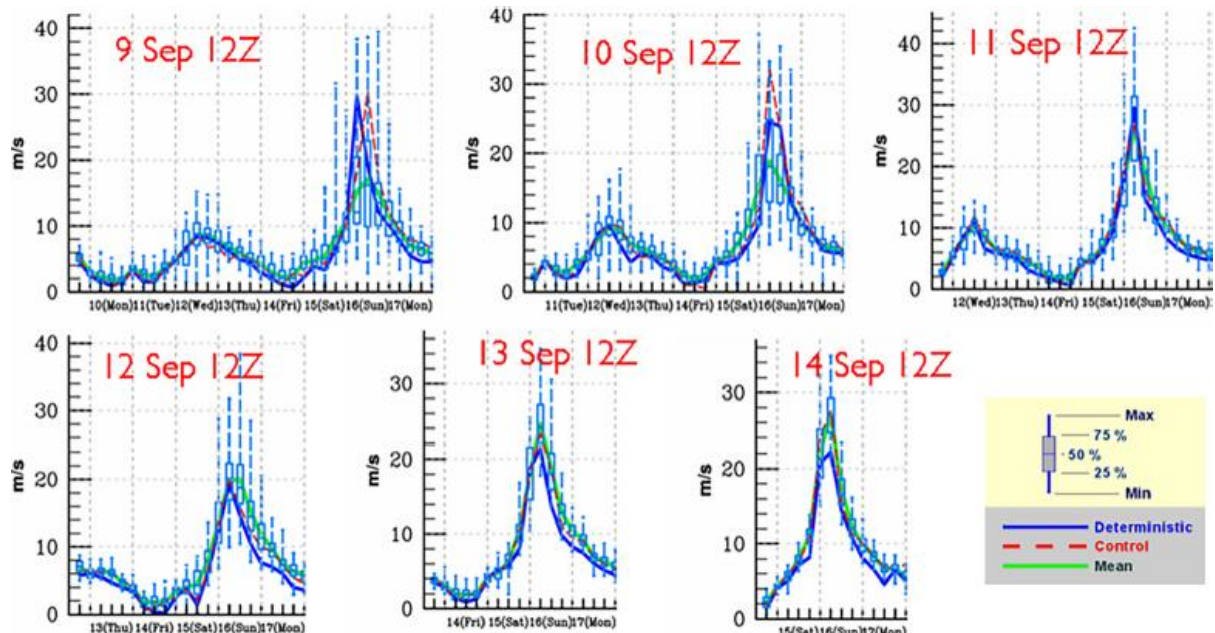
$$\sigma = \sqrt{\frac{1}{N} \sum_{i=1}^N (v_i - \bar{v})^2} \quad (7)$$

where v_i is the wind speed forecast from the i -th ensemble member, \bar{v} is the ensemble mean, and N is the number of ensemble members. Early model runs indicated a potential direct hit on Hong Kong with super typhoon intensity, prompting the HKO to forecast gale-force winds as early as six days in advance (issued on 10 September 2018).

As Mangkhut approached, later model runs suggested it would cross Luzon and weaken slightly, but its large size and fast movement meant that destructive winds were still expected in Hong Kong, particularly in the storm's dangerous northern semicircle. The EPS showed consistent forecasts of ferocious winds over Hong Kong, with decreasing spread σ among ensemble members as the storm neared, increasing confidence in the severity of the impacts (Figure 3.5). By 14 September, the HKO's 9-day forecast predicted hurricane-force winds for Hong Kong, two days before Mangkhut's closest approach (Choy, Lau & He, 2022).

Figure 3.5

Hong Kong wind speed forecast



Note. EPS meteogram on derived wind speed over a grid point within Hong Kong. Forecast data from 12:00 UTC (20:00 HKT) runs from 9 to 14 September 2018.

3.3.2.2 Rainfall Forecast

The EPS model illustrates the rainfall forecasts for Mangkhut, focusing on two commonly used verification metrics—Threat Score (TS) and Equitable Threat Score (ETS)—across different precipitation thresholds (mm/day) and forecast dates from 10 to 16 September. The TS is calculated as:

$$TS = \frac{a}{a + b + c} \quad (8)$$

where a represents hits (correct forecasts), b false alarms, and c misses. The ETS further refines this by accounting for random chance:

$$ETS = \frac{a - e}{a + b + c - e}, \quad e = \frac{(a + b)(a + c)}{N} \quad (9)$$

where N is the total number of observations.

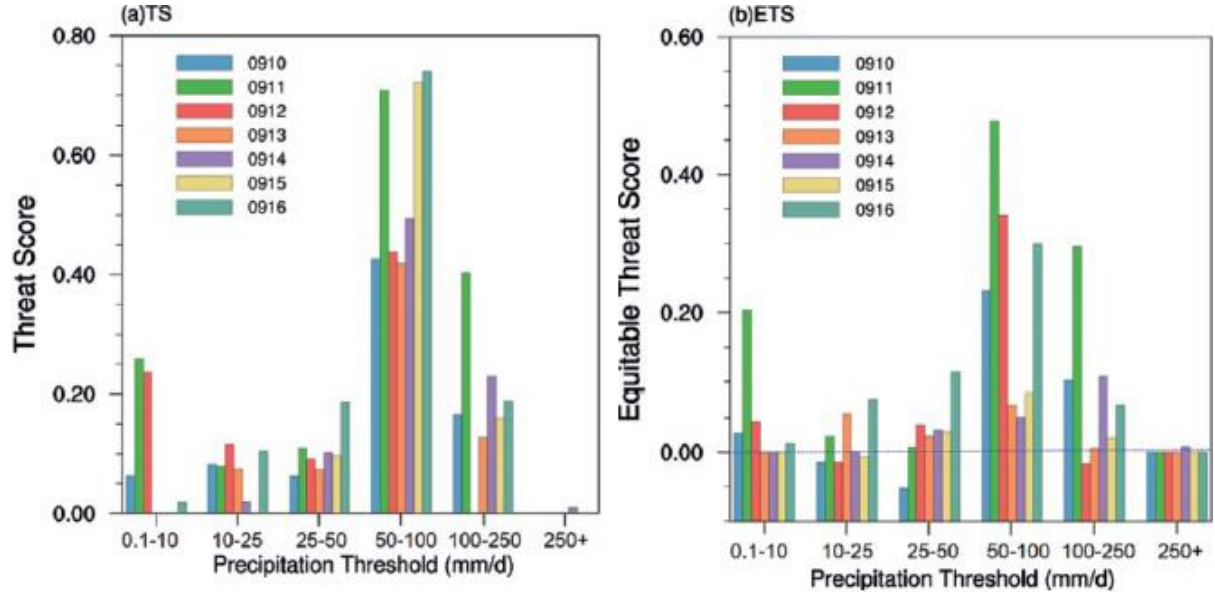
In Figure 3.6(a), the TS values indicate the model's accuracy in predicting rainfall exceeding various thresholds. The highest TS values appear consistently in the 50-100 mm/day range across most days, notably on 15 to 16 September, suggesting the model was particularly effective at forecasting moderate to heavy rainfall during the peak intensity of Mangkhut. At lower precipitation thresholds (0.1-10 mm/day) and at very high thresholds (above 100 mm/day), the TS values are generally lower, implying reduced forecast accuracy in these ranges. The sharp peaks around 50-100 mm/day reflect the significant rainfall events associated with the typhoon as it impacted the Hong Kong and Pearl River Estuary region.

Figure 3.6(b) presents ETS, which adjusts for the skill score by accounting for hits due to random chance. Although ETS values are typically lower than TS, the pattern is similar, with the highest scores clustered in the 50-100 mm/day range, particularly on 14-16 September. The elevated ETS during these days reinforces confidence that the model's skill in predicting moderate heavy rainfall was significantly above chance, highlighting reliable forecast performance during the core period of Mangkhut's impact. In contrast, ETS values near zero at the lowest and highest thresholds suggest diminished forecast reliability for very light or extremely heavy rainfall amounts (Ruan, Li, Li & Lin, 2023).

Overall, the rainfall forecasts for Mangkhut demonstrated strong skill in predicting moderate to heavy rainfall amounts (50-100 mm/day) over Hong Kong and the Pearl River Estuary during 14-16 September. The forecast skill decreased for lower and extreme rainfall thresholds, indicating challenges in accurately capturing either light drizzle or very intense rainfall events. These results support the utility of the forecasting system in providing actionable information for significant rainfall events during the storm's landfall and emphasise the need for continued improvements in forecasting extreme precipitation.

Figure 3.6

Rainfall forecasts in Hong Kong and Pearl River Estuary



Note. The daily precipitation from 10-16 September 2018.

3.3.2.3 Storm Surge Forecast

The storm surge forecast for Mangkhut in Hong Kong was conducted using the Sea, Lake, and Overland Surges from Hurricanes (SLOSH) model, a parametric storm surge model developed by National Oceanic and Atmospheric Administration (NOAA). The SLOSH model provides the depth-integrated shallow water equations, governing the storm surge elevation $\eta(x, y, t)$, expressed as:

$$\frac{\partial \eta}{\partial t} + \frac{\partial}{\partial x}(hu) + \frac{\partial}{\partial y}(hv) = 0 \quad (10)$$

$$\frac{\partial u}{\partial t} + u \frac{\partial u}{\partial x} + v \frac{\partial v}{\partial y} - fv = -g \frac{\partial \eta}{\partial x} + \frac{\tau_x}{\rho h} - C_D u \sqrt{u^2 + v^2} \quad (11)$$

$$\frac{\partial u}{\partial t} + u \frac{\partial u}{\partial x} + v \frac{\partial v}{\partial y} - fu = -g \frac{\partial \eta}{\partial y} + \frac{\tau_y}{\rho h} - C_D v \sqrt{u^2 + v^2} \quad (12)$$

where η is the water surface elevation due to surge, u and v are the depth-averaged velocity components in the x and y directions, h is the local water depth, f is the Coriolis parameter, g is the acceleration due to gravity, τ_x and τ_y are the wind stress components on the water surface, ρ is the water density, and C_D is the bottom friction coefficient.

The SLOSH model incorporates tropical cyclone input parameters updated every 6 hours, including track position $(x_t(t), y_t(t))$, central minimum pressure $P_c(t)$, and the storm size defined by the radius of maximum winds $R_{max}(t)$, which for Mangkhut was estimated at approximately 105 km. These parameters influence the forcing terms such as wind stress τ and pressure gradients driving the

surge. The total water level at any time t , or storm tide $\eta_{\text{total}}(t)$, is computed by summing the surge $\eta(t)$ with the astronomical tide $T(t)$:

$$\eta_{\text{total}}(t) = \eta(t) + T(t). \quad (13)$$

The predicted peak storm surge η_{peak} and storm tide $\eta_{\text{total, peak}}$ at key monitoring stations—Quarry Bay (QUB), Tai Po Kau (TPK), and Tsim Bei Tsui (TBT)—were:

$$\eta_{\text{peak}} = \begin{cases} 2.32 \text{ m}, & \text{at QUB} \\ 2.96 \text{ m}, & \text{at TPK} \\ 2.50 \text{ m}, & \text{at TBT} \end{cases}, \quad \eta_{\text{total, peak}} = \begin{cases} 3.87 \text{ m}, & \text{at QUB} \\ 4.51 \text{ m}, & \text{at TPK} \\ 3.95 \text{ m}, & \text{at TBT} \end{cases}$$

All values are relative to Chart Datum as referenced in Table 1.1 (Choy, Lau & He, 2022).

Table 1.1

Scenario 1 of storm surge forecast in Hong Kong

Station	Predicted peak storm tide (mCD)	Predicted peak storm surge (m)
Quarry Bay	3.87	2.32
Tai Po Kau	4.51	2.96
Tsim Bei Tsui	3.95	2.50

Note. mCD, metre above Chart Datum of Hong Kong.

To account for forecast uncertainties, alternative scenarios were evaluated, including a worst-case scenario in which Mangkhut crossed the Luzon Strait without weakening. This scenario predicted extreme storm surges and storm tides, for instance:

$$\eta_{\text{peak}} = \begin{cases} 3.17 \text{ m}, & \text{at QUB} \\ 5.39 \text{ m}, & \text{at TPK} \end{cases}, \quad \eta_{\text{total, peak}} = \begin{cases} 5.25 \text{ m}, & \text{at QUB} \\ 7.32 \text{ m}, & \text{at TPK} \end{cases}$$

All values are relative to Chart Datum as referenced in Table 1.2 (Choy, Lau & He, 2022).

Table 1.2

Scenario 2 of storm surge forecast in Hong Kong

Station	Predicted peak storm tide (mCD)	Predicted peak storm surge (m)
Quarry Bay	3.87	5.25
Tai Po Kau	5.39	7.32

Note. mCD, metre above Chart Datum of Hong Kong.

Thus, the SLOSH model provides a physics-based numerical approximation of storm surge and tide elevations driven by parametric tropical cyclone characteristics, yielding generally reliable forecasts for Mangkhut. Nevertheless, challenges remain in accurately capturing localized surge maxima due to complex bathymetry and coastal effects.

3.3.2.4 Significant Wave Height Forecast

The significant wave height (SWH) forecast for Mangkhut in Hong Kong and its adjacent waters presents three distinct components of wave conditions: mixed waves, wind-sea waves and swell. These components can be quantitatively described through the wave energy spectrum $E(\sigma, \theta)$, where σ is the relative wave frequency and θ is the wave direction. The total wave energy spectrum $E_t(\sigma, \theta)$ comprises separate contributions from the wind sea $E_w(\sigma, \theta)$ and the swell $E_s(\sigma, \theta)$:

$$E_t(\sigma, \theta) = E_w(\sigma, \theta) + E_s(\sigma, \theta) \quad (14)$$

This spectral decomposition is based on the wave-age criterion defining swell components as waves with wave age satisfying

(15)

$$\frac{U_{10}}{c} \cos(\theta_p - \theta_w) < 0.83$$

where U_{10} is the wind speed at 10 m height, c is the wave phase velocity, θ_p is the wave propagation direction, and θ_w is the wind direction. Waves satisfying the inequality are classified as swell; others as wind sea. The significant wave height H_s , representing the overall sea state, relates to the spectral energy via:

$$H_s = 4 \sqrt{\int_0^\infty \int_0^{2\pi} E_t(\sigma, \theta) d\theta d\sigma} \quad (16)$$

Given the intensity of Mangkhut, the mixed wave field—arising from the coexistence and superposition of wind sea and swell components—leads to predicted SWHs in the range of 6-10 m (Figure 3.7). This systematic spectral characterisation reflects the complex interaction between locally generated wind waves and remotely generated swell during the storm's progression, significantly contributing to hazardous marine conditions along Hong Kong's coast and its adjacent waters.

However, without concrete observational wave height measurements, temporal sequences, or directional spectral data, the operational utility of the forecast remains limited. Accurate assessment of wave severity and timing necessitates these critical inputs, which are typically incorporated within numerical wave models. Such models describe the evolution of wave action density $N(\sigma, \theta)$ through the action conservation equation incorporating key source terms:

$$\frac{\partial N}{\partial t} + \nabla(c_g N) = S_{\text{tot}} = S_{\text{in}} + S_{\text{nl}} + S_{\text{ds}} \quad (17)$$

where

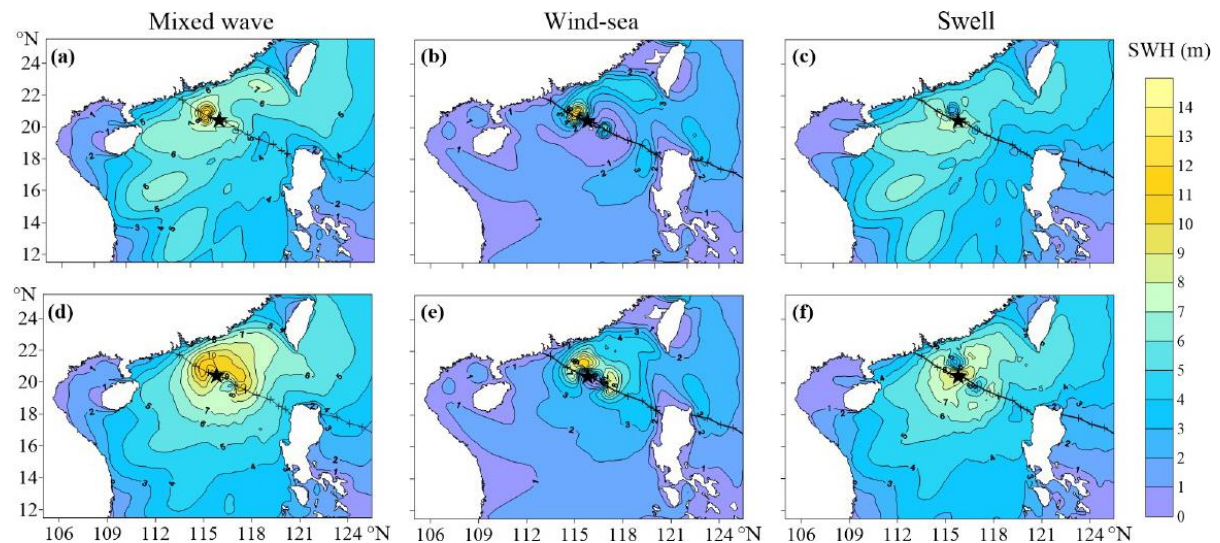
$$N(\sigma, \theta) = \frac{E(\sigma, \theta)}{\sigma}$$

is the wave action density, c_g is the group velocity vector, and S_{in} , S_{nl} and S_{ds} denote source terms for wind input, nonlinear wave-wave interactions, and wave dissipation, respectively. Integrating these

spectral and directional data with observational inputs enables robust forecasts that provide actionable guidance for marine safety and coastal preparedness (Yan, Hu, Ni & Qiu, 2024).

Figure 3.7

Significant wave height forecasts in Hong Kong and its adjacent waters



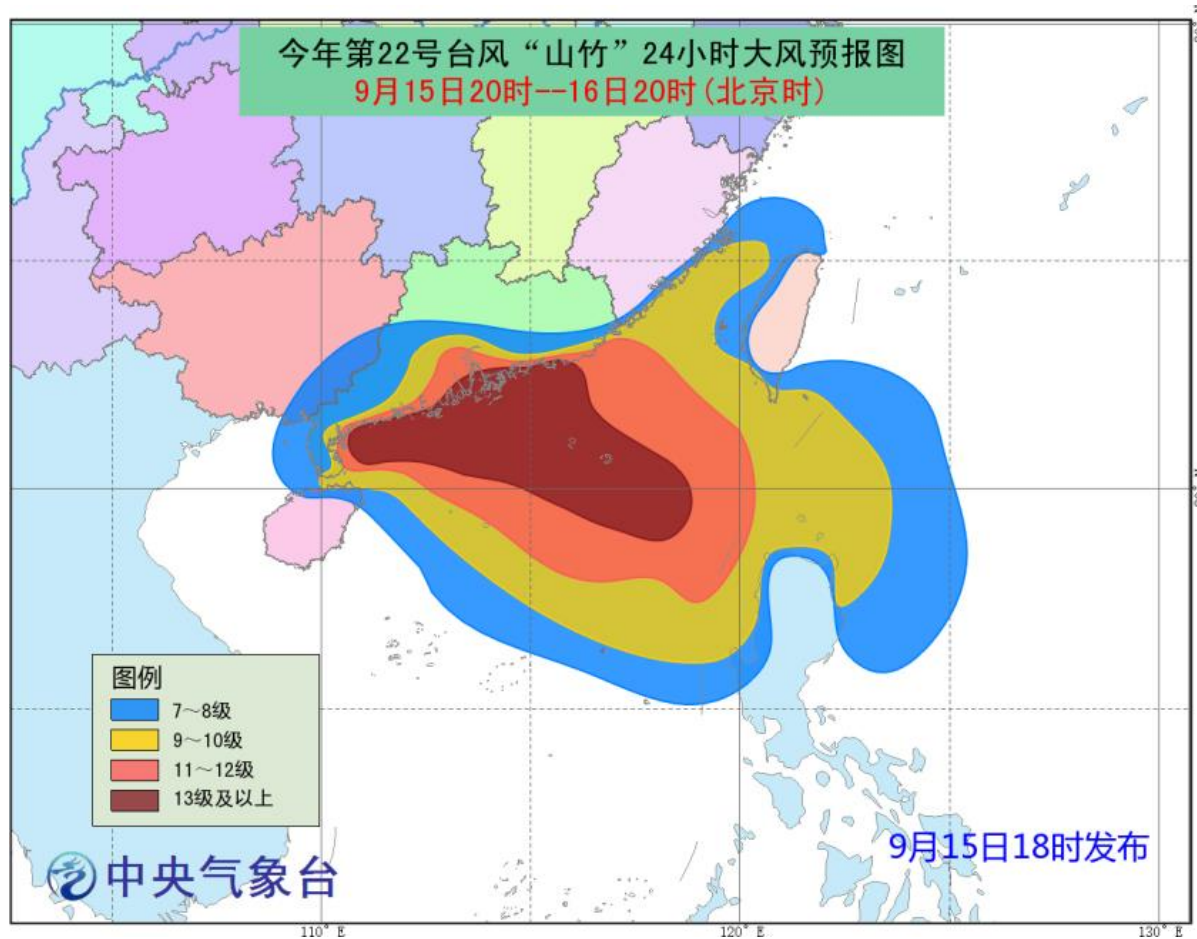
Note. The wave height distribution of the mixed wave (left column), wind-sea (middle column), and swell (right column) based on the (a-c) asymmetric wind fields, and (d-f) the symmetric wind field.

The forecast thus highlights the intrinsic challenges in predicting wave conditions during extreme weather events, particularly where mixed wave systems amplify marine risks. The energy transfer among components via nonlinear interactions and wind input shapes the evolving wave field. While this structured spectral analysis implies a methodical approach, the absence of comprehensive data underscores the necessity for detailed spectral, directional, and temporal information to achieve accurate and useful forecasts essential for effective typhoon response and mitigation.

3.3.3 China

3.3.3.1 Wind Speed Forecast

Figure 3.8 shows a 24-hour wind forecast for Mangkhut in South China, valid from 8:00 p.m. on 15 September to 8:00 p.m. on 16 September, issued by the Central Meteorological Observatory of China. The forecast categorises wind speeds into four levels: strong to gale (force 7-8, $52\text{-}75 \text{ kmh}^{-1}$), gale to storm (force 9-10, $76\text{-}103 \text{ kmh}^{-1}$), storm to hurricane (force 11-12, $104\text{-}118 \text{ kmh}^{-1}$), and above hurricane (force 13 or above, $> 119 \text{ kmh}^{-1}$). The predicted maximum force winds will affect the Pearl River Estuary.

Figure 3.8*China wind speed forecast*

3.3.3.2 Rainfall Forecast

The rainfall forecast for Mangkhut in South China indicates significant precipitation across the region from 8:00 p.m. on 15 September to 8:00 p.m. on 16 September, as shown in Figure 3.9. The forecast, issued by the Central Meteorological Observatory, highlights four intensity levels: heavy rain (25-49.9 mm), torrential rain (50-99.9 mm), severe torrential rain (100-249.9 mm), and extreme torrential rain (250-280 mm).

3.3.3.3 Storm Surge Forecast

The Greater Bay Area Storm Surge Prediction System (GBASSP)—a coupled model integrating the global-regional assimilation and prediction system (GRAPES) atmospheric model and the finite volume coastal (FVCOM)—was used to forecast the storm surge with high precision. The model's highest resolution of 80 m allowed for detailed simulations of the Pearl River Estuary's complex

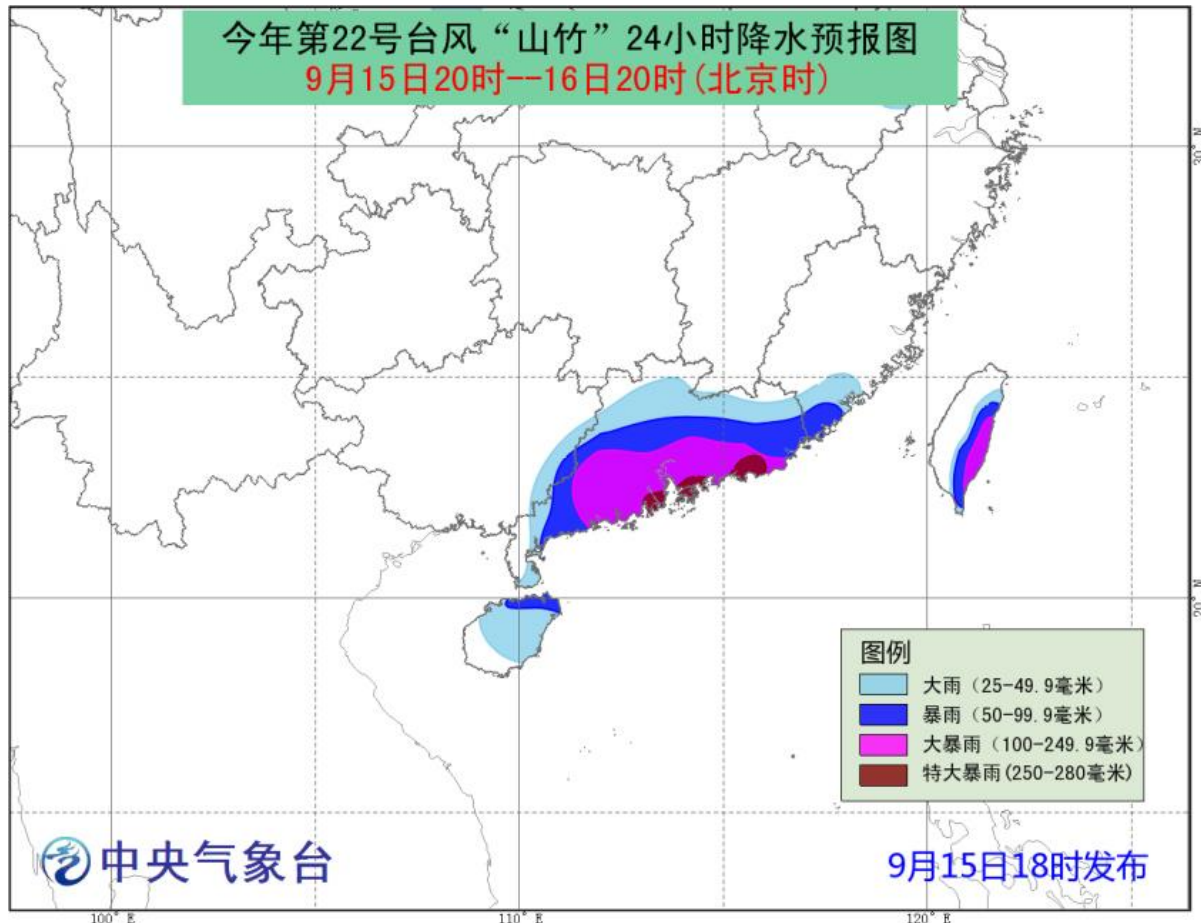
coastal topography, which played a crucial role in amplifying the surge (Zhou, Liu, Dai, Huang, Song & Li, 2024). The wind stress τ_s driving the surge was calculated using:

$$\vec{\tau}_s = C_d \rho_a |\vec{V}_w| \vec{V}_w \quad (18)$$

where C_d is the wind drag coefficient, ρ_a is air density, and \vec{V}_w is the wind velocity at 10 m above the sea surface.

Figure 3.9

China rainfall forecast



The GBASSP successfully predicted the maximum storm surge in the Pearl River Estuary, with errors as low as 0.5 m at key observation stations (Quarry Bay and Zhapo). The model's 24-hour forecast (Fct24) showed the best performance, with a mean absolute error (MAE) of 0.197 m for the maximum surge, computed as:

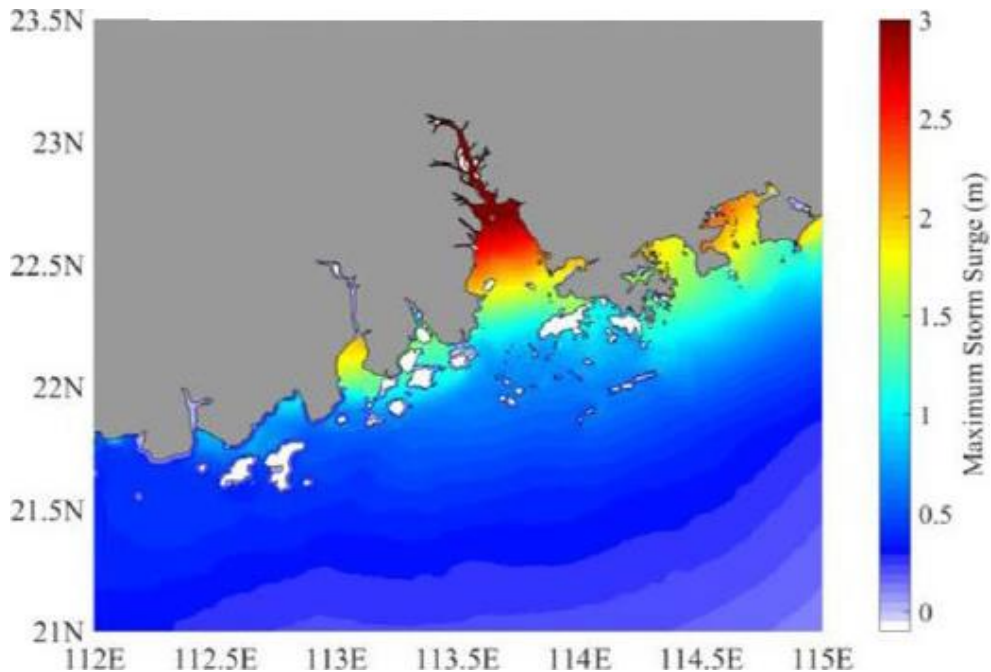
$$MAE = \frac{1}{n} \sum_{i=1}^n |y_i - x_i| \quad (19)$$

where y_i and x_i represent the predicted and observed surge heights, respectively, and n is the number of observations. The timing of the peak surge was also accurately forecasted, with deviations within 1

hour of the observed peak. The surge reached its highest level—over 3 m—at 1:00 p.m. on 16 September, coinciding with Mangkhut's landfall near Jiangmen city (Figure 3.10).

Figure 3.10

Predicted maximum storm surge for the next 72 hours in Pearl River Estuary



Note. The distributions of the storm surge when the maximum storm surge occurred (13:00:00 on 2018-09-16) during tropical cyclone Mangkhut from the results of Fct24. Fct24 denotes the results from the start time of the model, which is at least 24 h before Mangkhut made landfall. The time 2018-09-16 13:00:00 is when the increase in the water level in the model domain reached the maximum value during tropical cyclone Mangkhut (Zhou, Liu, Dai, Huang, Song & Li, 2024).

The storm surge was most severe in the eastern part of the Pearl River Estuary, where the trumpet-shaped coastline and strong southeasterly winds (exceeding 20 ms^{-1}) funnelled water inland (Figure 3.11). The GBASSP simulations revealed that wind stress τ_s and the pressure drop ΔP from Mangkhut were the primary drivers of the surge, while the shallow bathymetry of the Pearl River Estuary further amplified water levels. The bottom friction stress τ_b was modelled as:

$$(\tau_{bx}, \tau_{by}) = C_b \rho_w (u_b, v_b) \sqrt{u_b^2 + v_b^2} \quad (20)$$

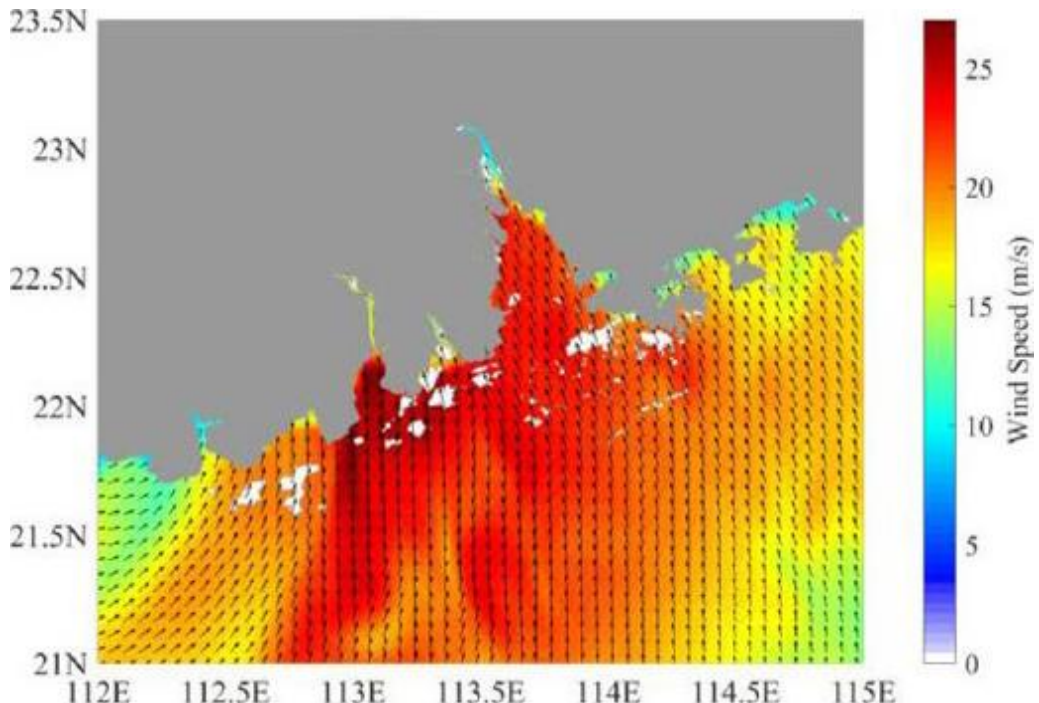
where C_b is the bottom drag coefficient, ρ_w is water density, and (u_b, v_b) are the near-bed current velocities. The model also captured the asymmetrical surge distribution, with higher surges on the typhoon's right side due to wind direction and coastal geometry.

The forecasting system provided early warnings at least two days before landfall, enabling timely evacuations and disaster preparedness. The forecasts were updated every hour, and the

system's computational efficiency—running in 70 minutes using 480 cores—made it suitable for real-time operations. The model's unstructured grid and wet/dry treatment for intertidal zones improved accuracy in predicting flood extent, particularly in low-lying urban areas such as Macau and Hong Kong (Figure 3.12).

Figure 3.11

Predicted 10 m wind for the next 72 hours in Pearl River Estuary



Note. The distributions of the wind speed at 10 m (Zhou, Liu, Dai, Huang, Song & Li, 2024).

Comparisons with other models highlighted the GBASSP's superior performance, boasting a relative error (RE) of 5.9%:

$$RE = \frac{AE}{x_i} \times 100\% \quad (21)$$

and a root mean square error (RMSE) of 0.21 m (Figure 3.12):

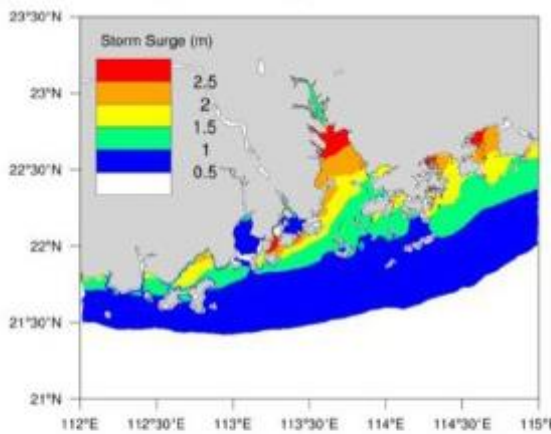
$$RMSE = \sqrt{\frac{1}{n} \sum_{i=1}^n (y_i - x_i)^2} \quad (22)$$

where n is the number of forecasted and observed values, x_i is the observed water level, and y_i is the forecasted water level. These metrics underscore the system's reliability in forecasting storm surges, particularly in complex coastal environments like the Pearl River Estuary. The model's unstructured grid and high resolution enabled it to capture localised surge variations effectively, which is critical for disaster preparedness in densely populated areas (Figure 3.13).

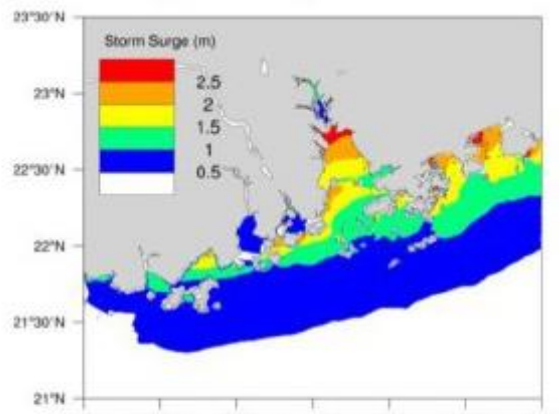
Figure 3.12

Storm surge warning for the next 72 hours in Pearl River Estuary

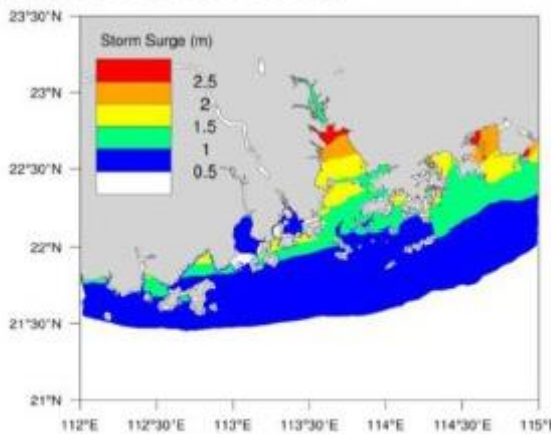
(a) 2018091400-2018091700



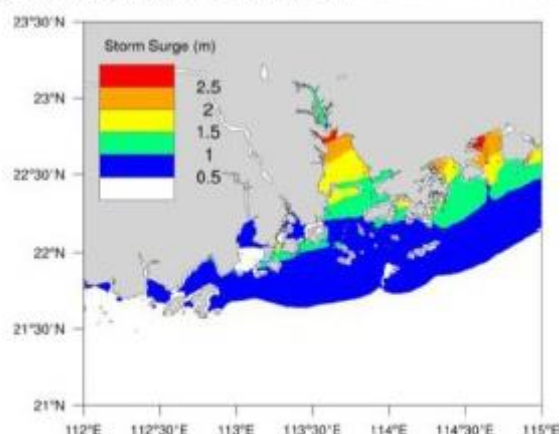
(b) 2018091412-2018091712



(c) 2018091500-2018091800



(d) 2018091512-2018091812

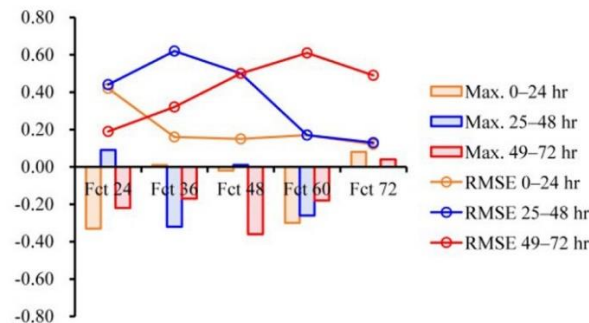


Note. The distribution of the storm surge when the maximum surge occurred before the two-day warning (Zhou, Liu, Dai, Huang, Song & Li, 2024).

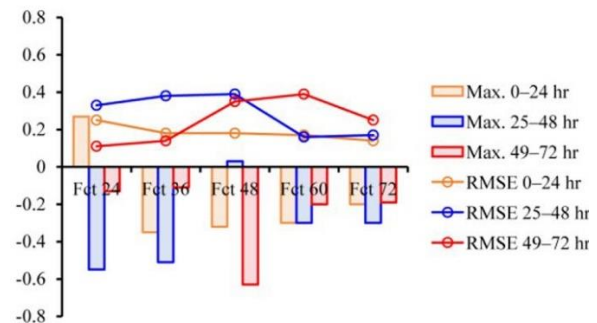
Figure 3.13

Error of predicted storm surge in Pearl River Estuary

(a) Zhapo



(b) Quarry Bay



Note. Root mean square error (RMSE) and maximum error (Max) of the GBASSP results at Quarry Bay station and Zhapo station during tropical cyclone Mangkhut.

The GBASSP proved highly effective in forecasting the storm surge from Mangkhut, offering accurate, high-resolution predictions that were critical for disaster mitigation. The model's success highlights the importance of advanced numerical coupling, fine grid resolution, and real-time operational capabilities in storm surge forecasting for vulnerable coastal megacities like those in the Greater Bay Area (GBA).

4. Meteorological Observations

4.1 Philippines Weather Stations

4.1.1 Wind Speed

Tropical cyclone Mangkhut, locally known as Ompong in the Philippines, struck the northern part of Luzon on 15 September, leaving a trail of devastation. As the typhoon entered the Philippine Area of Responsibility (PAR), PAGASA (2018) raised Tropical Cyclone Warning Signal (TCWS) No. 4 (171-220 kmh⁻¹ winds)—the highest warning level—over Cagayan, Isabela, and Apayao, while 37 provinces were placed under TCWS Nos. 1 to 3 as the storm advanced.

As it approached Luzon, surface stations recorded extreme wind speeds, with Aparri, Cagayan, experiencing the highest maximum sustained winds of 108 kmh⁻¹ and a peak gust of 176 kmh⁻¹. These winds were powerful enough to cause widespread structural damage, uproot trees, and disrupt power lines across the affected regions.

The storm's sheer size, spanning approximately 1400 km, amplified its destructive potential, with strong winds affecting not only coastal areas but also inland provinces. In Tuguegarao City, Cagayan, sustained winds reached 72 kmh⁻¹, with gusts peaking at 158 kmh⁻¹, while Basco, Batanes, recorded a notable gust of 140 km/h. Although these wind speeds were slightly lower than those of tropical cyclone Haima (Lawin) in 2016, they were still catastrophic, causing severe damage to infrastructure and agriculture. The interaction of Mangkhut's winds with Luzon's rugged terrain further intensified localised wind patterns, exacerbating destruction in mountainous areas such as the Cordillera Administrative Region.

PAGASA's wind observations highlighted the storm's relentless force, which persisted even as it weakened after landfall (Table 2.1). However, the damage had already been done, with the storm's fierce winds leaving a trail of devastation across northern and central Luzon.

4.1.2 Mean Sea Level Pressure

Mangkhut's (Ompong) intense circulation caused a dramatic drop in mean sea level pressure (MSLP), particularly in northern Luzon, where the storm made landfall (Table 2.2). The lowest recorded MSLP was observed in Tuguegarao City, Cagayan, at 949.0 hPa at 3:00 a.m. on 15 September, coinciding with the typhoon's closest approach. This sharp pressure decline reflected the

storm's extreme intensity, as lower pressure is directly associated with stronger tropical cyclones. The reading in Tuguegarao was notably lower than in surrounding areas, such as Aparri, Cagayan (953.3 hPa), and Laoag City, Ilocos Norte (965.7 hPa), highlighting the localised severity of Mangkhut's core as it traversed the region (PAGASA, 2018).

Table 2.1

Wind speed observations in the Philippines

Station	Maximum 10-minute Mean Wind Speed (km/h)	Maximum Gust (km/h)
Tuguegarao City, Cagayan	72	158
Aparri, Cagayan	108	176
Laoag City, Ilocos Norte	54	133

Table 2.2

Mean sea level pressure observations in the Philippines

Station	Mean Sea Level Pressure (hPa)
Tuguegarao City, Cagayan	949.0
Aparri, Cagayan	953.3
Laoag City, Ilocos Norte	965.7

4.1.3 Storm Surge

Figure 4.1 reveals the estimated storm surge heights (in metres) for a coastal region in the Philippines. Along the northeastern coast's curved shoreline, storm surge levels are most severe, reaching heights of 5.0 to 6.0 m. This tip of the peninsula shows the greatest storm surge risk, suggesting it is a critical zone for potential flooding and damage. The progressive elevation of surge heights from offshore toward this point reflects the local geography funnelling storm surge waters into this coastal zone, amplifying the flooding threat.

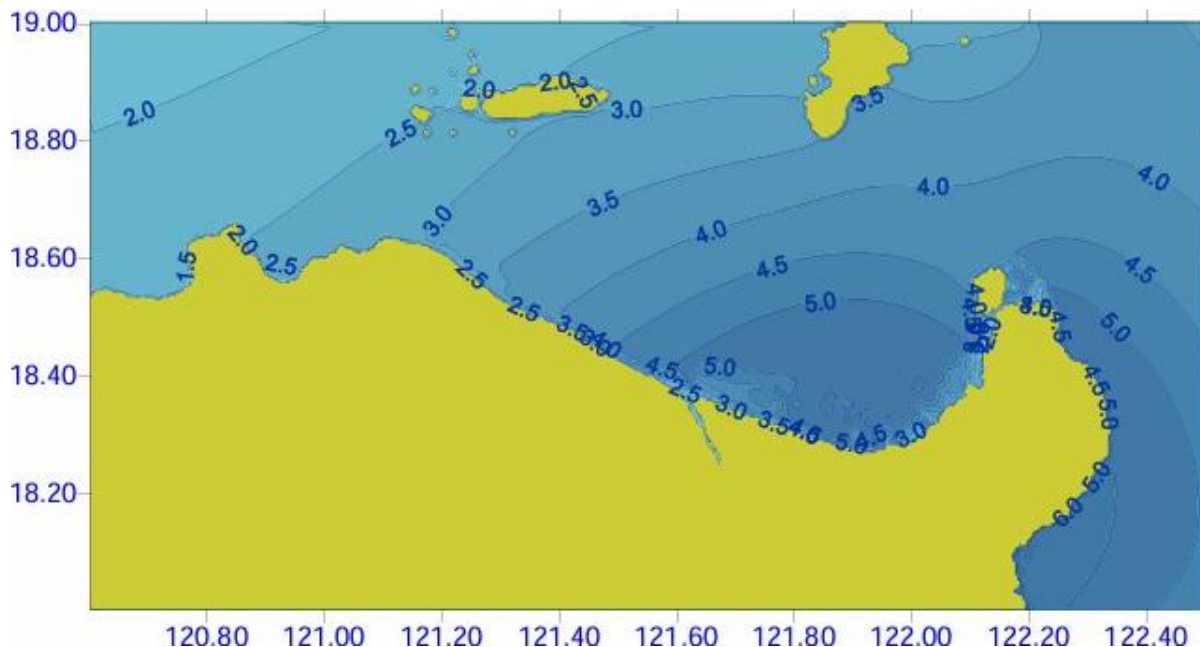
Moving westward and south along the coast, the storm surge values gradually reduce but remain significantly high, mostly ranging between 3.0 and 5.0 m. These levels still represent a substantial hazard to communities and infrastructure, necessitating robust preparedness and mitigation measures. The small islands off the coast experience lower surge heights, commonly between 2.0 and 3.0 m, likely benefiting from their position relative to the main surge flow and natural wave barriers.

Offshore waters away from the immediate coast show lower surge levels, decreasing to about 2.0 m or less, characteristic of open sea conditions where surge impacts are lessened. Overall, this map

highlights critical zones where storm surge impacts could be severe, emphasizing the need for targeted disaster risk reduction and coastal defence in the affected northern Philippine regions. Enhanced warning systems, evacuation plans, and resilient infrastructure should be prioritised for areas facing surge values above 4.0 m to mitigate the significant risk during major storm events.

Figure 4.1

Maximum storm surge and tide in the Philippines



4.1.4 Rainfall Distribution

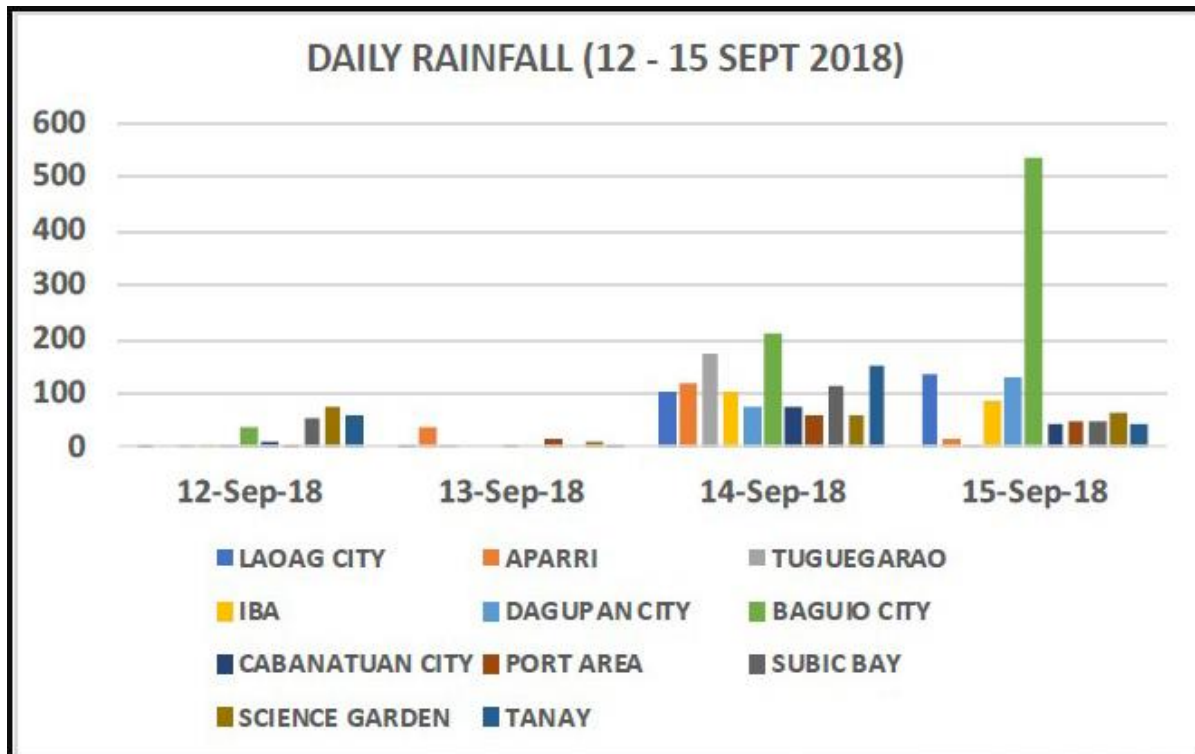
Mangkhut (Ompong) unleashed catastrophic rainfall across the Philippines, particularly in northern and central Luzon, from 12 to 15 September (Figure 4.2). The storm's immense size and slow movement exacerbated precipitation, with the Cordillera Administrative Region (CAR) and Ilocos Region bearing the brunt of the deluge. Baguio City, Benguet, recorded the highest 4-day rainfall total of 794 mm, surpassing the area's average September rainfall by 39.1%. This extreme accumulation triggered severe flooding and landslides, especially in mountainous areas where the terrain amplified runoff and soil saturation. The rainfall in Baguio was not only exceptional in volume but also in intensity, with a staggering 535 mm falling within 24 hours on 15 September—a record exceeding the 455 mm deluge caused by tropical cyclone Ketsana (Ondoy) in 2009.

Other areas experienced similarly disruptive rainfall, though to a lesser degree. Tanay, Rizal, and Laoag City, Ilocos Norte, recorded 249 mm and 239.4 mm of rain over four days, respectively—amounts equivalent to about half their typical September totals. Notably, Baguio also set a record for 6-hour rainfall, with 392 mm observed between 8:00 a.m. and 2:00 p.m. on 15 September, again

surpassing Ondoy's benchmarks. These short-term, high-intensity downpours overwhelmed drainage systems and caused rivers to swell, leading to flash floods in low-lying communities. Meanwhile, Tuguegarao City in Cagayan registered 172.2 mm of rain on 14 September, further compounding the storm's impact on agriculture and infrastructure in the Cagayan Valley.

Figure 4.2

Total daily rainfall distribution in the Philippines



Note. The daily rainfall from 12-15 September 2018 during the passage of tropical cyclone Mangkhut (PAGASA, 2018).

The rainfall distribution highlighted Mangkhut's disproportionate impact on Luzon's western and central mountain ranges. While some stations, like San Jose in Occidental Mindoro, recorded significant rainfall (165.9 mm on 13 September), PAGASA noted that these events may not have been directly tied to the tropical cyclone. The data underscored the storm's capacity to concentrate rainfall over specific regions, with the CAR's elevated geography acting as a catalyst for extreme precipitation. The resulting disasters included landslides and destroyed crops.

4.1.5 Upper-air Weather Measurements

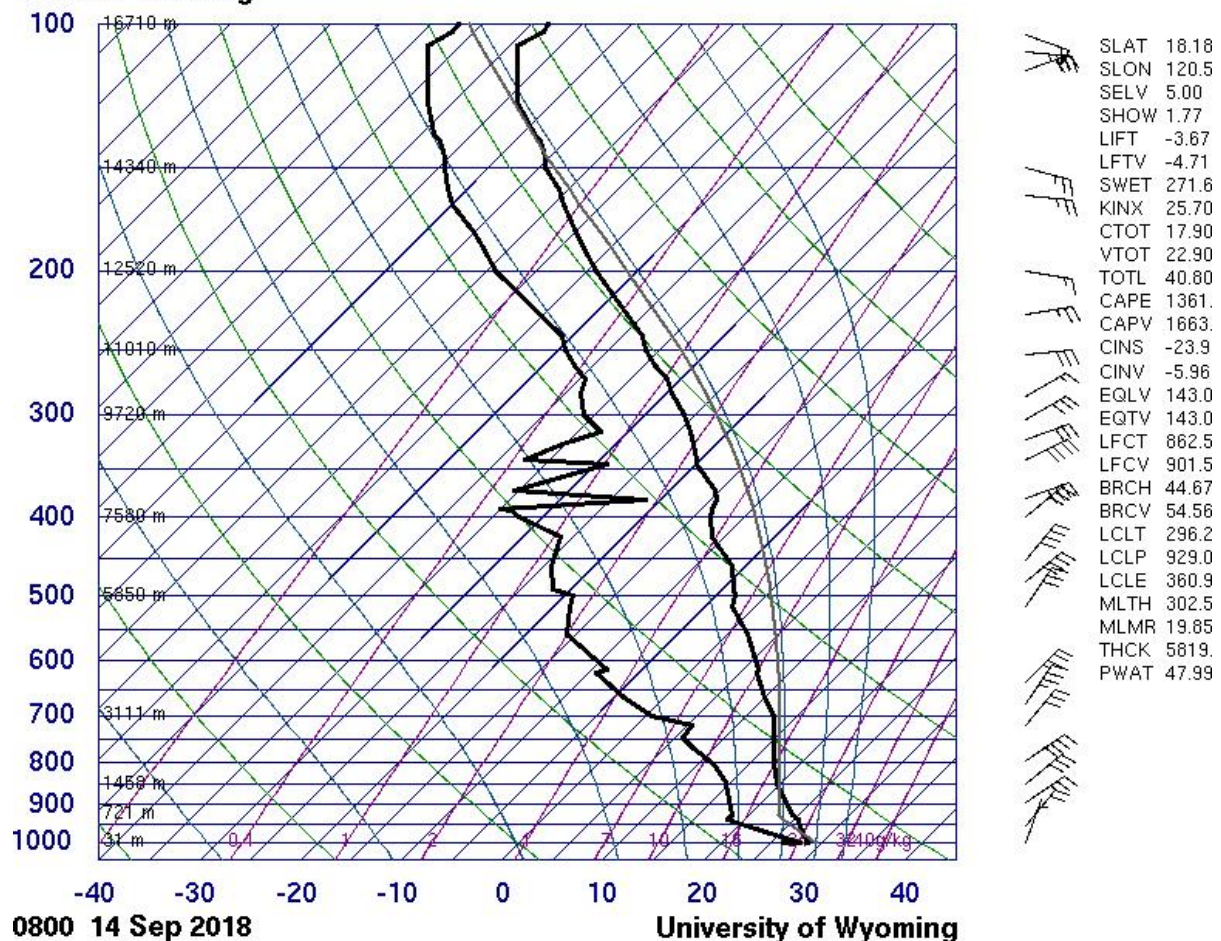
The upper-air weather measurements recorded at Laoag City (station RPLL) on 14 September, during Mangkhut's approach reveal critical atmospheric conditions that contributed to the storm's

intensity and associated severe weather (Figure 4.3). The skew-T log-P diagram and derived indices highlight an environment primed for extreme convection, with a Convective Available Potential Energy (CAPE) value of 1361 J kg^{-1} and a virtual CAPE (CAPV) of 1663 J kg^{-1} . These exceptionally high values indicate substantial atmospheric instability, providing the energy needed for intense thunderstorm development and sustained updrafts within Mangkhut's rainbands. The lifted index (LIFT) of -3.67 and the lifted index for virtual temperature (LFTY) of -4.71 further confirm strong convective potential, as negative values signify a heightened likelihood of severe weather.

Figure 4.3

Skew-T diagram in the Laoag, Philippines

98223 RPLI Laoag



The presence of deep moisture is evident in the precipitable water (PWAT) value of 47.99 mm, which is well above average for the region. This abundant moisture, combined with the storm's large circulation, fuelled the torrential rainfall observed across Luzon, including the record-breaking 794 mm 4-day total in Baguio City. The vertical wind profile, inferred from indices like the bulk Richardson number (BRCH: 44.67; BRCV: 54.56), suggests a favourable environment for organised convection with minimal wind shear, allowing Mangkhut to maintain its structure and intensity. The

level of free convection (LFC) at 901.5 hPa and the equilibrium level (EQLV/EQTV) near 143 hPa indicate that updrafts could penetrate deep into the troposphere, supporting the development of high-reaching thunderstorms and enhancing precipitation efficiency.

Additionally, the low-level convergence (CNS: -23.9) and convective inhibition (CINV: -5.96 J kg^{-1}) reveal that, while the atmosphere was highly unstable, weak capping allowed for the rapid release of convective energy. The mean layer mixing ratio (MLMR: 13.65 g kg^{-1}) and thickness (THCK: 5619 m) further reflect a warm, moist boundary layer typical of tropical cyclone environments. These upper-air observations collectively explain the extreme rainfall and sustained convection associated with Mangkhut, corroborating surface reports of flooding and landslides. The data underscore how advanced atmospheric profiling is essential for predicting the impacts of such high-intensity storms, particularly in regions vulnerable to tropical cyclones.

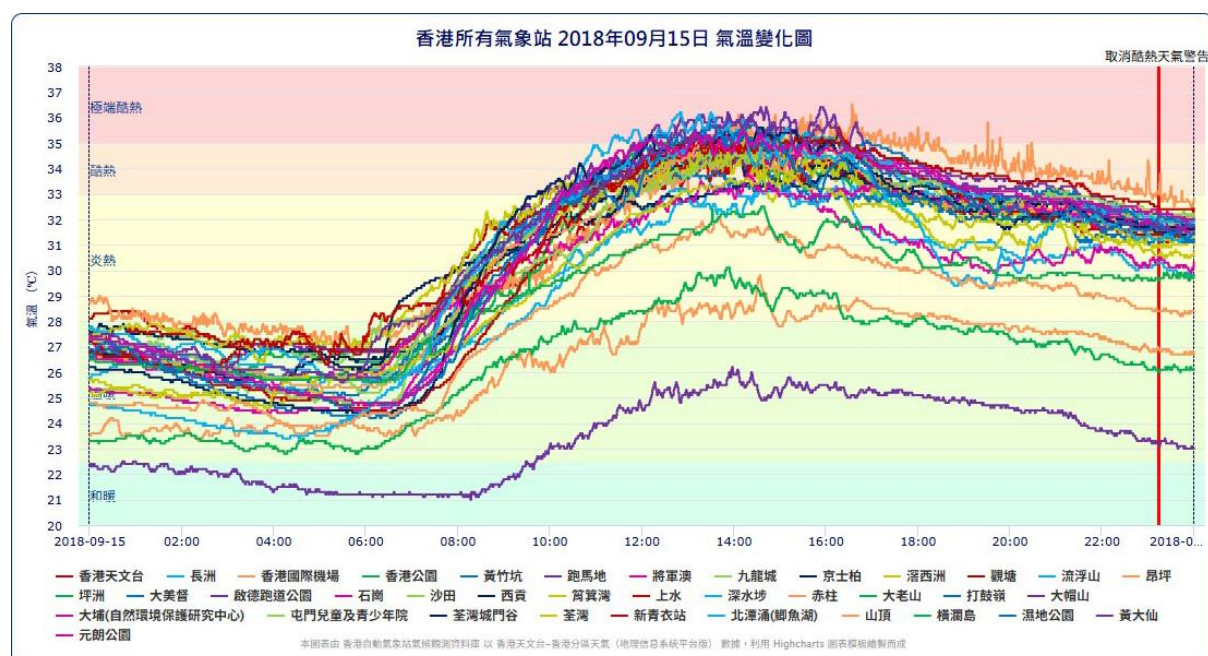
4.2 Hong Kong Weather Stations

4.2.1 Temperature

Under the subsidence effect ahead of Mangkhut's circulation, the weather would be hazy skies, very hot and fine over the southeastern China on 14 and 15 September. Temperature at the Hong Kong Observatory soared to 35.1°C on 15 September, the second highest record for September (Figure 4.4).

Figure 4.4

Hong Kong temperature observations



4.2.2 Wind Speed

Due to Mangkhut's rapid movement and extensive circulation, which posed a significant threat to Hong Kong, the HKO issued the Standby Signal No. 1 at 10:20 p.m. on 14 September, when the storm was approximately 1,110 km east-southeast of the territory. This surpassed the previous record for the greatest distance at the time of signal issuance—930 km, set by Carla in 1967.

On 15 September, local winds remained light to moderate northeasterlies. However, as Mangkhut steadily advanced toward the Guangdong coast, the HKO escalated the warning to Strong Wind Signal No. 3 at 4:20 p.m., when the storm was positioned about 650 km southeast of Hong Kong. By nightfall, winds intensified to fresh or strong northerlies.

Maintaining its trajectory toward the Pearl River Estuary, Mangkhut prompted the HKO to issue the No. 8 Northeast Gale or Storm Signal at 1:10 a.m. on 16 September, with the storm located approximately 410 km southeast of Hong Kong. Subsequently, winds strengthened further, reaching gale to storm force in offshore and elevated areas. Anticipating further intensification as the storm approached, the HKO raised the Increasing Gale or Storm Signal No. 9 at 7:40 a.m., when Mangkhut was situated about 200 km south-southeast of the territory. As wind speeds surged rapidly, the Hurricane Signal No. 10 was issued at 9:40 a.m., with the typhoon roughly 160 km south-southeast of Hong Kong. Notably, when Signals No. 8, 9, and 10 were issued, Mangkhut was at the farthest recorded distance from Hong Kong for each respective signal since 1961. The Hurricane Signal No. 10 remained in force for 10 hours, marking the second-longest duration for this warning signal since 1946, exceeded only by York's 11-hour record set in 1999.

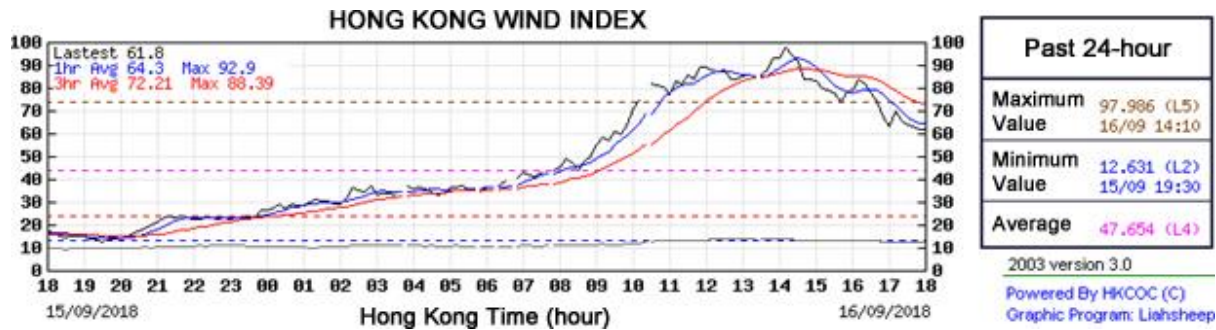
Mangkhut made landfall near Taishan, Guangdong, before dusk. As the storm moved away from Hong Kong and weakened, hurricane-force winds ceased to affect the region. Consequently, the HKO downgraded the warning to the No. 8 Southeast Gale or Storm Signal at 7:40 p.m., replacing Signal No. 10. With sustained wind abatement, the No. 3 Strong Wind Signal was issued at 5:20 a.m. on 17 September, followed by the No. 1 Standby Signal at 2:40 p.m. Finally, as Mangkhut dissipated inland, all tropical cyclone warnings were cancelled at 7:10 p.m. that evening.

During the passage of Mangkhut, exceptionally high wind speeds were recorded across Hong Kong, with the Hong Kong wind index reaching approximately 97.99 kmh^{-1} —the highest value among tropical cyclones necessitating No. 10 signals in the past three decades (Figure 4.5), exceeding those of York (1999), Vicente (2012), and Hato (2017). Waglan Island and Cheung Chau stations registered 60-minute mean wind speeds of 161 kmh^{-1} and 157 kmh^{-1} , respectively, representing the

second-highest measurements at these locations—surpassed only by Ellen's records in 1983. The storm generated widespread gusts exceeding 150 kmh^{-1} throughout the territory, with Tate's Cairn recording a peak gust of 256 kmh^{-1} , ranking third historically behind Wanda (1962) and Ruby (1964). Notably, the North Point anemometer within Victoria Harbour measured a 10-minute mean wind speed of 124 kmh^{-1} , marking the first recorded instance of sustained hurricane-force winds at this station since its commissioning in 1998. See more details in Tables 2.3 and 2.4.

Figure 4.5

Hong Kong wind index



Note. Time series of Hong Kong wind index on 15 and 16 September 2018.

Table 2.3

Maximum 60-minute mean wind speeds and gusts in Hong Kong

Station	Maximum 60-minute Mean Wind Speed				Maximum Gust			
	Direction	Speed (km/h)	Date	Time	Direction	Speed (km/h)	Date	Time
Bluff Head	-	101	16/9	15:00	-	157	16/9	14:00
Central Pier	E	99	16/9	13:00	E	169	16/9	12:30
Cheung Chau	E	151	16/9	15:00	E	212	16/9	14:10
Cheung Chau Beach	ENE	142	16/9	14:00	NE	209	16/9	12:01
Green Island	NE	124	16/9	11:00	NNE	229	16/9	10:29
Kai Tak	ESE	77	16/9	17:00	ENE	142	16/9	10:28
					ENE	142	16/9	13:59
Hong Kong International Airport	ESE	99	16/9	15:00	ESE	157	16/9	16:26
King's Park	E	67	16/9	15:00	NNE	161	16/9	15:00
Lau Fau Shan	ENE	96	16/9	14:00	ENE	166	16/9	12:40

Station	Maximum 60-minute Mean Wind Speed				Maximum Gust			
	Direction	Speed (km/h)	Date	Time	Direction	Speed (km/h)	Date	Time
North Point	E	110	16/9	13:00	E	171	16/9	12:51
Ping Chau	SSE	47	16/9	11:00	E	124	16/9	11:30
Sai Kung	NE	108	16/9	12:00	NE	180	16/9	11:43
Sha Chau	ESE	103	16/9	15:00	E	164	16/9	14:02
Sha Lo Wan	E	87	16/9	15:00	E	169	16/9	14:11
Sha Tin	NNE	47	16/9	11:00	NNE	149	16/9	11:00
Shek Kong	E	72	16/9	15:00	NE	164	16/9	11:22
Star Ferry (Kowloon)	E	79	16/9	14:00	E	135	16/9	13:48
Ta Kwu Ling	NNE	52	16/9	11:00	ENE	133	16/9	13:28
Tai Mei Tuk	ENE	139	16/9	13:00	ENE	198	16/9	12:08
Tai Mo Shan	ESE	167	16/9	15:00	ESE	250	16/9	14:05
Tai Po Kau	E	88	16/9	13:00	E	146	16/9	13:09
Tate's Cairn	ENE	158	16/9	12:00	ENE	256	16/9	10:33
Tseung Kwan O	NNE	52	16/9	11:00	NNE	153	16/9	10:40
Tsing Yi Shell Oil Depot	ESE	58	16/9	15:00	ESE	137	16/9	14:22
Tuen Mun Government Offices	SE	51	16/9	17:00	E	133	16/9	14:01
Waglan Island	NE	158	16/9	11:00	NE	220	16/9	10:14
Wetland Park	E	58	16/9	14:00	E	130	16/9	13:06
Wong Chuk Hang	ENE	54	16/9	14:00	ENE	173	16/9	13:40

Note. Maximum 60-minute mean wind speeds and maximum gust peak winds with associated wind directions recorded at various stations on 16 September 2018 by the HKO.

Table 2.4

Maximum 10-minute mean wind speeds and gusts in Hong Kong

Station	Maximum 10-minute Mean Wind Speed				Maximum Gust			
	Direction	Speed (km/h)	Date	Time	Direction	Speed (km/h)	Date	Time
Bluff Head	-	115	16/9	14:07	-	157	16/9	14:00

Station	Maximum 10-minute Mean Wind Speed				Maximum Gust			
	Direction	Speed (km/h)	Date	Time	Direction	Speed (km/h)	Date	Time
Central Pier	-	-	-	-	E	169	16/9	12:30
Cheung Chau	E	173	16/9	14:30	E	212	16/9	14:10
Cheung Chau Beach	ENE	159	16/9	13:19	NE	209	16/9	12:01
Green Island	NNE	144	16/9	10:37	NNE	229	16/9	10:29
Kai Tak	E	90	16/9	14:34	ENE	142	16/9	10:28
	E	90	16/9	14:35	ENE	142	16/9	13:59
Hong Kong International Airport	E	90	16/9	14:35	ENE	142	16/9	13:59
King's Park	E	80	16/9	14:21	NNE	161	16/9	15:00
Lau Fau Shan	ENE	110	16/9	13:12	ENE	166	16/9	12:40
North Point	E	124	16/9	-	E	171	16/9	12:51
Ping Chau	-	-	-	-	E	124	16/9	11:30
Sai Kung	NE	118	16/9	11:47	NE	180	16/9	11:43
	NE	118	16/9	11:56				
	NE	118	16/9	11:57				
	NE	118	16/9	12:00				
Sha Chau	SE	111	16/9	11:55	E	164	16/9	14:02
Sha Lo Wan	-	-	-	-	E	169	16/9	14:11
Sha Tin	NNE	58	16/9	12:30	NNE	149	16/9	11:00
Shek Kong	E	85	16/9	14:18	NE	164	16/9	11:22
Star Ferry (Kowloon)	E	90	16/9	14:03	E	135	16/9	13:48
Ta Kwu Ling	N	62	16/9	10:55	ENE	133	16/9	13:28
Tai Mei Tuk	ENE	153	16/9	12:16	ENE	198	16/9	12:08
Tai Mo Shan	-	-	-	-	ESE	250	16/9	14:05
Tai Po Kau	E	97	16/9	14:10	E	146	16/9	13:09
Tate's Cairn	ENE	189	16/9	10:38	ENE	256	16/9	10:33
Tseung Kwan O	NNE	66	16/9	10:26	NNE	153	16/9	10:40
Tsing Yi Shell Oil Depot	E	63	16/9	14:40	ESE	137	16/9	14:22
	E	63	16/9	14:41				
Tuen Mun Government Offices	SE	65	16/9	16:21	E	133	16/9	14:01

Station	Maximum 10-minute Mean Wind Speed				Maximum Gust			
	Direction	Speed (km/h)	Date	Time	Direction	Speed (km/h)	Date	Time
Waglan Island	NE	180	16/9	10:19	NE	220	16/9	10:14
Wetland Park	ENE	64	16/9	13:15	E	130	16/9	13:06
Wong Chuk Hang	ENE	69	16/9	12:08	ENE	173	16/9	13:40

Note. Maximum 10-minute mean wind speeds and maximum gust peak winds with associated wind directions recorded at various stations on 16 September 2018 by the HKO.

4.2.3 Mean Sea Level Pressure

As Mangkhut approached Hong Kong on 16 September, the MSLP experienced a dramatic drop. The lowest instantaneous mean sea-level pressure recorded at the Hong Kong Observatory Headquarters was 977.0 hPa at 1:28 p.m., while other stations measured even lower values: Hong Kong International Airport reported a devastating low of 973.9 hPa at 2:11 p.m., and Cheung Chau recorded 971.8 hPa at 2:10 p.m. Other stations across the region, including Ta Kwu Ling, Tai Po, Shatin, and Sheung Shui, reported similarly depressed pressures, with values ranging from approximately 970.0 hPa to 985.0 hPa during that critical early afternoon period when Mangkhut was nearest (Table 2.5).

Table 2.5

Hong Kong mean sea level pressure observations

Station	Lowest instantaneous mean sea-level pressure (hPa)	Date	Time
Hong Kong Observatory Headquarters	977.0	16/9	13:28
Hong Kong International Airport	973.9	16/9	14:11
King's Park	977.5	16/9	13:44
Ta Kwu Ling	981.3	16/9	12:52
Tai Po	980.5	16/9	13:17
Shatin	980.1	16/9	12:21
Sheung Shui	979.8	16/9	14:06
Lau Fau Shan	976.3	16/9	13:59
Cheung Chau	971.8	16/9	14:10
Waglan Island	973.5	16/9	12:10

Note. Time series of instantaneous mean sea-level pressures on 16 September 2018 by the HKO.

4.2.4 Storm Surge

Mangkhut followed a track typical of storms that generate severe storm surges in Hong Kong. As it passed to the south-southwest of the territory, its powerful east to southeasterly winds drove seawater toward the coast, causing significant water buildup. Mangkhut's vast circulation further amplified the surge by displacing a larger expanse of ocean, leading to an overall rise in water levels.

The storm surge elevated sea levels across Hong Kong by more than two metres, resulting in unprecedented flooding in many areas. Five of the six tide stations operated by the Hong Kong Observatory—Quarry Bay, Tai Po Kau, Tsim Bei Tsui, Tai Miu Wan, and Shek Pik—recorded historic surges. Quarry Bay recorded a surge of 2.35 m, while Tai Po Kau experienced an even more extreme rise of 3.40 m. Unfortunately, the Waglan Island tide station was damaged during the storm, preventing a complete record of peak water levels (Choy, Lau & He, 2022).

At Quarry Bay, the combined effect of the storm surge and astronomical tide pushed sea levels to 3.88 m above Chart Datum—surpassing the 3.57 m recorded during Typhoon Hato (2017) and falling just short of the all-time high of 3.96 m set by Wanda (1962). Similarly, Tai Po Kau reached a maximum water level of 4.71 m, second only to Wanda's record of 5.03 m (Choy, Lau & He, 2022). These observations highlight the exceptional intensity of Mangkhut's storm surge and its widespread impact on Hong Kong's coastal areas on 16 September. See more details in Table 2.6.

Table 2.6

Maximum storm surge and tide in Hong Kong

Station	Maximum Sea Level (above chart datum)			Maximum Storm Surge (above astronomical tide)		
	Height (m)	Date	Time	Height (m)	Date	Time
Quarry Bay	3.88	16/9	14:42	2.35	16/9	14:42
Shek Pik	3.89	16/9	14:16	2.34	16/9	14:16
Tai Miu Wan	4.19	16/9	13:41	2.77	16/9	13:41
Tai Po Kau	4.71	16/9	12:34	3.40	16/9	12:34
Tsim Bei Tsui	4.18	16/9	17:14	2.58	16/9	17:21

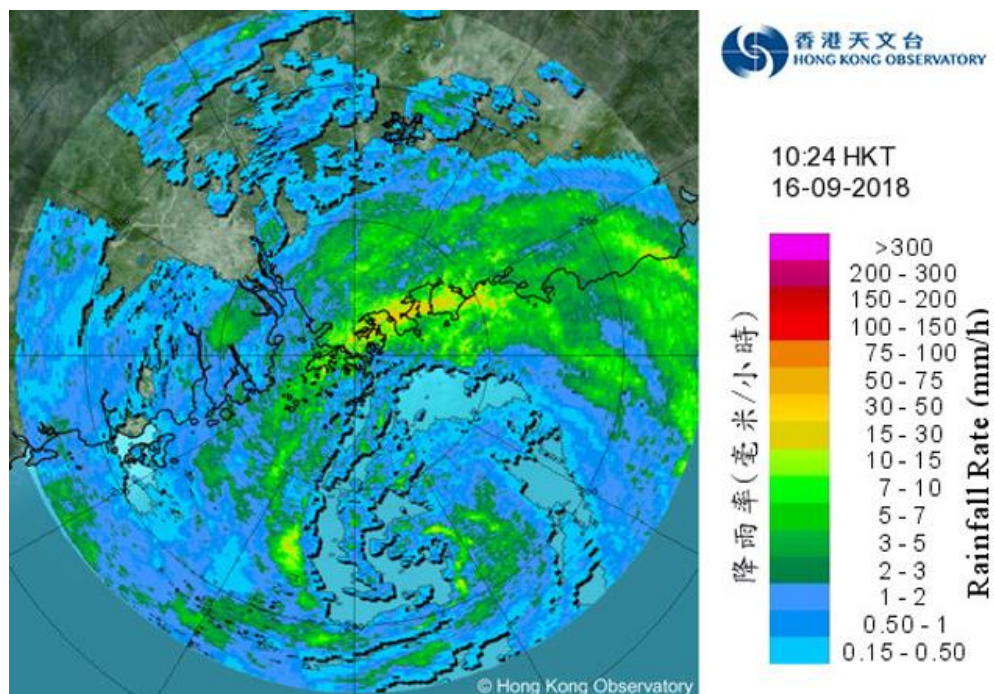
Note. Times and heights of the maximum sea level and the maximum storm surge recorded at tide stations in Hong Kong during the passage of tropical cyclone Mangkhut on 16 September 2018 by the HKO.

4.2.5 Rainfall Distribution

The extensive circulation of Mangkhut brought heavy rain and squalls weather to Hong Kong on 16 September. The dual-polarization S-band Doppler weather radar images illustrated that the storm's spiral rainbands were both intense and well-defined at 10:24 a.m. (Figure 4.6). Most parts of the territory saw over 150 mm of rain on that day (Figure 4.7). The HKO issued the Amber Rainstorm Warning at 9:10 a.m., which was upgraded to the Red Rainstorm Warning at 10:55 a.m., followed by the Special Announcement on Flooding in the northern New Territories at 11:25 a.m., and the Landslip Warning at 2:20 p.m.

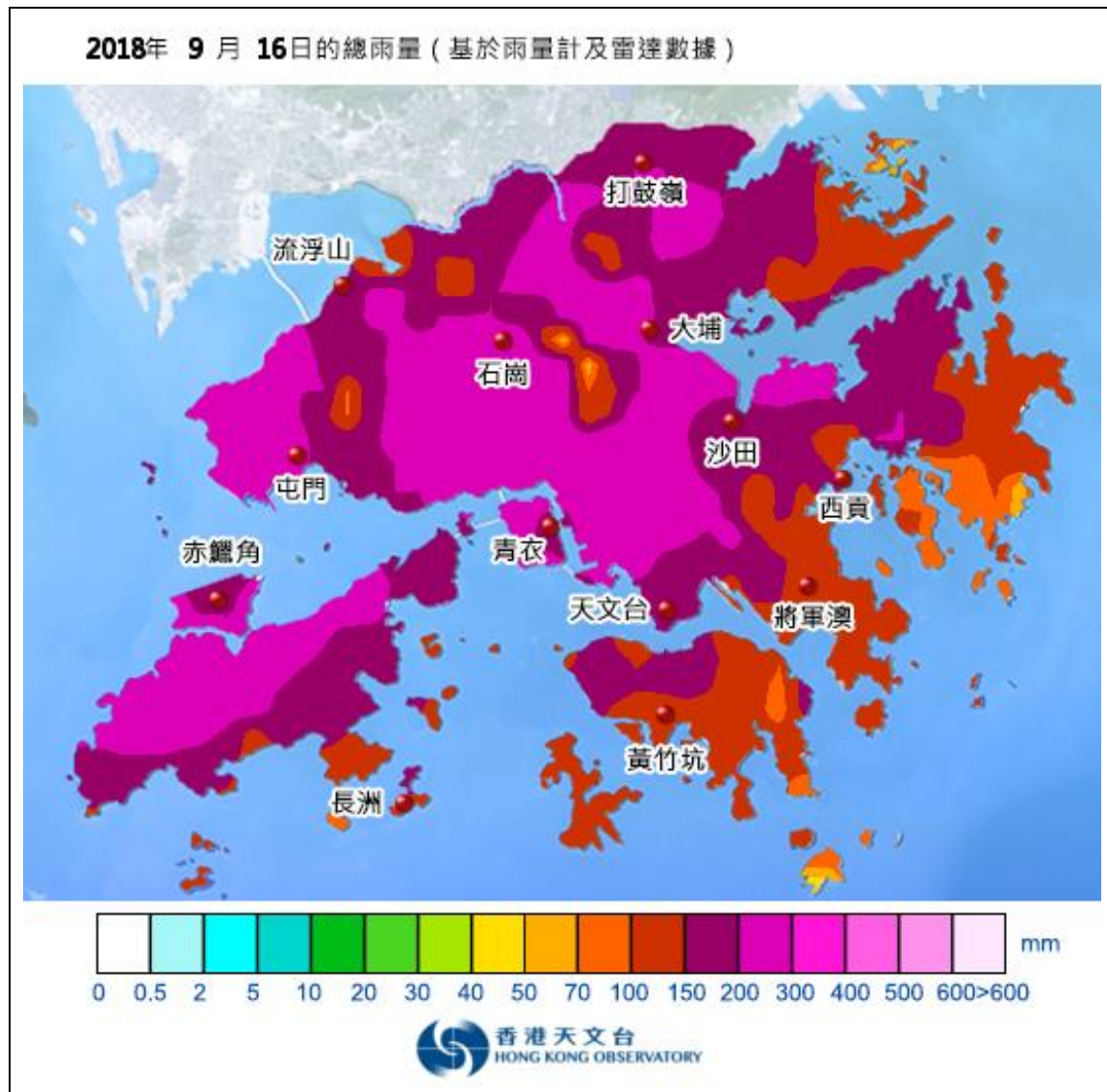
Figure 4.6

Radar image of intense spiral rainband of severe typhoon Mangkhut



Note. The intense spiral rainband of Mangkhut was affecting Hong Kong at 10:24 a.m. on 16 September 2018.

With Mangkhut receding and the rain tapering off, the Red Rainstorm Warning was lowered to Amber at 6:50 p.m. The Amber Rainstorm Warning was lifted at 10:30 p.m., followed by the cancellation of the Special Announcement on Flooding in the northern New Territories at 11:30 p.m. Table 2.7 shows the accumulated daily rainfall from 14-17 September.

Figure 4.7*Total daily rainfall distribution in Hong Kong*

Note. The distribution of rainfall during the passage of tropical cyclone Mangkhut on 16 September 2018 by the HKO.

Table 2.7*The accumulated daily rainfall distribution in Hong Kong*

Station	14/9	15/9	16/9	17/9	Total rainfall (mm)
Hong Kong Observatory (HKO)	0.0	Trace	167.5	12.0	179.5
Hong Kong International Airport (HKA)	0.0	Trace	191.5	4.2	195.7
Cheung Chau (CCH)	[0.0]	0.0	79.0	9.0	[88.0]
H23 Aberdeen	0.0	0.0	99.0	7.5	106.5

Station		14/9	15/9	16/9	17/9	Total rainfall (mm)
N05	Fanling	0.0	0.0	126.5	28.5	155.0
N13	High Island	0.0	0.0	[83.5]	2.0	[85.5]
K04	Jordan Valley	0.0	0.0	160.0	6.0	166.0
N06	Kwai Chung	0.0	0.0	214.0	22.5	236.5
H12	Mid Levels	0.0	0.0	143.0	22.0	165.0
N09	Sha Tin	1.5	0.0	223.0	0.0	224.5
H19	Shau Kei Wan	0.0	0.0	138.5	6.5	145.0
SEK	Shek Kong	[0.0]	0.0	279.0	41.5	320.5
K06	So Uk Estate	0..0	0.0	[253.0]	17.0	[270.0]
R31	Tai Mei Tuk	0.5	0.0	[150.5]	[3.5]	[154.5]
R21	Tap Shek Kok	0.0	0.0	213.0	36.0	249.0

Tung Chung (N17), Tuen Mun Reservoir (TMR) - data not available

Note: [] based on incomplete hourly data.

Note. The intense spiral rainband of Mangkhut brought heavy rain and squalls to Hong Kong from 14 to 17 September 2018 by the HKO.

4.2.6 Upper-air Weather Measurements

The upper-air weather measurement from King's Park, Hong Kong during Mangkhut on 16 September reveals a highly saturated and dynamically active atmosphere typical of a major tropical cyclone event. The Skew-T log-P diagram shows that the temperature and dew point profiles are nearly overlapped throughout the entire vertical extent, indicating a deep layer of atmospheric saturation (Figure 4.8). This is further confirmed by the PWAT value of 69.91 mm, which signifies an exceptionally high moisture load capable of supporting intense and prolonged heavy rainfall.

At the surface, the temperature is recorded at 300.4 K (27.3°C) with a mean layer mixing ratio of 17.73 g kg⁻¹, confirming a moisture-laden boundary layer with near-saturation conditions. The atmospheric stability parameters reveal a notable discrepancy: the modest CAPE values of 39.97 J kg⁻¹ (surface-based) and 52.84 J kg⁻¹ (virtual) contrast with the nearly neutral LIFT index of 0.04. This apparent contradiction likely reflects the sounding's capture of Mangkhut's outer rainband environment rather than its most unstable core region, where stronger convective activity would be expected.

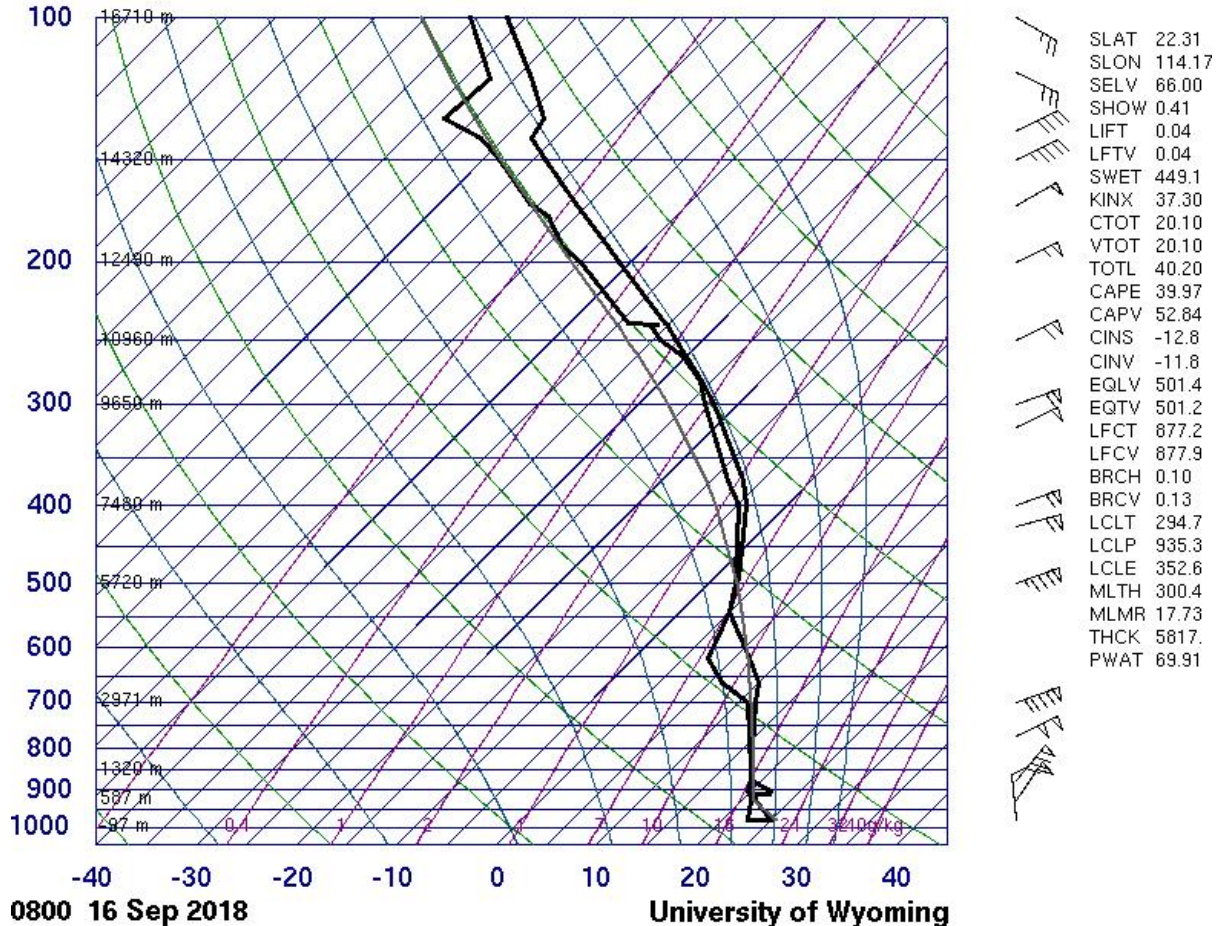
The wind profile is characterised by critical kinematic features, with storm-relative helicity (SWET) values of 449.1 m²s⁻² indicating significant rotational potential in the atmosphere. While not as extreme as some tropical cyclone soundings, this still demonstrates sufficient helicity to maintain

organised convection. The BRCH of 0.10 suggests a weak but present potential for organised convection at the time of observation.

Figure 4.8

Skew-T diagram in King's Park, Hong Kong

45004 Kings Park



The thermodynamic structure displays a deep, well-mixed boundary layer extending up to 877.2 hPa (LFCT), facilitating efficient vertical transport of moisture and momentum. This mixing depth, combined with the high moisture content, helps explain the effective rainfall production mechanisms observed during Mangkhut's passage. The EQLV at 501.4 hPa indicates cloud tops reaching into the mid-troposphere, consistent with the intense but not exceptionally deep convection typical of tropical cyclone rainbands.

These upper-air measurements collectively portray an atmosphere primed for heavy rainfall production, with the sounding's moderate instability metrics likely underestimating the more extreme conditions present in Mangkhut's inner core. The data provide valuable context for understanding how the typhoon's outer circulation contributed to Hong Kong's extreme weather, particularly when

combined with local topographic effects that enhanced precipitation in the northern territories. The sounding serves as an important reference point for studying the vertical structure of intense typhoons affecting highly urbanised coastal regions.

4.2.7 Wind Profilers

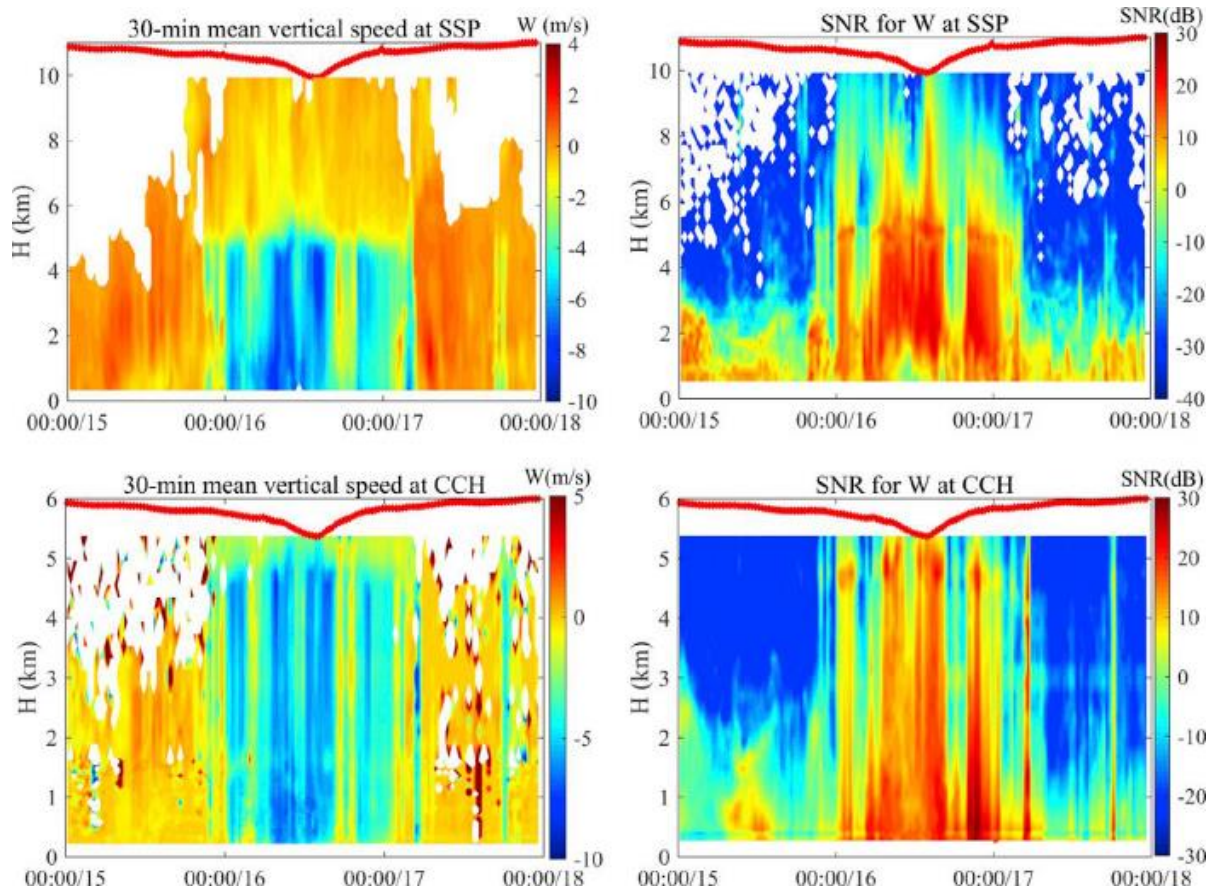
The wind profilers in Hong Kong played a crucial role in capturing the detailed evolution of wind characteristics during Mangkhut's passage. Situated at strategic locations including Sham Shui Po (SSP) and Cheung Chau (CCH), these profilers provided continuous vertical profiles of mean horizontal wind speed and direction across multiple altitudes with high temporal resolution. The data revealed significant variability in the boundary layer dynamics, reflecting the complex interactions between the tropical cyclone's structure and the local topography (He, He, Chen, Chan, Fu & Li, 2020).

During Mangkhut's approach and eventual landfall, the wind profilers detected exceptionally strong winds that peaked around noon on 16 September, coinciding with the closest passage of the typhoon to Hong Kong. Maximum 10-minutes mean wind speeds reached up to 55 ms^{-1} at CCH and 50 ms^{-1} at SSP, indicating near-surface wind intensities characteristic of a severe typhoon. These high wind speeds were sustained over several hours, particularly from early morning to mid-afternoon on 16 September, corresponding with the passage of stratiform rainbands across the region. The wind direction exhibited a dramatic shift during this period, rotating from a north-northeast orientation to the south-southeast as the storm centre moved relative to the observation sites, in agreement with the expected cyclonic circulation of Mangkhut (Figure 4.9).

One of the notable findings from the profiler data was the presence and variability of the tropical cyclone boundary layer (TBL) depth, which fluctuated in response to changing meteorological and topographic influences. At the SSP site, the TBL depth initially decreased from approximately 3 km at midnight to about 2 km around mid-morning, before gradually deepening again towards midnight the following day. Similarly, at the CCH site, the boundary layer depth decreased from around 2.5 km to 1 km over the same period, followed by relatively stable conditions thereafter. These variations were closely linked to the differing exposure of each site to prevailing winds and surrounding terrain. The rugged landforms near SSP allowed for a deeper, more turbulent boundary layer compared to the smoother, more open-sea exposure around CCH, where the TBL was consistently shallower.

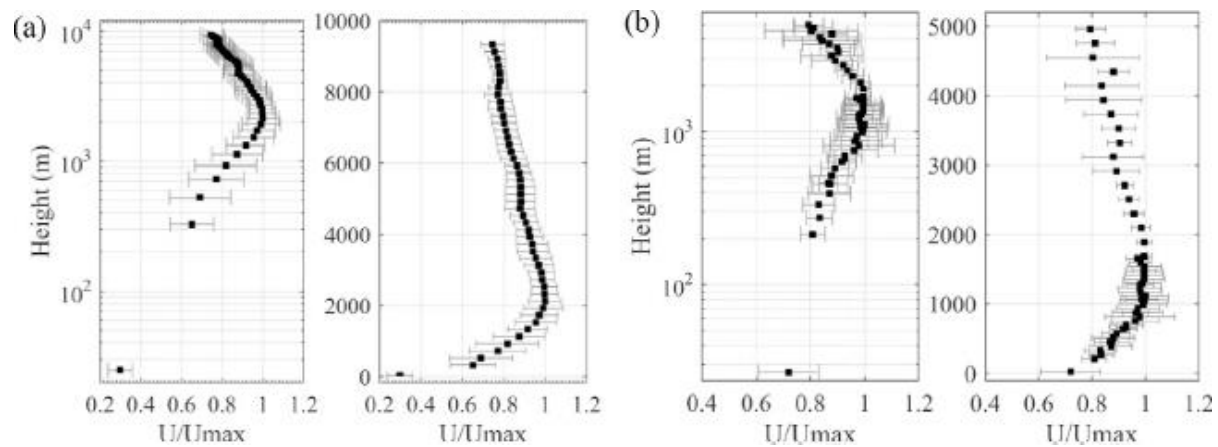
Figure 4.9

Mean horizontal wind speed and direction in Hong Kong



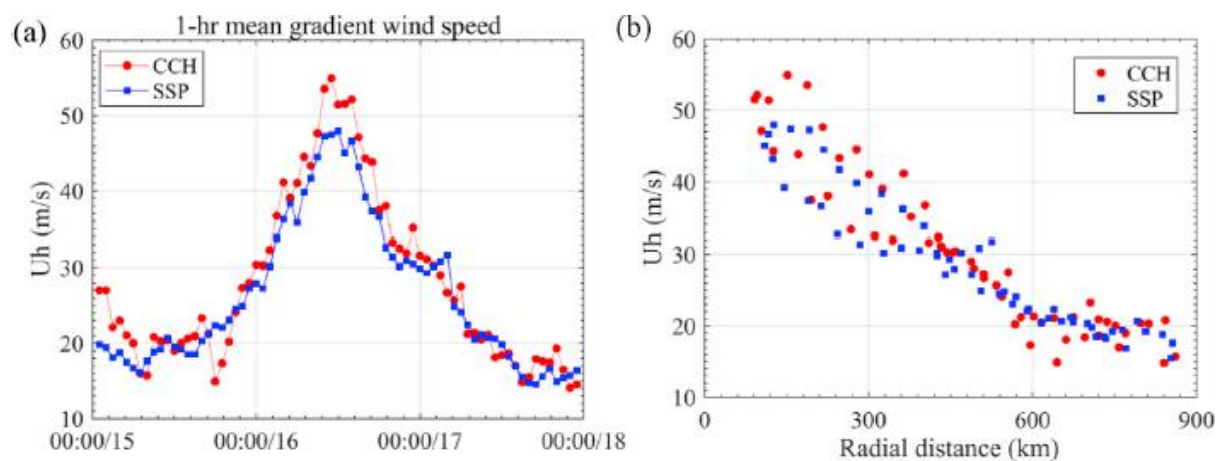
Note. Filled contour plots of mean horizontal wind speed (U) and direction (θ) from wind profilers at SSP and CCH (red lines denotes time history of the local normalised-pressure which reflects the storm-relative position of the site).

Vertical profiles of wind speed from both profilers demonstrated the existence of low-level jets (LLJs) within the inner region of the typhoon (Figure 4.10). These LLJs were predominantly centred between 1 and 3 km in altitude, although their exact height and strength varied depending on the site and the storm-relative position of the observation point. For instance, the jet maximum was observed around 2 km above SSP, accompanied by a marked decrease in wind speed with descending altitude below this level, indicative of surface frictional slowing and topographic shielding. At CCH, the LLJ was found slightly lower, near 1.5 km, and was less intense than at SSP. This vertical wind structure is closely associated with the super gradient wind dynamics typical of intense tropical cyclones, where winds near the surface are slowed by friction while stronger winds persist aloft.

Figure 4.10*Mean profiles of normalised speed in Hong Kong*

Note. Mean profiles of normalised speed (U/U_{\max}) above (a) Sham Shui Po and (b) Cheung Chau based on records during 9:00 a.m. to 2:00 p.m. on 16 September when Mangkhut's most inner region passed through Hong Kong.

Furthermore, the differences in surface wind measurements between sites underscored the significant impact of local terrain on wind flow patterns during the typhoon. While wind speeds near the surface varied considerably—reduced to 30% of the gradient wind at the rugged SSP site versus 72% at the more exposed CCH—the gradient wind speeds at higher altitudes above these locations showed much less variation (Figure 4.11). This finding suggests that, despite site-specific influences at near-surface levels, the broader wind field aloft remains relatively consistent and can be reliably characterised by gradient winds, which are vital for engineering and meteorological modelling.

Figure 4.11*Gradient wind speed from wind profiles in Hong Kong*

Note. Gradient wind speed recognised as the maximum mean speeds from wind profiles at Cheung Chau and Sham Shui Po—(a) time history; (b) radial distribution.

Overall, the wind profilers in Hong Kong during Mangkhut provided critical insights into the temporal and vertical variation of wind speeds and directions, the depth of the TBL, and the presence of LLJs within the cyclone's structure. These observations highlight the complex interplay between meteorological forces and local geographical features and emphasize the importance of detailed, high-resolution vertical wind profiling for understanding and mitigating the impacts of severe tropical cyclones on urban coastal environments.

4.2.8 Dropsonde

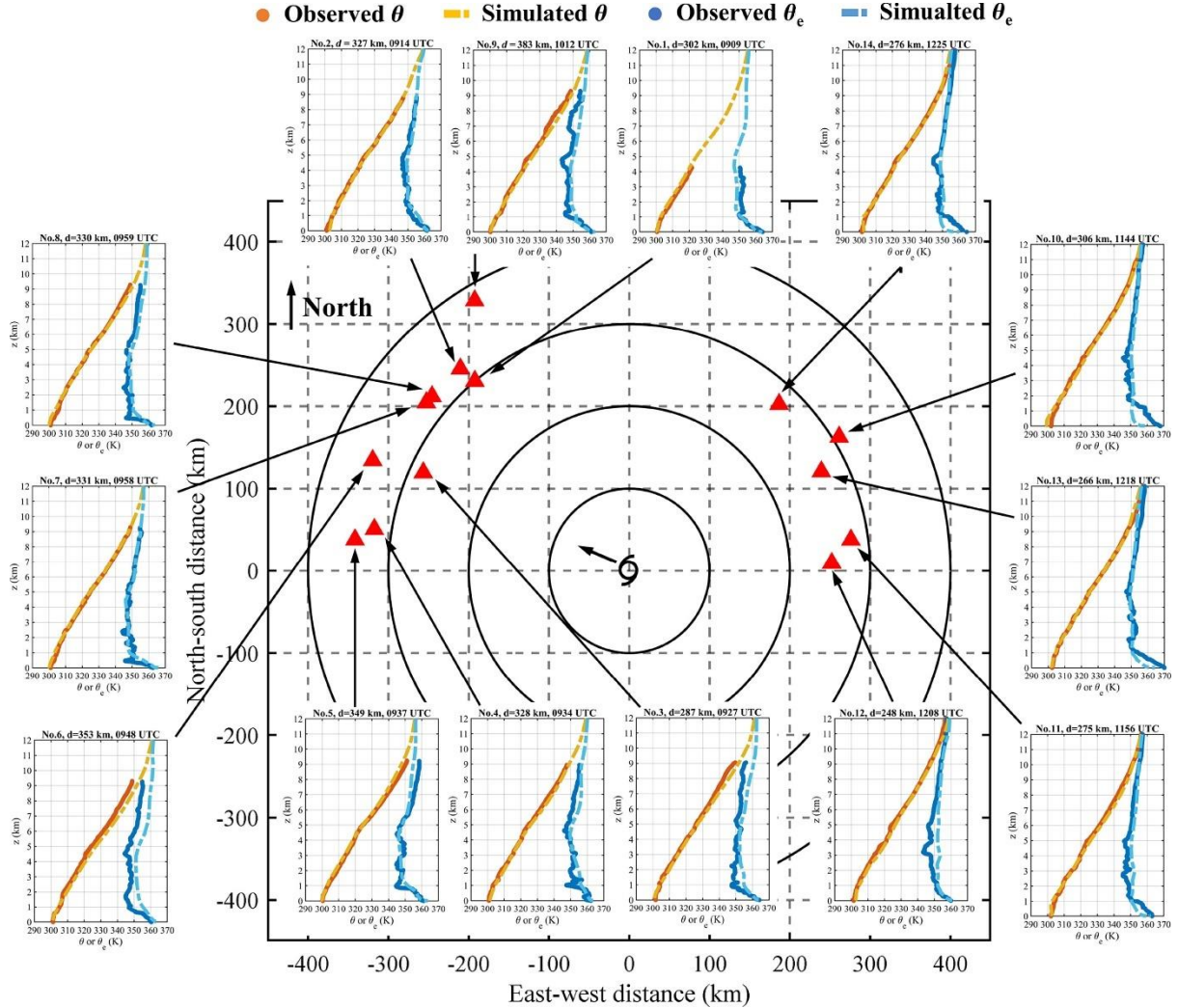
The dropsonde observations conducted by the HKO during Mangkhut provided critical insights into the storm's kinematic and thermodynamic structure as it intensified over the northern part of the South China Sea. These dropsondes, launched from a fixed-wing aircraft operated by the Government Flying Service (GFS), captured vertical profiles of wind speed, direction, temperature, humidity, and pressure from approximately 10 km altitude down to the surface. The data revealed strong inflow within the lower atmospheric boundary layer (below 3 km), consistent with Mangkhut's intensification trend. This inflow was observed across multiple quadrants of the storm, indicating a well-developed and symmetric circulation pattern, corroborated by satellite imagery showing extensive convective activity around the cyclone (He, Hon, Chan & Li, 2021).

Thermodynamic profiles from the dropsondes highlighted a steep gradient in equivalent potential temperature within the boundary layer, signalling atmospheric instability conducive to Mangkhut's intensification. This instability was observed uniformly around the storm, further supporting satellite-derived evidence of widespread convective development. The dropsonde data also confirmed the presence of a textbook warm-core structure, with higher equivalent potential temperatures near the storm's centre—a hallmark of intense tropical cyclones (Figure 4.12). These observations were pivotal for the real-time assessment of Mangkhut's intensity and provided valuable validation for NWP models.

The HKO's dropsonde missions during Mangkhut were constrained by operational limitations, such as the number of launch points and flight timing, yet they still yielded unprecedented three-dimensional data for tropical cyclones in the South China Sea. The dropsondes' high sampling frequency (4 Hz for wind and 2 Hz for thermodynamic variables) ensured detailed vertical resolution, capturing fine-scale features such as the inflow layer and boundary layer stability (Figure 4.13). These measurements were particularly valuable because they were taken while Mangkhut was still over open water, providing a clearer picture of the storm's natural evolution before landfall interactions complicated its structure.

Figure 4.12

Vertical profiles of potential temperature and equivalent potential temperature in Mangkhut

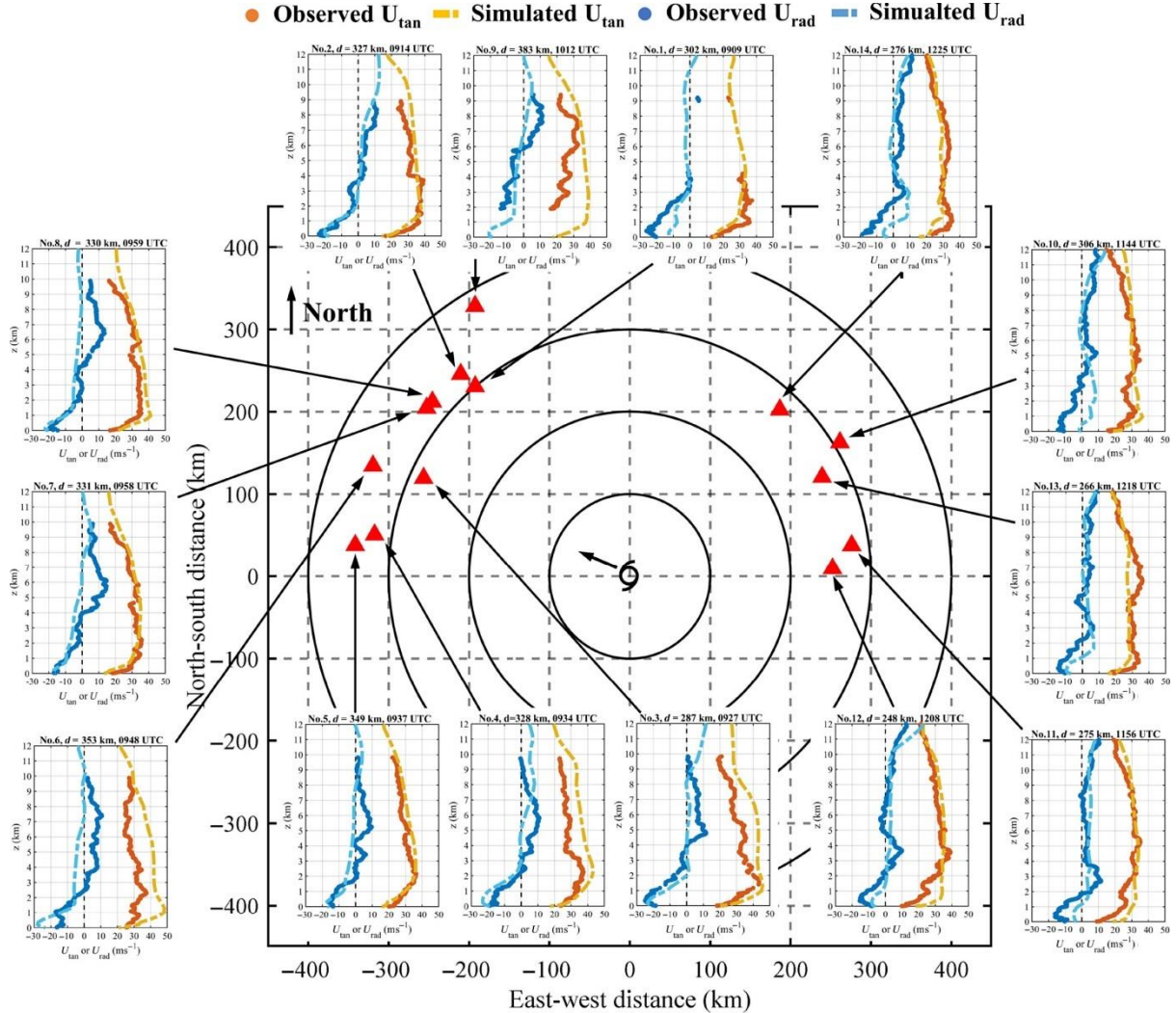


Note. Vertical profiles of potential temperature and equivalent potential temperature in Mangkhut at 5:00-8:00 p.m. on 15 September 2018. Red triangles represent dropsonde locations. Orange solid dots and dashed lines and respectively represent observed and simulated potential temperature θ (in K). Blue solid dots and dashed lines and respectively represent observed and simulated equivalent potential temperature θ_e (in K). z represents height above mean sea level (in km). d represents distance from storm centre (in km).

Comparisons with the Asian Aviation Meteorological Centre's WRF (AAMC-WRF) model simulations showed that the model reproduced key features observed by the dropsondes, including the inflow layer and boundary layer instability. However, discrepancies were noted, such as slight overestimations of potential temperature and tangential wind speed maxima near 1 km altitude. These findings underscore the model's strengths in capturing the broad dynamics of intensifying cyclones while highlighting areas for improvement in simulating finer-scale thermodynamic details.

Figure 4.13

Vertical profiles of tangential and radial wind speeds in Mangkhut



Note. Vertical profiles of tangential and radial wind speeds in Mangkhut at 5:00-8:00 p.m. on 15 September 2018. Red triangles represent dropsonde locations. Orange solid dots and dashed lines and respectively represent observed and simulated tangential wind speed U_{\tan} (in ms^{-1}), anti-clockwise positive. Blue solid dots and dashed lines and respectively represent observed and simulated radial wind speed U_{rad} (in ms^{-1}), outflow positive. z represents height above mean sea level (in km). d represents distance from storm centre (in km).

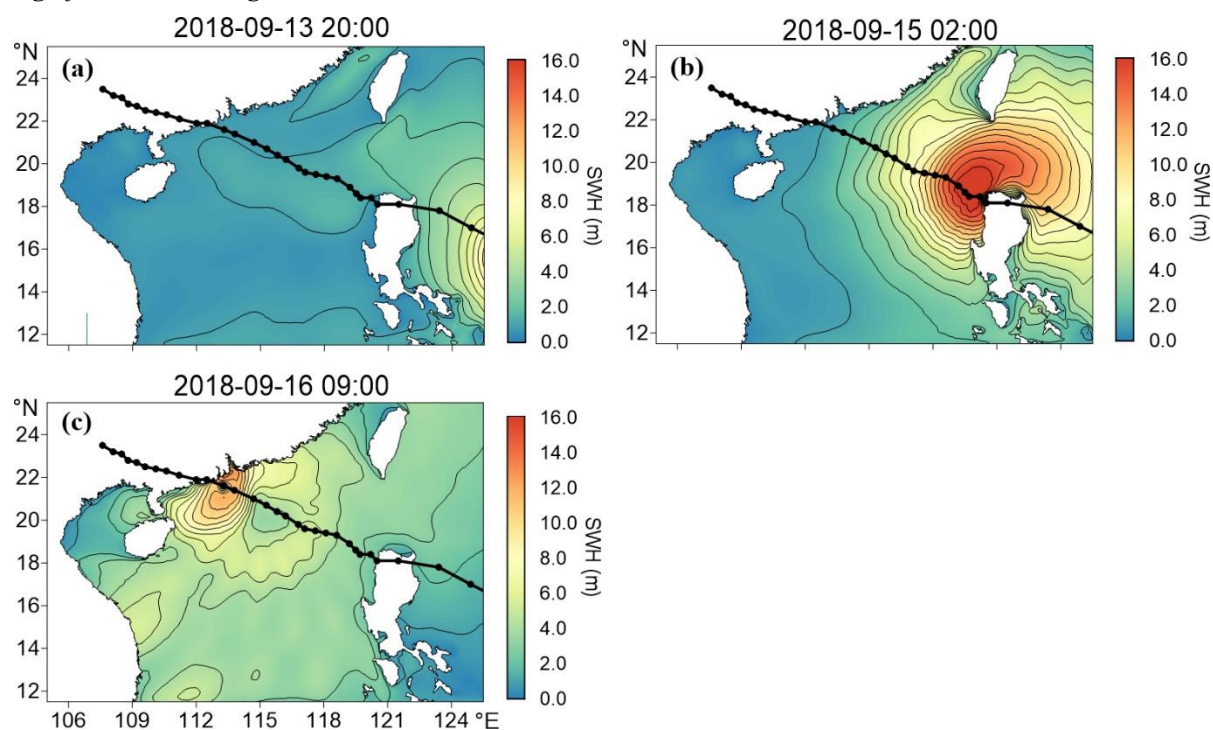
Overall, the dropsonde observations during Mangkhut demonstrated their utility in enhancing real-time cyclone monitoring and NWP model validation. The data provided a unique, observationally grounded understanding of the processes driving Mangkhut's intensification, complementing satellite and radar-based analyses. The success of these missions has paved the way for more extensive dropsonde deployments in future tropical cyclone events, promising further advances in forecasting and risk assessment for the South China Sea region.

4.2.9 Significant Wave Height at Buoy

As Mangkhut traversed the South China Sea, the wave field developed a counterclockwise rotation, mirroring the tropical cyclone's wind direction, with the highest wave heights typically observed on the right side of the cyclone's track due to the combined effects of wind speed and cyclone motion. The model results indicated that the maximum significant wave heights near the coast of Guangdong, including Hong Kong, reached up to 6 m as the storm approached. This extreme wave activity was driven by the intense cyclonic wind stress, which generated large waves that propagated toward the coast (Figure 4.14). However, upon entering shallower waters, the waves began to break and dissipate due to topographic changes and a reduced wind radius, leading to a rapid decline in wave heights (Yan, Hu, Ni & Qiu, 2024).

Figure 4.14

Significant wave height in South China Sea



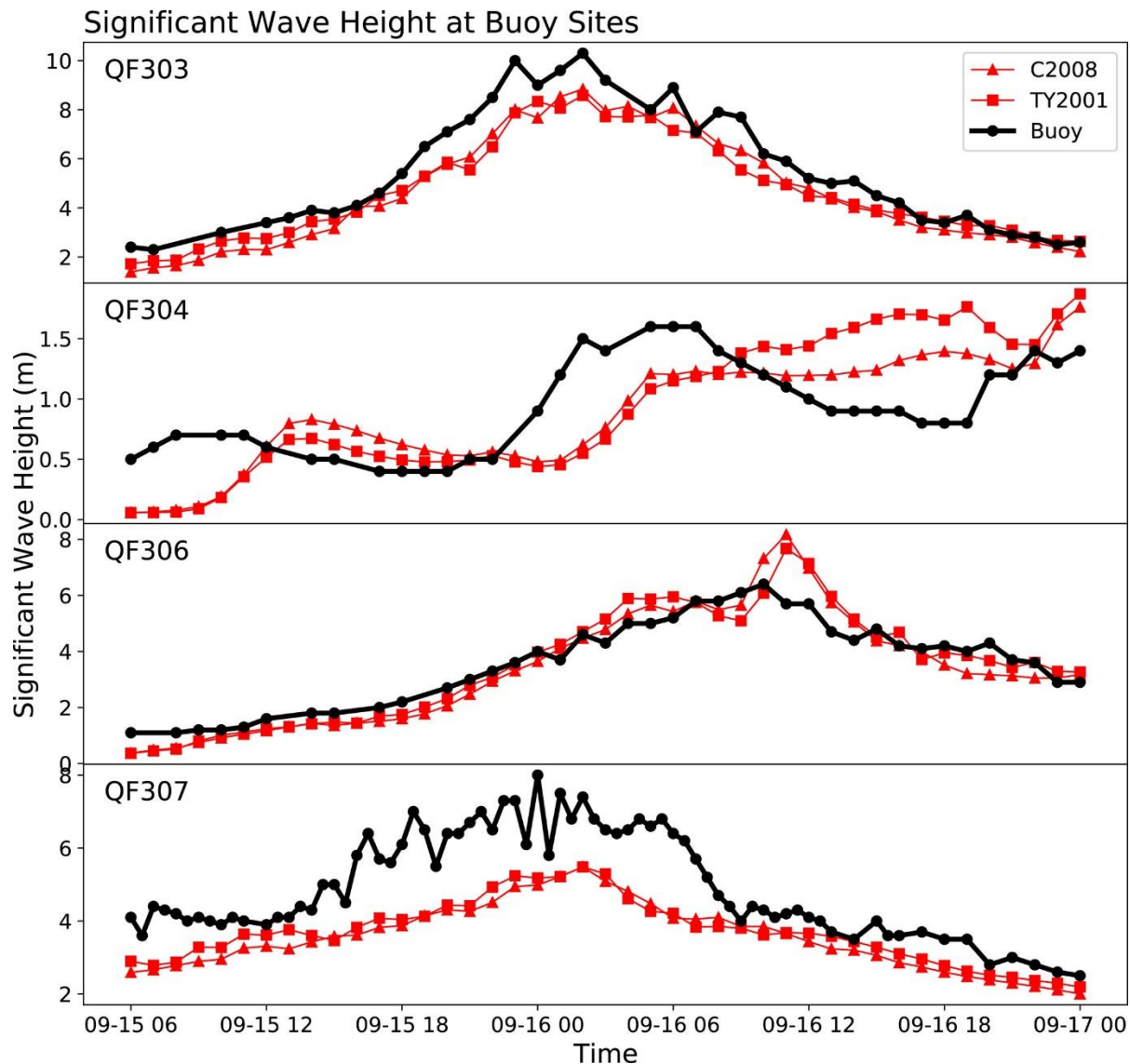
Note. Spatial distribution of significant wave height from 13 and 15-16 September during the passage of tropical cyclone Mangkhut.

The validation of significant wave heights using buoy data demonstrated a strong agreement between simulated and observed values, with correlation coefficients exceeding 0.9 at most stations. For instance, buoy stations QF303 and QF305, located to the right of the tropical cyclone's track, recorded maximum wave heights of 10.4 m and 10.2 m, respectively, while QF306, situated on the left side, observed a lower maximum of 7.1 m (Figure 4.15). The temporal lag between wind speed

and wave height was minimal—approximately 1 hour—highlighting the rapid response of wave development to the tropical cyclone’s wind field.

Figure 4.15

Maximum wave heights in South China Sea



Note. Significant wave height (m) from model based on C2008 and TY2001 (coloured lines) and observations (black line) at buoy site QF303, QF304, QF306, and QF307.

In Guangdong, wave conditions during Mangkhut were particularly severe due to the region’s proximity to the storm’s path and its exposure to the right-side wind field, where wave energy was concentrated.

4.3 China Weather Stations

4.3.1 Wind Speed

The wind speed in Taishan, Guangdong, during Mangkhut was exceptionally high, prompting the China Meteorological Administration (CMA) to issue red alerts for extreme winds. Mangkhut made landfall in Taishan on 16 September. The highest mean wind speeds recorded at the Taishan Nuclear Power Plant, Neilingding South of Shenzhen, Mangyu Dao of Shenzhen, Xichong Base of Shenzhen and Zhuhai were 210 kmh^{-1} , 147 kmh^{-1} , 124 kmh^{-1} , 120 kmh^{-1} and 117 kmh^{-1} , while the gusts peaked at Sanmen Island of Huizhou, Xichong Base of Shenzhen, Neilingding South of Shenzhen and Mangyu Dao of Shenzhen were 226 kmh^{-1} , 189 kmh^{-1} , 173 kmh^{-1} and 165 kmh^{-1} . These extreme winds caused catastrophic damage, including collapsed buildings, uprooted trees, and widespread power outages, underscoring the typhoon's unprecedented intensity.

Table 2.8

Maximum mean wind speeds and gusts in Pearl River Estuary

Station	Maximum Mean Wind Speed (km/h)	Maximum Gust (km/h)
Neilingding South	147	173
Xichong Base	120	189
Mangyu Dao	124	165
Taishan Nuclear Power Plant	210	-
Sanmen Island	-	226

Note. Maximum mean wind speeds and maximum gust peak winds with recorded at various stations on 16 September 2018 by the CMA.

4.3.2 Mean Sea Level Pressure

Mangkhut was associated with exceptionally low MSLP across Pearl River Estuary as it made landfall, reflecting its intense cyclonic circulation. The lowest instantaneous MSLP recorded at the Taishan Nuclear Power Plant was 965.7 hPa.

4.3.3 Storm Surge

Mangkhut caused significant storm surge impacts in the Pearl River Estuary, which were comprehensively analysed using an assimilated tropical cyclone wind-pressure field model combined with the TELEMAC-2D hydrodynamic model (Lai, Li, Wang, Chen, Feng, Yuan, Li, Liu, Kong & Xu,

2025). The wind-pressure field model employed a gradient wind balance to derive surface winds from the tropical cyclone's pressure distribution, expressed as:

$$V_g(r) = \sqrt{\frac{r}{\rho} \frac{\partial P}{\partial r} + \left(\frac{fr}{2}\right)^2} - \frac{fr}{2} \quad (23)$$

where $V_g(r)$ is the gradient wind speed at radius r , ρ is air density, $\frac{\partial P}{\partial r}$ is the radial pressure gradient, and f is the Coriolis parameter. This wind field was then coupled with the TELEMAC-2D model, which solved the depth-averaged shallow water equations:

$$\frac{\partial h}{\partial t} + \nabla \cdot (hu) = 0 \quad (24)$$

$$\frac{\partial u}{\partial t} + u \cdot \nabla u = -g\nabla\eta + \frac{\tau_s - \tau_b}{\rho h} + v\nabla^2 u \quad (25)$$

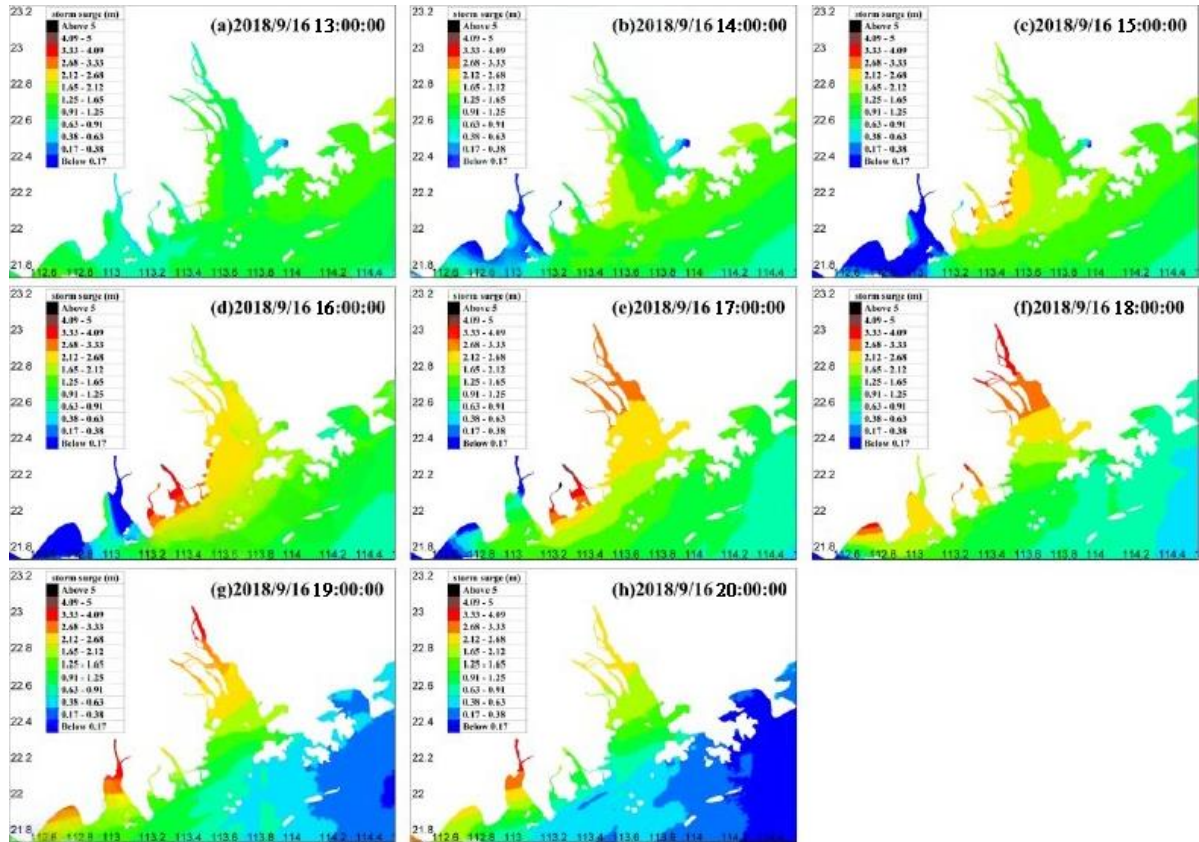
where h is water depth, u is depth-averaged velocity, η is water surface elevation, τ_s and τ_b are surface wind stress and bed shear stress, and v is eddy viscosity. The model captured the complex process whereby, prior to landfall, strong winds pushed water toward the western shore of the estuary, creating a distinctive west-high, east-low surge pattern due to wind forcing. The surge level exhibited a rising and falling trend over time, with most affected areas reaching peak storm surge at or shortly after the time of landfall.

The storm surge in the Pearl River Estuary demonstrated a distinct pattern of progressive intensification, beginning early on 16 September and peaking around 6:00 p.m. Early in the morning, surge levels near the estuary's coastlines rose from low values (below 0.17 m offshore) to more moderate surges (between 0.91 and 1.65 m) concentrated centrally in the estuary. As Mangkhut approached landfall, surge heights escalated substantially, particularly in shallow and enclosed areas such as the Modaomen Waterway and Lingdingyang Bay, where localised surges exceeded 5 m (Figure 4.16). The TELEMAC-2D analysis revealed that these extreme surges were amplified by the nonlinear advection terms in the momentum equations, chiefly in areas where the estuary's bathymetry funnelled water into narrowing channels.

Spatially, the highest storm surges were concentrated in the western region, especially near shallow bay-top areas, while the eastern regions experienced relatively lower surge levels. The surge distribution was strongly influenced by the tropical cyclone's path and regional bathymetry, with surge heights and timing shifting eastward as the landfall location changed. This sensitivity indicates the critical role of the landfall location on surge impact, as areas closer to the tropical cyclone's radius of maximum wind speed experienced amplified surge heights.

Figure 4.11

Storm surge in the Pearl River Estuary

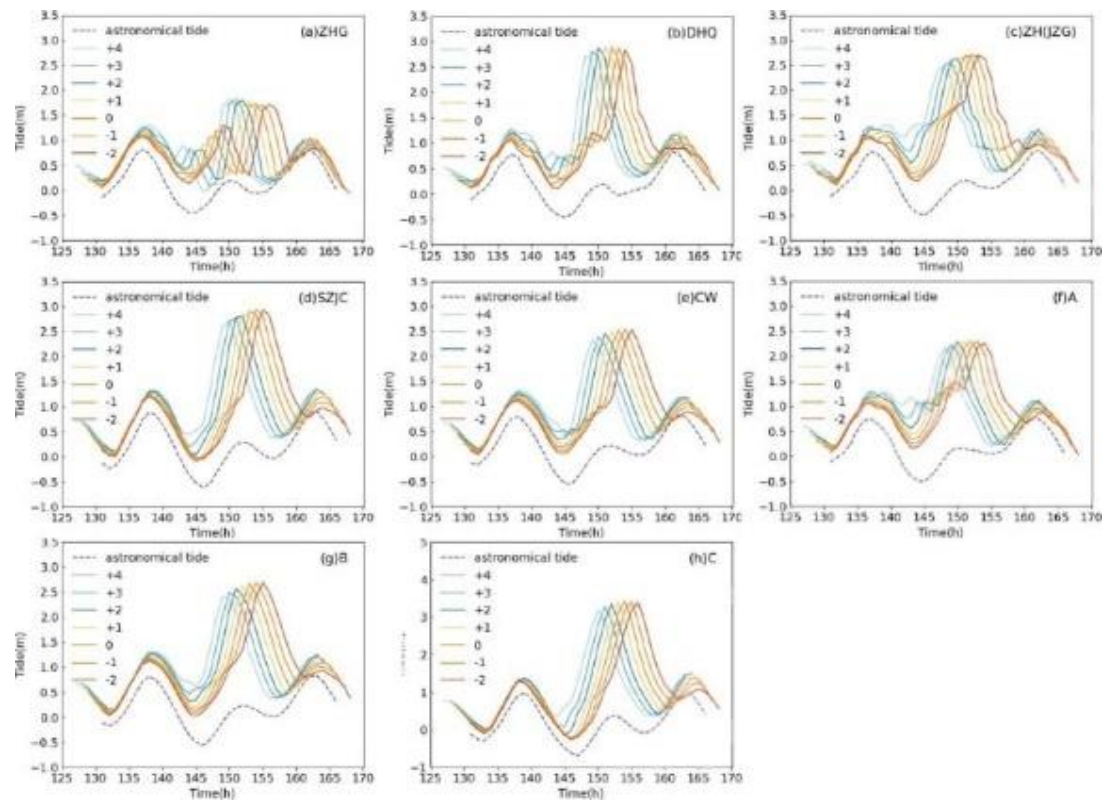


Note. Spatial distribution of storm surge in the Pearl River Estuary at 1:00 p.m. to 8:00 p.m. on 16 September 2018 (Lai et al., 2025).

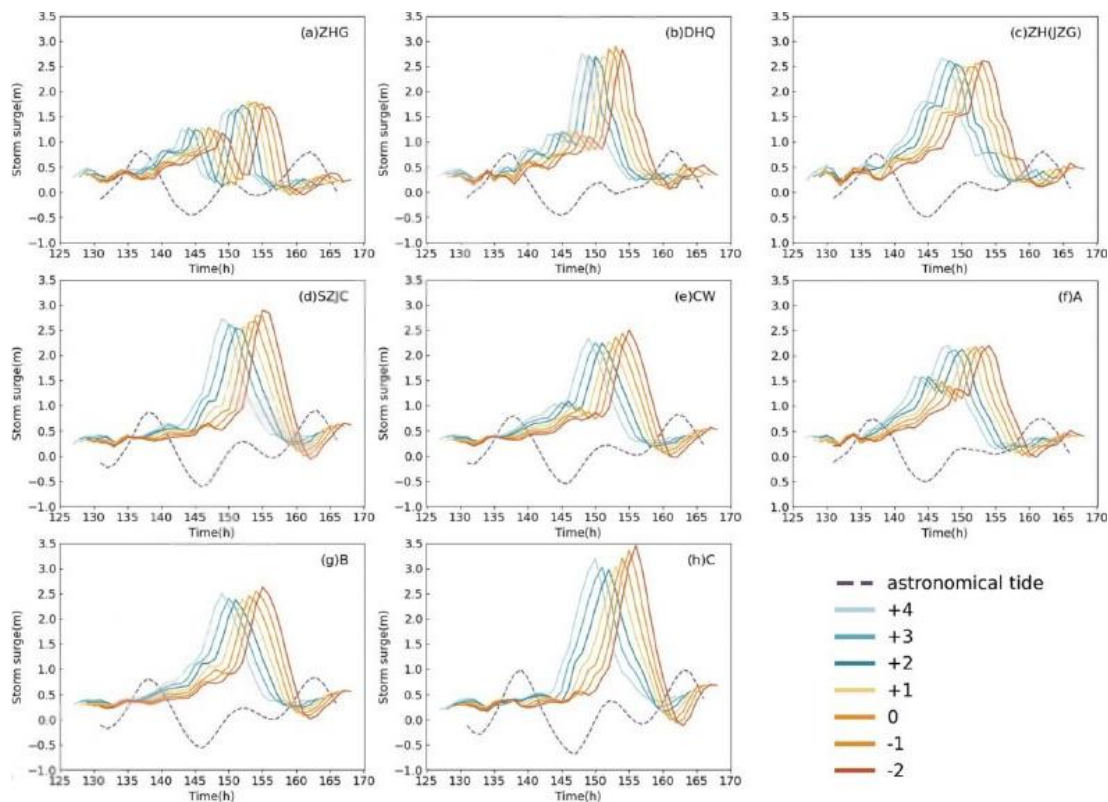
Temporal analysis highlighted the interaction between storm surge and astronomical tides (Figure 4.17). Both the model and observations demonstrated that Mangkhut's storm surge was smaller during high astronomical tide periods compared to low tide, consistent with theoretical findings on tide-surge interaction (Figure 4.18). The TELEMAC-2D results further quantified this damping effect through the nonlinear coupling term $\eta_{\text{surge}} \propto \eta_{\text{tide}}^{-\alpha}$, where α is an empirical coefficient representing tidal phase modulation. However, the total water level (storm tide) was typically higher when the peak surge coincided with high tides, increasing the risk of flooding.

Figure 4.17

Time series of storm surge and astronomical tides at each station in the Pearl River Estuary

**Figure 4.18**

Time series of the storm surge at each station in the Pearl River Estuary



Changes in tropical cyclone parameters also affected the surge response. A lower minimum central pressure intensified the peak surge, especially in shallow coastal areas and inner bays, underscoring their sensitivity to pressure changes, as quantified by the inverted barometer effect:

$$\Delta\eta = \frac{P_a - P_c}{\rho g} \quad (26)$$

where $\Delta\eta$ is the surge height caused by pressure difference, P_a is the reference atmospheric pressure (usually around standard sea level pressure), P_c is the central pressure of the cyclone (lower than P_a), ρ is the density of seawater and g is the acceleration due to gravity. Moreover, variations in Mangkhut's forward speed had complex effects: slower movement increased water levels before and after landfall, lengthening the surge duration, while the timing of the peak surge shifted accordingly.

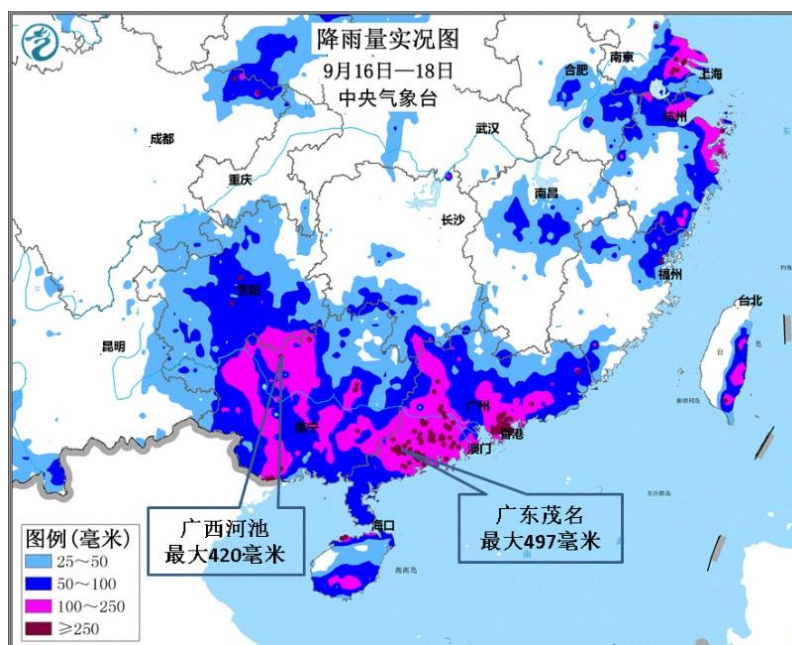
These observations highlight the complex interplay among tropical cyclone characteristics, bathymetry, and tidal effects on storm surge impacts, providing critical insights for coastal disaster preparedness in the Pearl River Estuary.

4.3.4 Rainfall Distribution

Under the circulation of Mangkhut, there was heavy rain and squall thunderstorms over South China. The total rainfall recorded at Maoming, Sijiu, and Taishan was 497 mm, 379 mm, and 157 mm, respectively, while most parts of the territory received over 200 mm of rain between 16 and 18 September (Figure 4.19).

Figure 4.19

Total rainfall distribution in South China from 16 to 18 September 2018



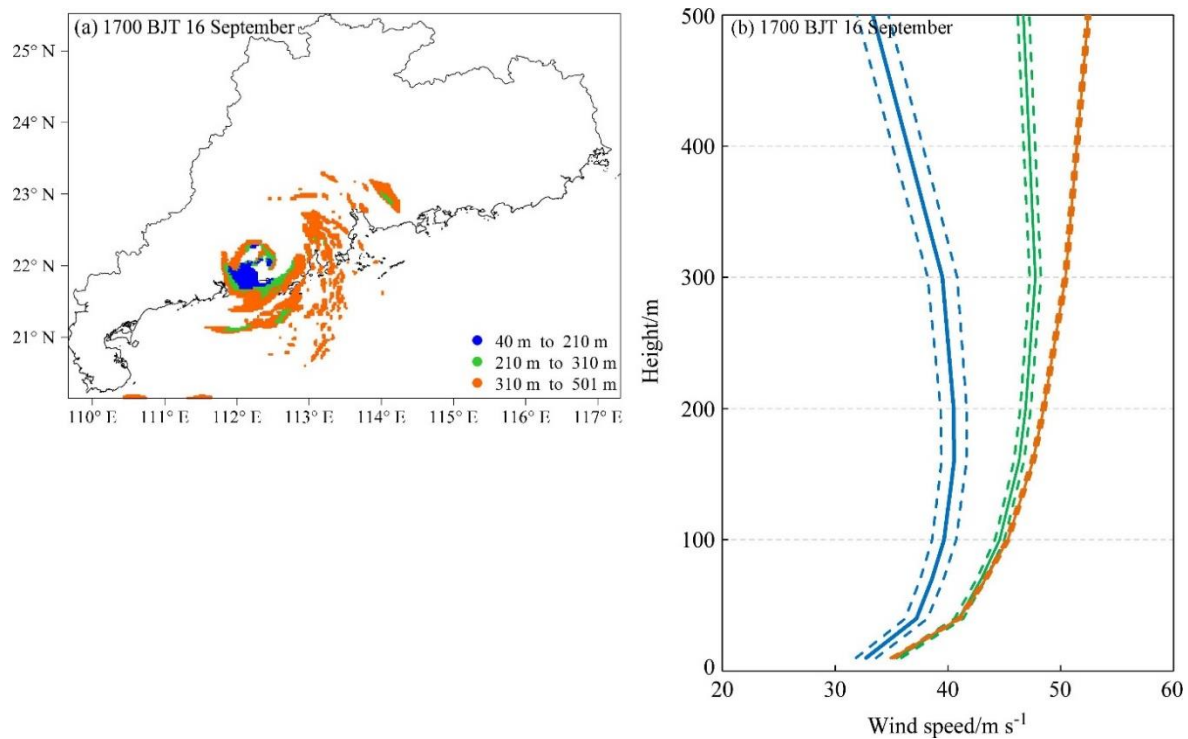
4.3.5 Wind Profilers

The wind profiler at Taishan during Mangkhut revealed significant variations in wind speed across different altitudes, as shown in Figure 4.20 (Rui, Rong & Dajun, 2022). At lower heights of 0-100 m, wind speeds ranged from 20 to 30 ms⁻¹, indicating strong surface-level winds typical of a severe typhoon. As altitude increased to 200-300 m, wind speeds intensified to 40-50 ms⁻¹, reflecting enhanced momentum transfer and turbulence aloft. The highest recorded speeds, up to 60 ms⁻¹, occurred near 400 m, likely due to the tropical cyclone's intense core circulation and jet-like features at mid-levels.

These profiles underscore the tropical cyclone's multi-layered wind structure, with wind speeds escalating at higher elevations. Such data are critical for understanding storm dynamics, assessing structural risks, and improving predictive models for future tropical cyclones. The pronounced shear between layers also highlights potential hazards for aviation and tall infrastructure.

Figure 4.20

Mean wind profilers in Taishan of Jiangmen City



Note. The heights (lower than 500 m) of maximum wind speed (a) during the landfall of Mangkhut on 16 September 2018. The maximum wind speed denotes the maximum value of the horizontal wind speeds in the different heights. Typical wind profiles of winds averaged over the blue, green, and orange areas in (b). The solid and dashed lines denote the mean value and 95% confidence level, respectively.

5. Disaster Statistics

5.1 Philippines Damage Situation

Mangkhut (locally named Ompong) made landfall in Baggao of Cagayan province, on 15 September, leading to widespread devastation across Luzon (Table 3.1). The storm resulted in approximately 82 deaths, with most fatalities caused by landslides triggered by intense rainfall (Figure 5.1). In addition to the fatalities, there were 138 injuries and 2 people reported missing.

Table 3.1

Assessment of damages and direct economic loss in the Philippines

Casualties	
Death	82 people
Injure	138 people
Disappearance	2 people
Natural Hazard	
Flooring	402 cases
Electricity Outages	198 cases
Damages	
House	210,500
Road	325
Bridge	8
Loss of Economic	
Agriculture	₱26,769,717,988.00
Infrastructure	₱7,161,016,082.22
Total Cost of Damage	₱33,930,734,070.22

The storm severely impacted agriculture, infrastructure, and human settlements, affecting over 600,000 families across 31 provinces (National Disaster Risk Reduction and Management Council [NDRRMC], 2018). The total cost of damage was ₱33,930,734,070.22 (US\$595,370,036.36), including agricultural losses of ₱26,769,717,988.00 (US\$469,718,336.74) and infrastructure damages of ₱7,161,016,082.22 (US\$125,651,699.62).

The agricultural sector suffered catastrophic losses, with approximately 80% of crops destroyed in Claveria, Cagayan (Figure 5.2). More than 171,932 farmers were affected, particularly in the Cordillera Administrative Region (CAR), where livelihoods were severely disrupted (Dadey, 2018).

Figure 5.1

The catastrophic landslide in Itogon, Benguet



Note. Majority of the casualties were caused by landslides. The victims were either buried by falling soil, hit by rocks or carried away by the debris (Cordillera Disaster Response and Development Services [CorDisRDS], 2018).

Figure 5.2

Damage to agriculture and livelihood in Conner, Apayao



Note. Corn field damaged by tropical cyclone Mangkhut in Conner, Apayao (CorDisRDS, 2018).

Housing infrastructure was heavily damaged, with 210,500 houses reported as damaged or destroyed in Regions I, II, III, and CAR (Figure 5.3; Dadey, 2018). The number of damaged homes rose sharply from 1,264 to 44,599 within 24 hours, highlighting the tropical cyclone's rapid and destructive impact. Thousands were displaced, with 13,949 families (54,935 persons) initially sheltering in 390 evacuation centres, although many began returning home to assess the damage (Dadey, 2018).

Humanitarian response efforts were coordinated by the IOM, the Philippine government, and local agencies. Emergency shelter kits and non-food items were mobilised for 2,000 families, while displacement tracking and mental health support were prioritised. The Department of Social Welfare and Development (DSWD) collaborated with IOM to address gaps in shelter and camp management; however, challenges persisted in accessing remote areas and restoring basic services such as power, which was only partially restored in 111 of the 198 affected areas.

Figure 5.3

Damage to gymnasium in Luzon



Note. Mangkhut destroyed a gymnasium used by the community of Buguey in northern Luzon (Morgerman, 2018).

5.2 Hong Kong Damage Situation

Mangkhut, which struck Hong Kong on 16 September, was one of the most powerful storms recorded in the region (Table 3.2), causing widespread destruction across the city (Choy, Wu, Lee & HKFI, 2020). Although no fatalities were reported, the storm caused significant casualties with 458 injuries mainly due to flying debris, shattered glass, and structural damages. Approximately 1,800 people were displaced, with around 20,000 individuals seeking emergency refuge during the storm, reflecting the scale of human disruption.

Table 3.2

Assessment of damages and direct economic loss in Hong Kong

Casualties	
Death	0 people
Injure	458 people
Disappearance	0 people
Victim	322 people
Temporary Shelter(s)	
No. of Opening	53
Displaced Persons	1800 people
Natural Hazard	
Flooding	83 cases
Landslide	18 cases
Electricity Outages	> 40000 households
Fresh Water Outages	16 places
Property Damage(s)	
No. of Fallen Trees	61388 trees
Damages of Smashed Windows or Glass Curtain Walls	500 cases
No. of Damages of Sewage Treatment Works	3 unit
Damages of Building	1930 cases
Infrastructure Damage(s)	
Public Beaches	41 sites
Public Swimming Pool	4 unit
Waterfront Promenades	22 unit
Sports Ground	4 unit
Stadium	4 unit
Water Sports Centre	5 unit
Rest Garden	130 unit

Infrastructure Damage(s)	
Road	5 sites
Traffic Lights	170 unit
Construction Sites	5
Fill Bank	1 site
Harbour	18
Seawalls and Breakwaters	8 sites
Radar Stations	2
Agricultural Losses	
Farmland	567 hectares
Crops	4143 tons
Pond Fish	885 tons
Transportation Damage(s)	
Railway Damages	5 sites
No. of Ships Lost	708
Telecommunication Facility Damage(s)	
Transmitting Station	1 site
Traffic Impacts (Suspension Services)	
Bus	2 – 2.5 days
Tram	1 day
MTR (East Rail Line from Tai Po Market to Sheung Shui Station)	1.5 – 2 days
Light Rail (Part of Route)	1.5 – 2 days
Ferry	1 day
International Airport	889 flights
Emergency Help	
Save Our Souls	20000 people
Direct Economic Losses	
Amount	HK\$4,598,145,635

Note. At least 35 years were damages not seen in Hong Kong during the passage of Mangkhut.

The storm's extreme winds and heavy rainfall led to unprecedented infrastructural destruction. A record 61,388 trees were uprooted or toppled—the highest number documented in a single event—contributing to injuries and widespread transport obstructions (Figure 5.4). Structural damage was extensive, with 1,930 reported incidents, including shattered glass curtain walls in commercial districts such as Hung Hom, Wan Chai, Central, and Mong Kok (Figure 5.5), as well as broken windows in residential buildings across Tseung Kwan O. Critical public amenities suffered severe impairment, including damage to 41 public beaches (Figure 5.6), 22 waterfront promenades (Figure 5.7), four stadiums (Figure 5.8), and 170 traffic light units.

Figure 5.4

Fallen trees in many parts of the territory



Note. The passage of Mangkhut resulted in fallen trees in many parts of the territory (Kung, 2018).

The storm's torrential rainfall and 3 to 5 m storm surges triggered severe flooding, particularly in low-lying coastal areas (Figure 5.9). Neighbourhoods such as Tai O, Lei Yue Mun, and Tsang Tai Uk experienced waist-deep inundation, forcing large-scale evacuations (Figure 5.10). Seawater intrusion submerged underground car parks in Heng Fa Chuen and Tseung Kwan O (Figure 5.11), destroying hundreds of vehicles. Low-lying infrastructure, including cycle tracks along the Shing Mun River (Sha Tin) and Lam Tsuen River (Tai Po), was extensively flooded (Figure 5.12). Landslides exacerbated the damage, with reports of slope failures in Sai Kung and the New Territories, which blocked major roads and delayed recovery efforts (Figure 5.13).

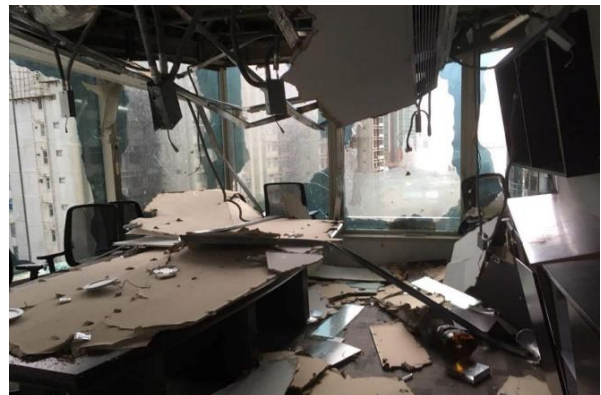
During Typhoon Mangkhut's onslaught, Hong Kong's sea, land, and air transport systems were paralysed (Choy, Wu, Lee & HKFI, 2020). Fallen trees and flooding forced the closure of major roads, delaying the full resumption of public transport until the following day. The majority of public bus services remained suspended, while MTR's East Rail Line and Light Rail operated at limited capacity. Ferry services experienced prolonged delays due to damaged terminals, and Hong Kong International Airport cancelled 889 flights amid the chaos. Power outages affected over 40,000 households, with 13,500 enduring blackouts lasting more than 24 hours; some remote areas remained

without electricity for up to four days. Freshwater supply was interrupted in 16 locations due to pump failures, compounding residents' hardships.

Figure 5.5

Shattered glass curtain walls in commercial districts

Hung Hom



Wan Chai



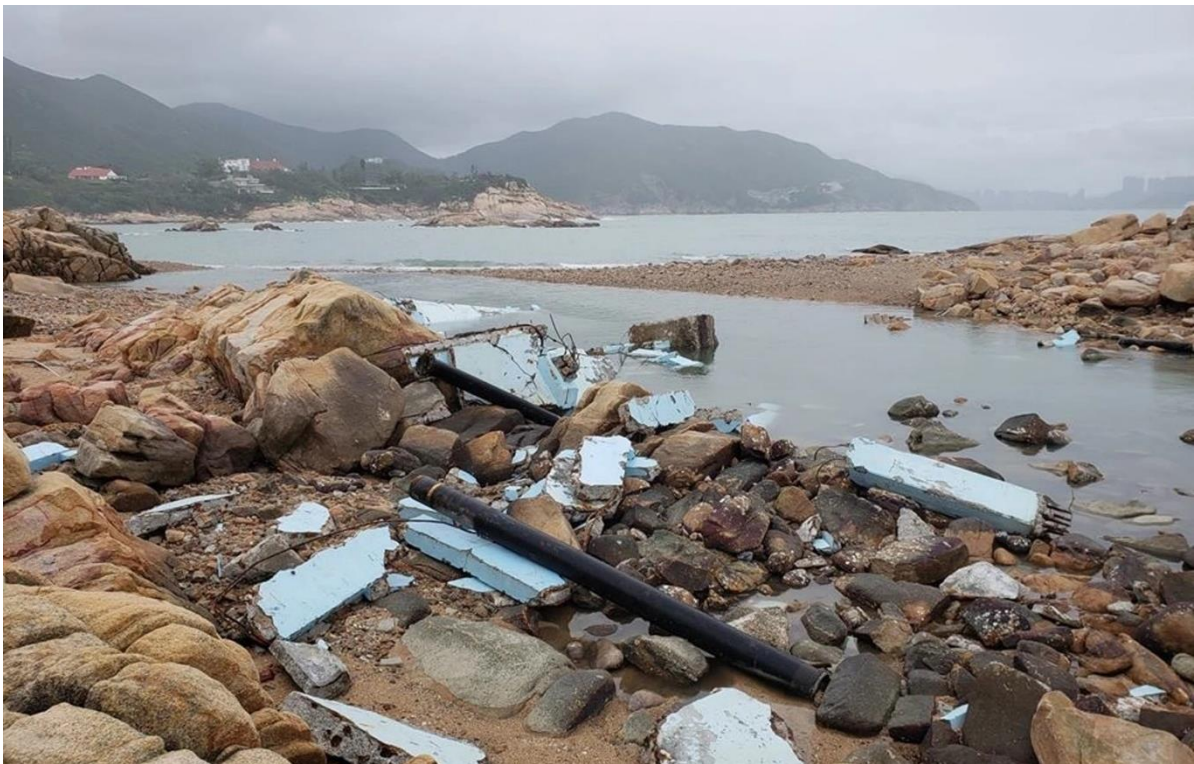
Mong Kok



Note. Shattered glass curtain walls during the passage of Mangkhut (Wong; Shun; Tang, 2018).

Figure 5.6

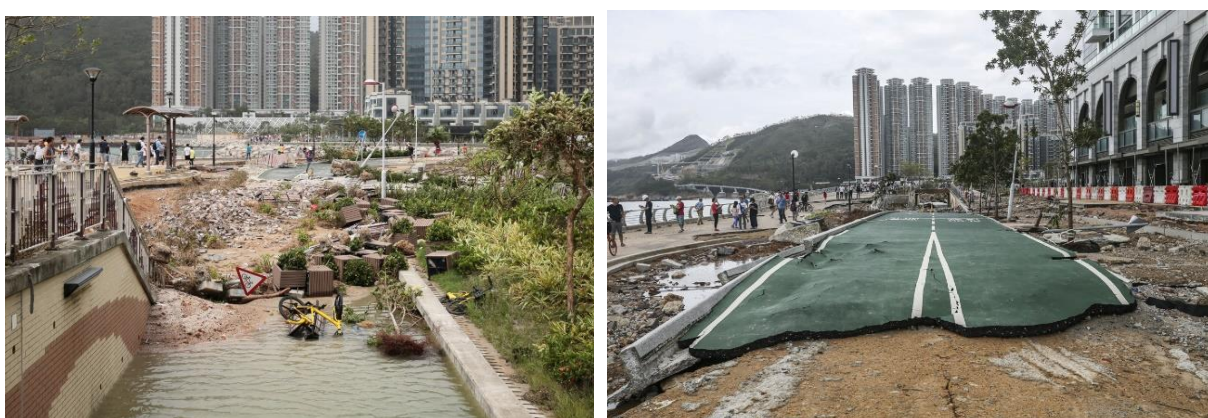
Damage to Lovers Bridge in Shek O beach



Note. The well-known tourist spot “Lovers Bridge” in Shek O was totally destroyed by the monster tropical cyclone Mangkhut on 16 September 2018 by Hon.

Figure 5.7

Damage to Tseung Kwan O South waterfront promenade



Note. The promenades and facilities in the TKO Waterfront Park were substantially damaged (Kao, Cheung, Xinqi & Cheung, 2018).

Figure 5.8

Damage to the Siu Sai Wan Sports Ground in Chai Wan



Note. The Siu Sai Wan Sports Ground was damaged by Mangkhut (Lam, 2018).

Figure 5.9

Severe flooding in low-lying coastal areas

Heng Fa Chuen



Tseung Kwan O

Note. Severe inundation triggered by storm surge and huge waves were observed in a number of coastal areas (Fong; Lai; Liu; Chan; Wong; Bastille Post, 2018).

Figure 5.10

Flooding in Tai O and Lei Yue Mun

Tai O**Lei Yue Mun**

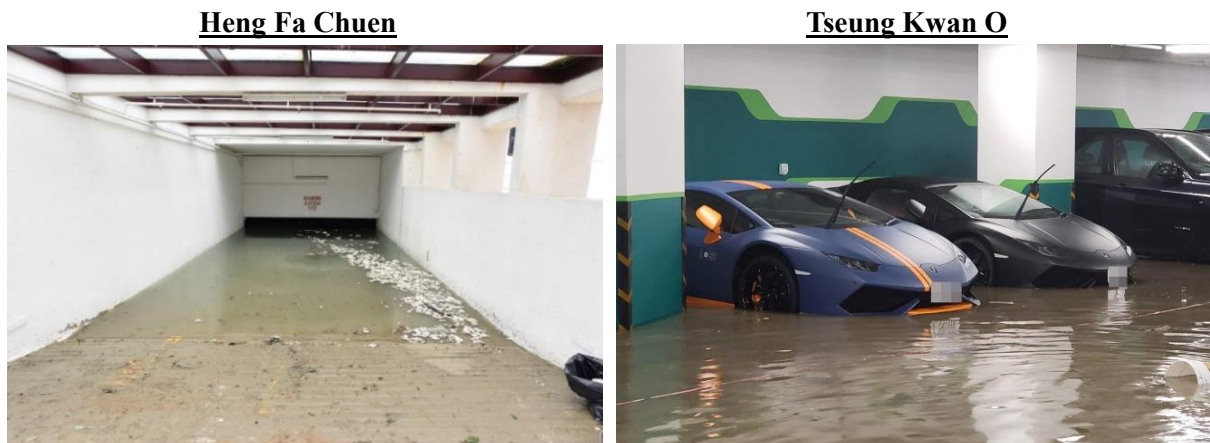
Note. The flood caused by seawater intrusion submerged houses during the evacuation (Nip, 2018).

The agricultural sector suffered devastating losses, including 567 hectares of ruined farmland, 4,143 tons of destroyed crops, and 885 tons of lost pond fish. Coastal industries were equally affected,

with hundreds of vessels sunk or severely damaged by high waves and storm surges (Figure 5.14). The total direct economic loss reached HK\$4,598,145,635 (US\$585,762,600.50), encompassing property damage, infrastructure repairs, and business interruptions.

Figure 5.11

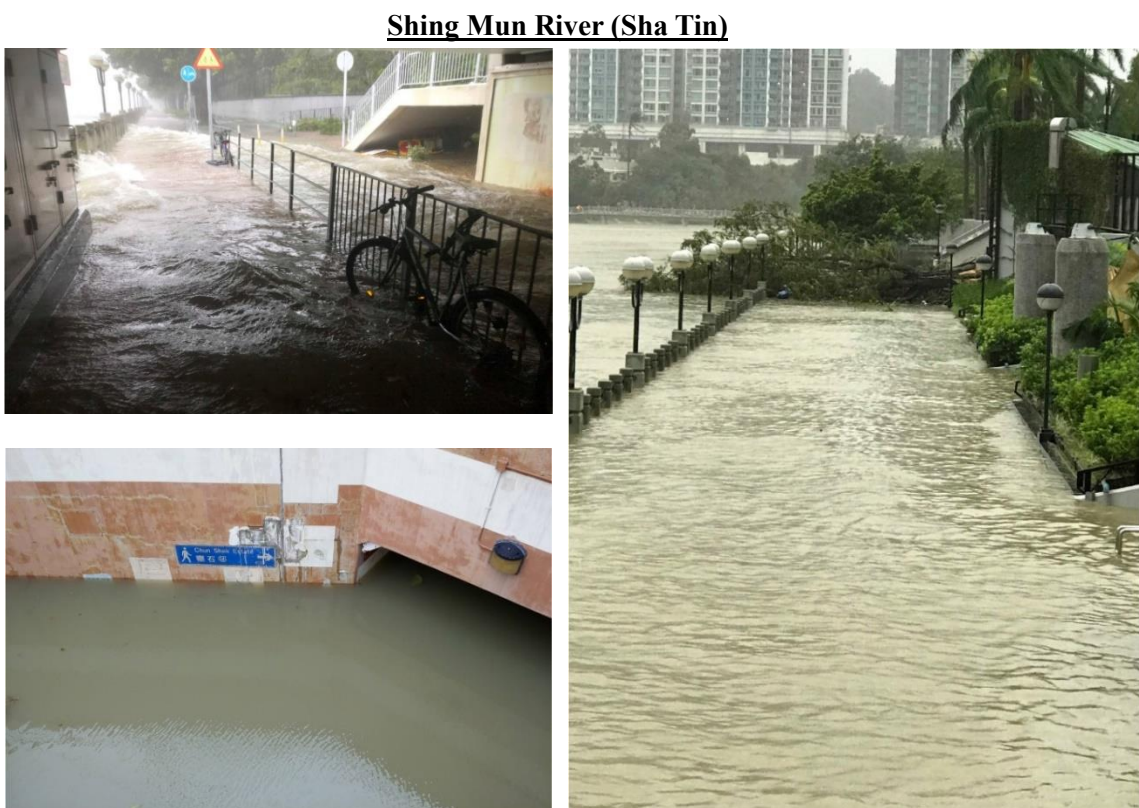
Seawater intrusion submerged underground car parks in Heng Fa Chuen and Tseung Kwan O



Note. Sea water flowed into the estates and underground car parks in Hung Fa Chuen and Tseung Kwan O south, submerging a number of private vehicles inside (Chan; Sing Tao Daily, 2018).

Figure 5.12

Severe flooding in cycle tracks along the Shing Mun River and Lam Tsuen River



Lam Tsuen River (Tai Po)



Note. The cycle tracks and subways near Shing Mun River in Shatin, Lam Tsuen River in Tai Po were inundated (Tang; Chan; Ho, 2018).

Figure 5.13

Landslide in Sai Kung



Note. Landslides, including slope failures in Sai Kung that blocked major roads, worsened the damage. (Hong Kong Slope Safety, 2018)

Overall, Mangkhut's multifaceted impacts—record-breaking tree losses, structural destruction, catastrophic flooding, landslides, and prolonged utility failures—highlight Hong Kong's vulnerability

to extreme tropical cyclones. The event underscores the need for enhanced climate resilience in urban planning, particularly in coastal defence and the protection of critical infrastructure.

Figure 5.14

Vessels sunk or severely damaged by high waves and storm surges in Sham Wan and Sai Kung

Sham Wan



Sai Kung



Note. The powerful storm surges and high waves generated by Mangkhut produced extensive damage to maritime vessels in Sham Wan and Sai Kung, with hundreds of boats either severely damaged or sunk (Asia Boating Limited; Hong Kong Boating Industry Association [HKBIA], 2018). The Sai Kung area was notably impacted, suffering significant destruction as luxury yachts, dinghies, and other watercraft were violently tossed ashore or battered by the extreme conditions.

5.3 China Damage Situation

Mangkhut wreaked havoc across Guangdong and Guangxi provinces when it made landfall on 16 September, leaving a trail of human casualties and widespread destruction (Table 3.3). The storm led to at least six fatalities and several injuries in Guangdong province, with a few additional injuries occurring in Guangxi (Xinhua, 2018). More than 3 million residents were forcibly evacuated across both provinces, and over 49,000 fishing boats were recalled to port for safety measures, with many people losing their properties to the catastrophic winds and flooding (Figure 5.15).

Table 3.3

Assessment of damages and direct economic loss in China

Casualties	
Death	6 people
Injure	Few people
Disappearance	0 people
Victim	330,000,000 people
Damages	
House	5,500 suites
Agricultural Loss	174.4 hectare
Loss of Economic	
Total Cost of Damage	¥52,000,000,000

Figure 5.15

Severe flooding in Yangchun, Guangdong province



Note. Mangkhut caused severe flooding in Yangchun, Guangdong, inundating vast areas, damaging homes, disrupting transportation, and leading to widespread waterlogging and significant agricultural losses in the region. (Chu, 2018).

In the Guangxi Zhuang Autonomous Region, Mangkhut's impact displaced roughly 45,000 people and affected about 69,400 residents. The storm caused widespread damage to buildings, coastal infrastructure, and triggered flooding and landslides that blocked major roads, complicating

relief efforts (Figure 5.16). About 2.5 million people sought refuge in shelters throughout southern China as the typhoon disrupted transportation services—including suspensions of ferries, trains, and flights—and caused power outages across multiple cities.

Figure 5.16

Fallen billboard in Tengxian, Guangxi province



Note. The fallen billboard in Guangxi from Mangkhut suffered structural collapse due to strong winds, causing debris on the ground and highlighting the storm's destructive force in urban areas (Guangxi Meteorological Bureau [GMB], 2018).

The total direct economic loss in mainland China due to Mangkhut was estimated at around ¥52,000,000,000 (approximately US\$7,240,828,400), reflecting severe damage to housing, agriculture, transportation infrastructure, and public utilities. Coastal flooding, storm surge, and landslides added to the extensive destruction of property and the displacement of large populations. The Chinese government and local authorities undertook large-scale evacuations and relief operations to manage the crisis and minimise casualties.

6. Discussion

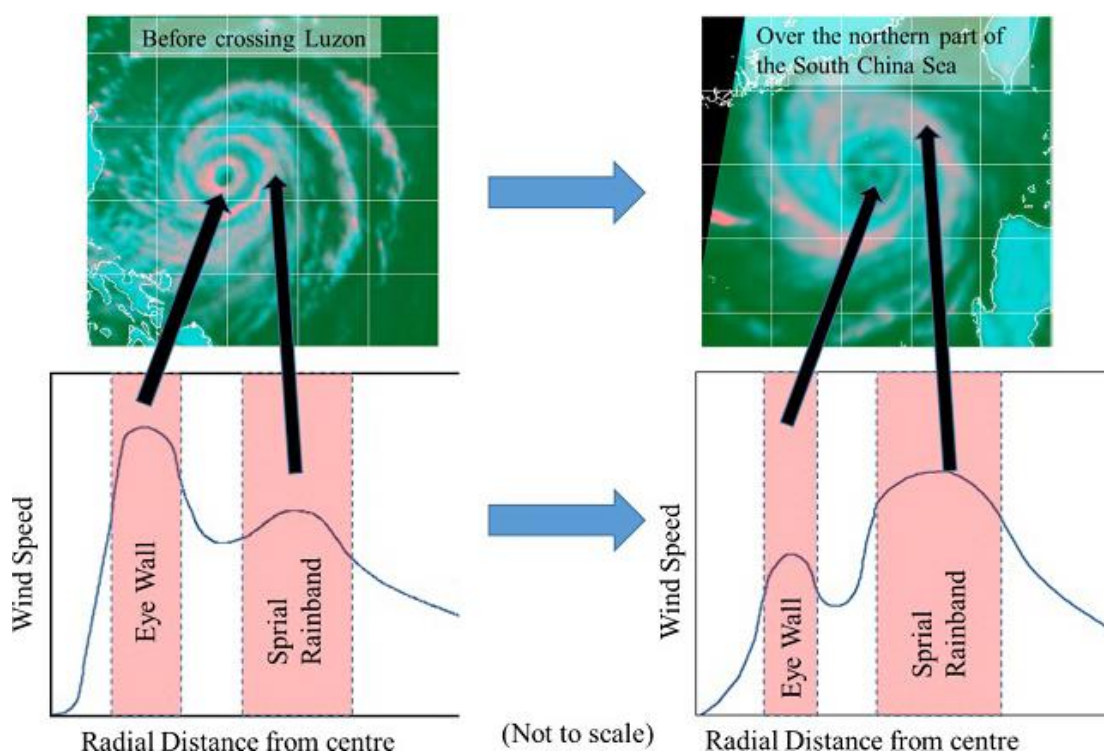
6.1 Special Wind Structure of Mangkhut

Mangkhut exhibited a special and complex wind structure characterised by an extensive circulation, intense spiral rainbands, and rapid movement, which together caused destructive winds over a wide area including Hong Kong.

Initially, before Mangkhut crossed Luzon, it displayed a typical mature tropical cyclone wind structure with strongest winds confined to a highly convective eyewall detected in microwave satellite imagery (Figure 6.1). However, after weakening from land interaction over northern Luzon, although the eyewall re-formed in the South China Sea, its convection was significantly weaker. In contrast, the spiral rainbands located 100 to 200 km from the storm centre remained intense and structurally intact (Choy & Wu, 2018). Radar images showed that these strong spiral rainbands swept across Hong Kong as Mangkhut skirted south-southwest of the city, delivering sustained destructive winds throughout the day (Figure 6.2).

Figure 6.1

Change in the wind structure of Mangkhut before and after crossing Luzon

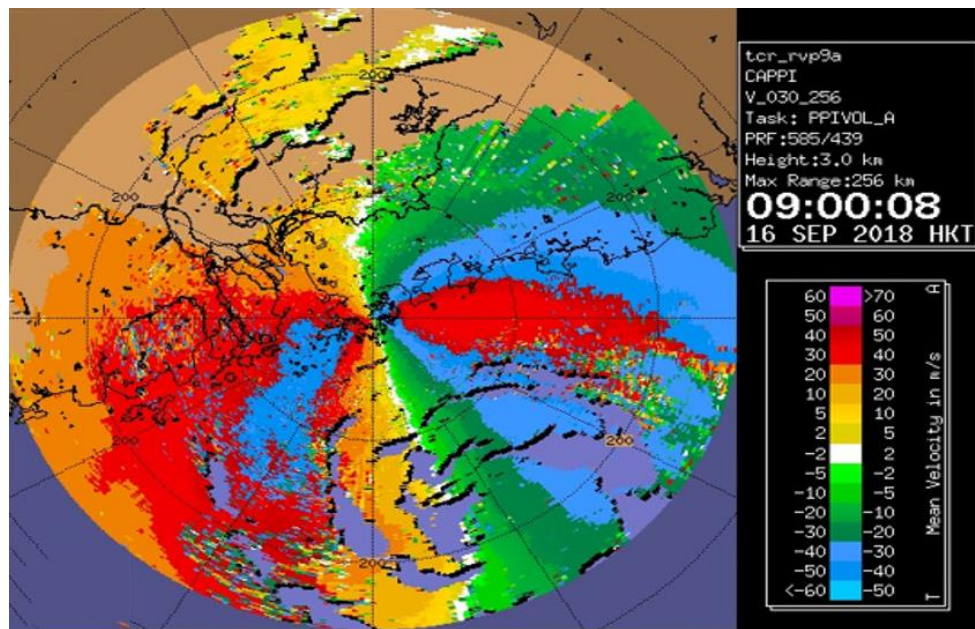


Note. Microwave satellite images of and diagram illustrating the change of wind structure of Mangkhut before crossing Luzon at 9:30 p.m. on 14 September 2018 and over the northern part of South China Sea at 0:30 a.m. on 16 September 2018.

Additionally, Mangkhut moved rapidly west-northwestward at speeds up to 35 kmh^{-1} —one of the fastest among historical No. 10 Hurricane Signals in Hong Kong. Because Hong Kong lay in the storm’s dangerous right semicircle for an extended period, the combination of the tropical cyclone’s wind speeds and its translational velocity led to especially fierce and persistent winds.

Figure 6.2

Strong spiral rainbands sweep across Hong Kong during Mangkhut’s passage



Note. Radar imagery showing the Doppler velocity at 9:00 a.m. on 16 September 2018. The image revealed the radial winds at 1 km (i.e. the velocity of rain echoes relative to the radar, and positive (negative) values indicates rain echoes moving away from (towards) the radar). The image showed that the radial wind over the outer spiral rainband was higher than that near the eyewall.

Surface observations confirmed that wind speeds over Hong Kong, contributed mainly by the strong spiral rainbands, were stronger than those nearer to the storm centre such as Macao and Zhuhai. Maximum 60-minute mean wind speeds at stations like Waglan Island and Cheung Chau reached 161 kmh^{-1} and 157 kmh^{-1} respectively, some of the highest on record. Gusts exceeded 150 kmh^{-1} broadly, with a peak gust of 256 kmh^{-1} at Tate’s Cairn.

Unlike many tropical cyclones where the eyewall mostly dominates the strongest winds, Mangkhut’s wind structure near Hong Kong was dominated by intense spiral rainbands combined with its rapid forward speed and extensive circulation. This unique configuration produced widespread, intense, and prolonged destructive winds, making Mangkhut one of the most impactful typhoons in the region’s recent history.

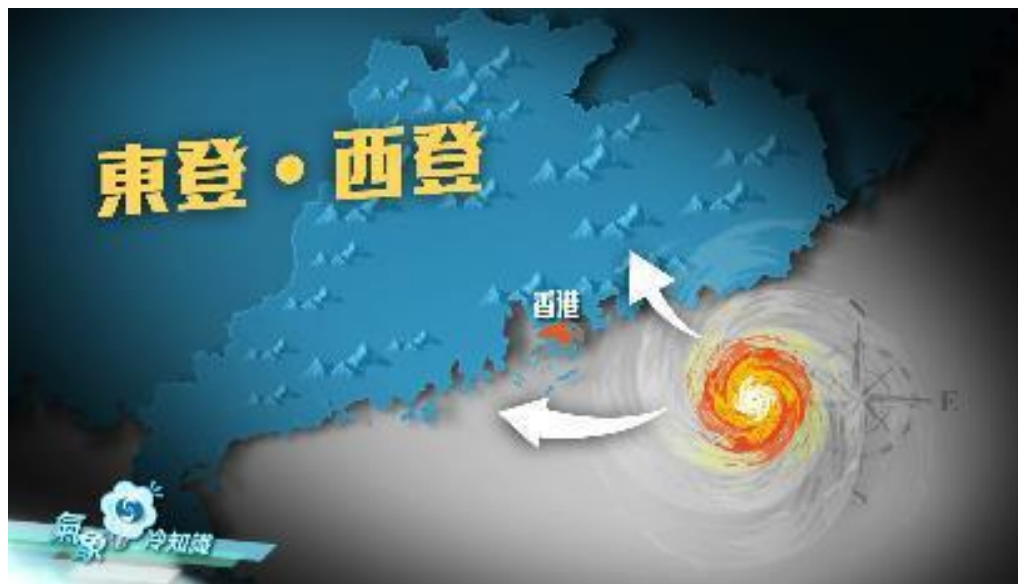
6.2 Enhanced Public Awareness of Disaster Preparedness in Social Media

The HKO significantly enhanced disaster preparedness for super typhoon Mangkhut in 2018 through a comprehensive, multi-channel public communication strategy. By leveraging both traditional and social media, the Observatory ensured the timely dissemination of critical weather information, raised public awareness, and fostered community engagement to mitigate risks (Tsoi, Lee, Yeung & Shum, 2019).

Six days before Mangkhut's expected impact, HKO began widely disseminating early warnings, forecast paths, and risk assessments across various media channels. Leveraging its newly launched social media platforms, such as Facebook and Instagram, the Observatory used engaging multimedia content—including videos, animations, and infographics—to explain the typhoon's characteristics and potential hazards in a clear, accessible way. This “infotainment” approach helped raise public awareness and comprehension of the storm's severity and the necessary precautions. For instance, the Observatory released an educational video explaining how typhoon impacts vary depending on whether they make landfall east or west of Hong Kong (Figure 6.3)—garnering over 770,000 views, a record-high engagement for the agency. Another video on storm surges (Figure 6.4), released on 15 September, reached 500,000 users.

Figure 6.3

East vs. West Landing

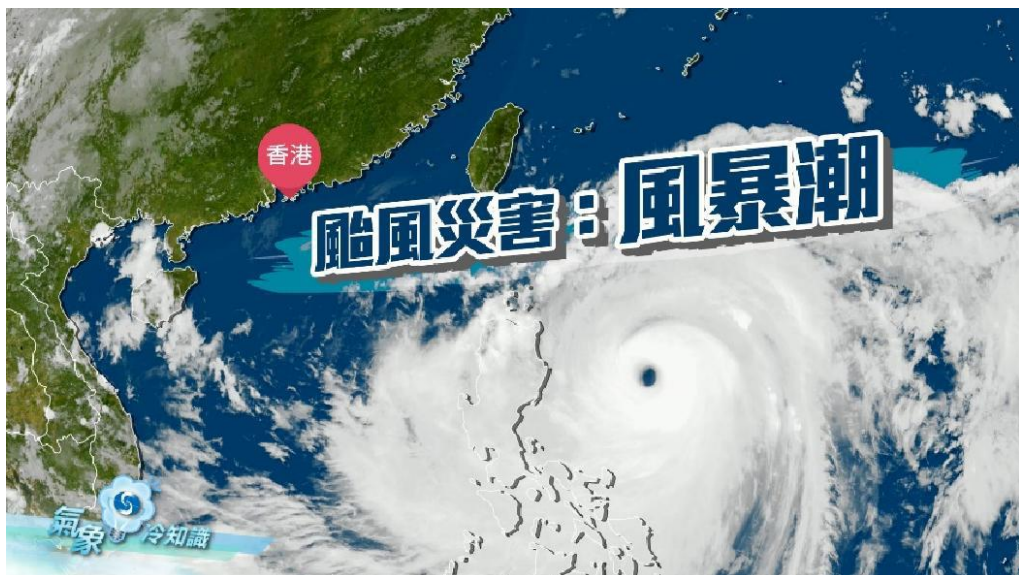


HKO's ongoing communication during Mangkhut involved frequent updates through press conferences, live broadcasts on television and radio, and real-time posts on social media. These updates included easily understandable explanations about the meaning of different warning signals,

expected wind conditions, storm surge risks, and the importance of timely protective actions. By coordinating messages across all media, the Observatory ensured that accurate and consistent information reached diverse segments of the population promptly.

Figure 6.4

Typhoon disaster: storm surge



Moreover, social media platforms allowed for interactive engagement, enabling the public to ask questions, share local observations, and provide feedback. This two-way communication strengthened community involvement and allowed HKO to adjust its messaging to address misconceptions or emerging concerns, further enhancing preparedness.

During and after Mangkhut, the Observatory also collected crowdsourced photos and videos from residents to better assess disaster impacts and enhance public education. The extensive use of robust communication technologies and strategic messaging significantly contributed to improved public understanding and readiness, helping to mitigate Mangkhut's destructive effects in Hong Kong.

Overall, the integration of traditional and innovative social media communication underpinned the effective dissemination of timely and tailored disaster preparedness information before and during Mangkhut, showcasing a successful model for public engagement in severe weather events.

6.3 Clearance and Repair Work in the Aftermath of Mangkhut

Although the Hong Kong government was widely commended for its proactive disaster preparedness ahead of super typhoon Mangkhut, its post-disaster management drew sharp criticism

for underestimating the extensive cleanup timeline and the challenges in restoring transportation services.

The onslaught of Mangkhut on 16 September, left Hong Kong reeling from widespread damage, including uprooted trees, severe flooding, and disrupted infrastructure. The storm's ferocity paralysed the city's transport networks, with roads blocked by debris and public transport services suspended. In response, the Hong Kong Education Bureau (EDB) announced a two-day suspension of classes to ensure student safety. Most universities also cancelled classes. However, the government's decision not to extend the suspension to workplaces triggered massive congestion during morning rush hours, as millions of commuters struggled to navigate the crippled transport system.

The government's selective suspension policy sparked intense public anger, with many questionings why offices remained open while schools were closed. Social media platforms were flooded with images and videos of overcrowded buses, stranded commuters, and gridlocked streets, amplifying frustration over the lack of coordination in post-disaster recovery (Figure 6.5). The masses argued that the failure to declare a citywide work stoppage not only endangered public safety but also highlighted poor crisis management. The controversy intensified as frontline workers, particularly those in essential services, faced extreme difficulties reporting to duty amid the chaos.

Figure 6.5

Public transportation heavily disrupted in Tai Wai station



Note. Services on the East Rail Line were paralysed due to fallen trees and damaged cables, causing major delays and crowding (Lo, 2018).

The transport meltdown following Mangkhut forced the Hong Kong government to review its extreme weather response policies. While officials defended the decision by citing economic considerations, the public outcry underscored the need for clearer guidelines on work suspensions during major disasters. The incident became a catalyst for discussions on urban resilience, prompting calls for better contingency planning to minimise disruption during future storms. Despite the criticism, the disaster also showcased community solidarity, with volunteers and emergency crews working tirelessly to clear debris and restore normalcy. Nevertheless, the post-Mangkhut chaos remains a cautionary tale about balancing economic priorities with public safety in disaster recovery.

7. Conclusion

Super Typhoon Mangkhut (1822) was an exceptionally intense and destructive tropical cyclone that showcased the complex interactions between atmospheric, oceanic, and geographical factors leading to rapid intensification and prolonged high-intensity phases. Its well-defined structure, characterized by a distinct eye, symmetrical central dense overcast, strong convective hot towers, and expansive spiral rainbands, facilitated the maintenance of its super typhoon status with maximum sustained winds reaching up to 250 kmh^{-1} and central pressure as low as 900 hPa.

Mangkhut's rapid intensification was driven by favourable environmental conditions including high sea surface temperatures (about 30°C), low vertical wind shear, and excellent upper-level outflow, amplified further by oceanic heat content and dynamic potential intensity factors. Despite weakening over the mountainous terrain of northern Luzon, the storm reorganised over the South China Sea, maintaining a broad and powerful wind field that inflicted severe damage across the Philippines, Hong Kong, and southern China.

The societal impacts were profound and multifaceted, with the Philippines suffering substantial agricultural and infrastructure losses, including nearly 45,000 houses damaged and an economic loss exceeding ₱33 billion. Hong Kong experienced record-breaking wind speeds, the highest number of uprooted trees in a tropical cyclone event, extensive damage to public amenities, transportation disruptions, and economic losses of HK\$4.6 billion. Southern China, particularly Guangdong province, faced large-scale flooding, property damage, and significant agricultural losses.

Mangkhut also exposed critical gaps in disaster preparedness and emergency response coordination. The challenges in early warning, infrastructure resilience, and public communication were evident from the impacts and controversies around government decisions in the aftermath, especially regarding work and school suspensions.

Forecasting efforts, leveraging advanced techniques such as the Advanced Dvorak Technique and Ensemble Prediction Systems, proved valuable for predicting Mangkhut's track and intensity, although localized surge and wave impacts posed ongoing challenges due to complex coastal dynamics.

This case study highlights the urgent need to integrate meteorological science with socio-economic and institutional frameworks to strengthen resilience against future high-intensity tropical cyclones. Improvements in forecasting accuracy, infrastructure design, community awareness, and

coordinated emergency management are imperative to mitigate the devastating effects of such natural disasters. In a changing climate, where extreme tropical cyclone activity may intensify, lessons from Mangkhut underscore the importance of sustained investments in mitigation and adaptation strategies to safeguard vulnerable populations and infrastructures.

Acknowledgements

The authors thank Philip Fong, C.B. Lai, Kris Cheng, Roy Liu, Winson Wong, K.K Ho, Holmes Chan, Felix Wong, M.H. Leung, T.H. Lui, C.T. John Li, Waly Lee, Ms. Yeung, Leo Chan, Anson Tang, David Lam, Ms. Wen, Y.N. Susanna Lee, T. Kung, W.K. Chow, Helen Ho, H.M. Kong, C.K. Fung, Andy Ho, M.L. Wan, K.C. Lai, T.C. Lee, K.T. Lau, Ryan Leung, C.M. Shun, Mr. Tang, Mr. Shek, Mr. Yu, T.C. Yan, S.K. Hon, C.Y. Chan, Josh Morgerman, Mr. Lo, Mrs. Chu, Ernest Kao, Elizabeth Cheung, Su Xinqi, Tony Cheung and Mrs. Lam for their captured the photos. The institutions also thank Civil Aid Service, Hong Kong China News Agency, Asia Boating Limited, Hong Kong Boating Industry Association, Hong Kong Slope Safety, Cordillera Disaster Response and Development Services and Guangxi Meteorological Bureau for their valuable photos.

References

- Asia Boating Limited. (2018, September 17). Boats in Hong Kong Destroyed by the Typhoon Mangkhut on Sept 16 2018. *Asia Boating Limited*. <https://asia-boating.com/boats-yachts-hong-kong/boats-in-hong-kong-typhoon-mangkhut-on-sept-16-2018/>.
- Chan, H. (2020, March 31). Heng Fa Chuen seaside housing estate cleans up after Typhoon Mangkhut brings floods and destruction. *Hong Kong Free Press (HKFP)*. <https://hongkongfp.com/2018/09/17/heng-fa-chuen-seaside-housing-estate-cleans-typhoon-mangkhut-brings-floods-destruction/>.
- Chang, R., Zhu, R. & Zhao, D. (2022). Strong Wind Characteristics of the Lower Boundary Layer (0–300 m) during the Landfall of a Typhoon. *Chinese Journal of Atmospheric Sciences*, 46(5), 1071-1086. <http://www.iapjournals.ac.cn/dqkx/article/doi/10.3878/j.issn.1006-9895.2108.21071>.
- Cheung, C. (2024, September 5). Hidden Hong Kong: 11 worst typhoons in Hong Kong's history. *Localiz*. <https://www.localiz.com/post/culture-history-timeline-worst-typhoons-storms-hong-kong>.
- Choy, C. H. & Kok, M. H. (2014, January 13-15). *Study New Development of Tropical Cyclone Observatory* (RN1100). Paper presented at the 28th Guangdong-Hong Kong-Macao Seminar on Meteorological Science and Technology, Hong Kong.
- Choy, C. H., Lau, D. S. & He, Y. H. (2022). Super typhoons Hato (1713) and Mangkhut (1822), part I: analysis of maximum intensity and wind structure. *Weather*, 77(9), 314-320.
- Choy, C. H., Lau, D. S. & He, Y. H. (2020). Super typhoons Hato (1713) and Mangkhut (1822), part II: challenges in forecasting and early warnings. *Weather*, 77(9), 324-331.
- Choy, C. & Wu, M. C. (2018, October 29). *A wake up call from Mangkhut. Observatory's Blog*. <https://www.hko.gov.hk/en/blog/00000216.htm>.
- Choy, C. H., Wu, M. C., Lee, T. C. & HKFI (2020). Assessment of the damages and direct economic loss in Hong Kong due to Super Typhoon Mangkhut in 2018. *Tropical Cyclone Research and Review*, 9(4), 193-205.

Chu, K. C. (2018, September 18). Typhoon Mangkhut Leaves 5 Dead, 1 Missing in Mainland China with ¥5.2 Billion Economic Losses. *Hong Kong 01 (HK01)*. <https://www.hk01.com/%E5%8D%B3%E6%99%82%E4%B8%AD%E5%9C%8B/237206/%E9%A2%B1%E9%A2%A8%E5%B1%AB-%E9%A2%A8%E7%81%BD%E9%87%8D%E5%89%B5%E5%85%A7%E5%9C%B0%E9%87%805%E6%AD%BB1%E5%A4%B1%E8%B9%A4-%E7%B6%93%E6%BF%9F%E6%90%8D%E5%A4%B1%E9%81%9452%E5%84%84>.

Comments Editorial Office. (2018, September 17). Typhoon Mangkhut: East Rail Line Overrun by Sea of Commuters as Lantau Highway Upgrade Threatens Worker Nightmare. *Hong Kong 01 (HK01)*. <https://www.hk01.com/01%E8%A7%80%E9%BB%9E/236483/%E9%A2%B1%E9%A2%A8%E5%B1%E7%AB%B9-%E6%9D%B1%E9%90%B5%E7%B7%9A%E9%A9%9A%E7%8F%BE%E4%BA%BA%E9%A0%AD%E6%B5%B7-%E6%9D%B1%E5%A4%A7%E5%B6%BC%E5%8A%A0%E5%BC%B7%E7%89%88%E5%8B%A2%E4%BB%A4%E6%89%93%E5%B7%A5%E4%BB%94%E6%9B%B4%E5%B4%A9%E6%BD%B0>.

Cordillera Disaster Response and Development Services (CorDisRDS). (2018, September 18). *Typhoon Ompong: Impacts on Cordillera Region*. Citizens' Disaster Response Center. <https://www.cdrc-phil.com/typhoon-ompong-impacts-on-cordillera-region/>.

Creepy, J. (2020, March 31). ‘A human disaster’: Piles of styrofoam washed up by Typhoon Mangkhut highlight Hong Kong’s marine trash problem. *Hong Kong Free Press (HKFP)*. <https://hongkongfp.com/2018/09/19/human-disaster-piles-styrofoam-washed-typhoon-mangkhut-highlight-hong-kongs-marine-trash-problem/>.

Dadey, K. (2018). *The Philippines - Typhoon Mangkhut Situation Report*. International Organization for Migration (IOM).

Department of Atmospheric Science. (2018). *Upper Air Sounding*. University of Wyoming, College of Engineering. https://weather.uwyo.edu/upperair/sounding_legacy.html.

Department of Development Bureau (DEVB). (2021, January 3). *Unforgettable experience: emergency response to typhoon damage. My Blog Archives*. https://www.devb.gov.hk/en/home/my_blog/index_id_423.html.

ESCAP/WMO Typhoon Committee (2018, November 5-9). *Member Report (China)*. Paper presented at the 13th Integrated Workshop, Chiang Mai, Thailand.

ESCAP/WMO Typhoon Committee (2018, November 5-9). *Member Report (Philippines)*. Paper presented at the 13th Integrated Workshop, Chiang Mai, Thailand.

Getty Images. (2018, September 16). *TOPSHOT-HONG KONG-PHILIPPINES-WEATHER-TYPHOON-MANGKHUT*. <https://www.gettyimages.hk/detail/%E6%96%B0%E8%81%9E%E7%85%A7%E7%89%87/man-wades-across-the-floods-in-heng-fa-chuen-during-the-approach-%E6%96%B0%E8%81%9E%E7%85%A7%E7%89%87/1033996990?adppopup=true>.

Guangxi Meteorological Bureau (GMB). (2018, December 18). This Year's Strongest Typhoon 'Mangkhut' Crosses Guangxi: Severe Wind and Flood Disasters. *Guangxi Meteorological Bureau (GMB)*. http://gx.cma.gov.cn/ztlm/2018gxsdtqqhsjpx/201812/t20181218_127260.html.

He, J., Hon, K. K., Chan, P. W. & Li, Q. S. (2022). Dropsonde observations and numerical simulations for intensifying/weakening tropical cyclones over the northern part of the South China Sea. *Weather*, 77(9), 332-338.

He, S. & Li, Y. (2018, September 16). 2 killed as Typhoon Mangkhut makes landfall in Guangdong. *China Daily*. https://global.chinadaily.com.cn/a/201809/16/WS5b9dd125a31033b4f4656458_2.Html.

He, Y. C., He, J. Y., Chen, W. C., Chan, P. W., Fu, J. Y. & Li, Q. (2020). Insights from Super Typhoon Mangkhut (1822) for wind engineering practices. *Journal of Wind Engineering & Industrial Aerodynamics*, 203, 104238.

Hong Kong Observatory (HKO). (2018). *Tropical Cyclones in 2018*. Hong Kong Observatory (HKO). HONGKONGUIDE. (2018, September 17). "Lovers Bridge" in Shek O destroyed by Typhoon Mangkhut. HONGKONGUIDE.

Houze, R. A., Chen, S. S., Smull, B. F., Lee, W. C. & Bell, M. M. (2007, March 2). Hurricane Intensity and Eyewall Replacement. *Science*, 315, 1235-1239.

Japan Meteorological Agency (JMA). (2018). *Himawari Real-time*. National Institute of Information and Communications Technology (NICT) Science Cloud. <https://himawari8.nict.go.jp/>.

- Kang, S. K., Kim, S. H., Lin, I. I., Park, Y. H., Choi, Y., Ginis, I., Cione, J., Shin, J. Y., Kim, E. J., Kim, K. O., Kang, H. W., Park, J. H., Bidlot, J. R. & Ward, B. (2024). The North Equatorial Current and rapid intensification of super typhoons. *Nature Communications*, 15, 1742.
- Kao, E., Cheung, E., Xinqi, S. & Cheung, T. (2018, September 18). Hong Kong faces days of uncertainty as it struggles to recover from monster storm Typhoon Mangkhut. *South China Morning Post (SCMP)*. <https://www.scmp.com/news/hong-kong/health-environment/article/2164607/hong-kong-faces-days-uncertainty-it-struggles>.
- Kitamoto Laboratory. (2018). *Digital Typhoon: Typhoon 201822 (MANGKHUT)*. National Institute of Informatics (NII). <https://agora.ex.nii.ac.jp/digital-typhoon/summary/wnp/s/201822.html.en>.
- Kong, W. (2011). To the east, to the west? (Effects of landfall position). *Hong Kong Observatory (HKO)*. https://www.hko.gov.hk/en/education/tropical-cyclone/weather-effects-and-impact/0016_6-to-the-east-to-the-west-effects-of-landfall-position.html.
- Lai, C., Li, R., Wang, Z., Chen, Y., Feng, S., Yuan, X., Li, X., Liu, M., Kong, L. & Xu, C. Y. (2025). *Formation Mechanism of Typhoon-Induced Storm Surge and Key Influencing Factors: A Case Study of the Pearl River Estuary*. Social Science Research Network (SSRN). <http://dx.doi.org/10.2139/ssrn.5291478>.
- Leung, H. Y. (2018, September 17). Mangkhut Aftermath: Office Worker's Defeated Stance Before Fallen Tree Goes Viral – "I Must Work" Meme Storm. *Hong Kong 01 (HK01)*. <https://www.hk01.com/%E7%86%B1%E7%88%86%E8%A9%B1%E9%A1%8C/236430/%E9%A2%B1%E9%A2%A8%E5%B1%B1%E7%AB%BB-%E6%89%93%E5%B7%A5%E4%BB%94%E7%AB%99%E5%A1%8C%E6%A8%B9%E5%89%8D-%E8%83%8C%E5%BD%B1%E5%8B%81%E7%84%A1%E5%A5%88-%E6%88%91%E8%A6%81%E8%BF%94%E5%B7%A5-%E6%94%BB%95%9C%96%E7%98%8B%E5%82%B3>.
- Li, Z., Tam, C. Y., Li, Y., Lau, N. C., Chen, J., Chan, S. T., Lau, D. S. D. & Huang, Y. (2022). How Does Air-Sea Wave Interaction Affect Tropical Cyclone Intensity? An Atmosphere-Wave-Ocean Coupled Model Study Based on Super Typhoon Mangkhut (2018). *Earth and Space Science*, 9.
- Liu, S. (2018, September 15). The National Meteorological Center issued red warning of typhoon to address Mangkhut. *National Meteorological Center (NMC)*. https://www.cma.gov.cn/en2014/news/News/201809/t20180915_478054.html.

- Morgerman, J. (2018). *iCyclone Chase Report: MANGKHUT 2018*. iCyclone.
- National Disaster Risk Reduction and Management Council (NDRRMC). (2018). *Preparedness Measures and Effects of TY “OMPONG” (I.N. MANGKHUT)*. Republic of the Philippines.
- Now TV News. (2018, September 16). Bikeway Submerged as Shing Mun River Overflows. *Now TV News*. <https://news.now.com/home/local/player?newsId=320453>.
- Olander, T. L. & Velden, C. S. (2015). *ADT – Advanced Dvorak Technique: Users’ Guide (McIDAS Version 8.2.1)*. University of Wisconsin-Madison.
- Pamintuan, J. P. P. & Bagtasa, G. (2025). Sensitivity of WRF tropical cyclone simulations in the Philippines to different SST data. *Dynamics of Atmospheres and Oceans*, 111, 101578.
- Regional and Mesoscale Meteorology Branch (RMMB). (2018). *WP262018 - Typhoon (>=96 kt) MANGKHUT*. Regional and Mesoscale Meteorology Branch (RMMB). https://rammb-data.cira.colostate.edu/tc_realtime/storm.asp?storm_identifier=wp262018.
- Ruan, Z., Li, J., Li, F. & Lin, W. (2024). Simulation Study on the Autumn Typhoon Mangkhut (2018) in 10.5 Days over the South China Sea: Microphysical Characteristics and latent heat budget. *Meteorologische Zeitschrift*, 33(2), 131-144.
- Sing Tao Daily. (2018, September 17). Mangkhut Hits Hong Kong: Lamborghini “Stuck in Water”, Power and Water Outage in Lohas Park, Tseung Kwan O. *Sing Tao Daily*. <https://www.stheadline.com/article/1814429/%E5%B1%B1%E7%AB%B9%E8%A5%B2%E6%B8%AF%E5%B0%87%E8%BB%8D%E6%BE%B3%E5%98%89%E6%82%85%E5%81%9C%E6%B0%84%E5%81%9C%E9%9B%BB-%E6%9E%97%E5%AF%B6%E5%A0%85%E5%B0%BC%E5%9C%A8%E6%B0%B4%E4%B8%AD%E5%A4%AE>.
- Song, S. H. (2018, September 17). Classroom Perspectives: The Power of Mangkhut. *SYMediaLab*. <https://www.sy medialab.com/talk/%E3%80%90%E6%95%99%E5%AD%B8%E9%9A%A8%E7%AD%86%E3%80%91%E5%B1%B1%E7%AB%B9%E7%9A%84%E5%A8%81%E5%8A%9B/>.

South China Morning Post (SCMP). (2018, September 17). Typhoon Mangkhut: Aftermath. *South China Morning Post (SCMP)*. <https://www.scmp.com/photos/hong-kong/2164587/typhoon-mangkhut-aftermath?page=5>.

Tropical Tidbits. (2018). *Numerical Model Prediction*. Tropical Tidbits. https://www.tropicaltidbits.com/analysis/models/?model=ecmwf®ion=wpac&pkg=z500_mslp&runtimes=2018091418&fh=12.

Tsoi, T. S., Lee, F. Y., Yeung, K. C. & Shum, C. T. (2019, March 6-8). *From Traditional to Social Media – Public Communication Strategy of the Hong Kong Observatory* (RN1362). Paper presented at the 33rd Guangdong-Hong Kong-Macao Seminar on Meteorological Science and Technology combined with the 24th Conference on Meteorological Business Collaboration, Hong Kong.

Uson, M. C. C., Rivera, P., Celebre, C. P., & Monteverde, M. C. A. (2019, November 10-15). *Development of a Storm Surge Forecasting and Warning System for the Philippines*. Department of Science and Technology, Philippine Atmospheric, Geophysical and Astronomical Services Administration (PAGASA). http://waveworkshop.org/16thWaves/Presentations/GG1%20Development%20of%20a%20Storm%20Surge%20Forecasting%20%20and%20Warning%20System%20for%20the%20Philippines_MCUson.pdf.

Velden, C., Harper, B., Wells, F., Beven, J. L., Zehr, R., Olander, T., Mayfield, M., Guard, C., Lander, M., Edson, R., Avila, L., Burton, A., Turk, M., Kikuchi, A., Christian, A., Caroff, P. & McCrone, P. (2006). The Dvorak Tropical Cyclone Intensity Estimation Technique: A Satellite-Based Method that Has Endured for over 30 Years. *Bulletin of the American Meteorological Society*, 87(9), 1195-1210.

Weather Division. (2018). *Typhoon Ompong (Mangkhut / 1822) Summary Report*. Philippine Atmospheric, Geophysical and Astronomical Services Administration (PAGASA).

Weather Division. (2020). *DOST-PAGASA Annual Report on Philippine Tropical Cyclones*. The Government of the Republic of the Philippines.

Wenweipo News. (2018, September 17). Super Typhoon Makes Direct Hit on Taishan - All Four Nuclear Plants Remain Unaffected. *Wenweipo News*. <http://news.wenweipo.com/2018/09/17/IN1809170003.htm>.

Wong, W. L. (2018, September 17). Typhoon Mangkhut Downgraded to Severe Tropical Storm - HKO Issues No. 3 Signal on “Blue Monday”. *Hong Kong 01 (HK01)*. <https://www.hk01.com/%E7%A4%BE%E6%9C%83%E6%96%B0%E8%81%9E/236258/%E9%A2%B1%E9%A2%A8%E5%B1%B1%E7%AB%B9-%E9%99%8D%E7%82%BA%E5%BC%B7%E7%83%88%E7%86% B1%E5%B8%B6%E9%A2%A8%E6%9A%B4-%E5%A4%A9%E6%96%87%E5%8F%B0-%E8%97%8D%E8%89%B2%E6%98%9F%E6%9C%9F%E4%B8%80-%E8%BD%893%E8%99%9F%E9%A2%A8%E7%90%83>.

Xinhua. (2018, September 17). 4 dead as Super Typhoon Mangkhut slams south China. *Xinhuanet*. http://www.xinhuanet.com/english/2018-09/17/c_137473935.htm.

Yan, Y., Hu, M. & Qiu, C. (2024). Simulated Directional Wave Spectra of the Wind Sea and Swell under Typhoon Mangkhut. *Atmosphere*, 15(10), 1174.

Yeung, H. Y. (2013). “Convective Hot Tower” Signatures and Rapid Intensification of Severe Typhoon Vicente (1208). *Tropical Cyclone Research and Review*, 2(2), 96-108.

Zhang, W. J., Hui, W., Lyu, W. T., Cao, D., Li, P., Zheng, D., Fang, X. & Zheng, Y. (2020). FY-4A LMI Observed Lightning Activity in Super Typhoon Mangkhut (2018) in Comparison with WWLLN Data. *Journal of Meteorological Research*, 34, 336-352.

Zhou, M., Liu, C., Dai, G., Huang, H., Song, Q. & Li, M. (2024). A real-time storm surge prediction system for the Guangdong–Hong Kong–Macao Greater Bay Area under the background of typhoons: model setup and validation. *Natural Hazards*, 121, 3473-3498.

Appendix I: Classification of Tropical Cyclones

A. Philippines

The Philippine Atmospheric, Geophysical and Astronomical Services Administration (PAGASA) classifies tropical cyclones into five categories based on 10-minute average sustained winds (Figure S1.1).

Table S1.1

Classification of tropical cyclones by maximum sustained 10-minute wind speed in the Philippines

Tropical Cyclone Classification	Maximum 10-minute Mean Wind near the Centre
Tropical Depression	30 to 61 km/h
Tropical Storm	62 to 88 km/h
Severe Tropical Storm	89 to 117 km/h
Typhoon	118 to 222 km/h
Super Typhoon	223 km/h or above

B. Hong Kong

Tropical cyclones are classified by the World Meteorological Organization (WMO) based on maximum sustained wind speeds near their centre. In Hong Kong, these classifications use 10-minute mean wind speeds, defined as follows in Table S1.2 (HKO, 2009).

Table S1.2

Classification of tropical cyclones by maximum sustained 10-minute wind speed in Hong Kong

Tropical Cyclone Classification	Maximum 10-minute Mean Wind near the Centre
Tropical Depression	41 to 62 km/h
Tropical Storm	63 to 87 km/h
Severe Tropical Storm	88 to 117 km/h
Typhoon	118 to 149 km/h
Severe Typhoon	150 to 184 km/h
Super Typhoon	185 km/h or above

C. China

The CMA classifies tropical cyclones based on 2-minute mean maximum sustained wind speeds near the storm centre, following national standards adapted from World Meteorological Organization

(WMO) guidelines. The system categorises cyclones into six tiers, with distinct Chinese terminology for public warnings (Table S1.3).

Table S1.3

Classification of tropical cyclones by maximum sustained 2-minute wind speed in China

Tropical Cyclone Classification	Maximum 2-minute Mean Wind near the Centre
Tropical Depression	41 to 62 km/h
Tropical Storm	63 to 87 km/h
Severe Tropical Storm	88 to 117 km/h
Typhoon	118 to 149 km/h
Severe Typhoon	150 to 184 km/h
Super Typhoon	185 km/h or above

Appendix II: Tropical Cyclone Warning Signals

A. Philippines

The tropical cyclone warning signals in the Philippines, issued by the PAGASA, are known as the tropical cyclone wind signals. These signals serve as alert levels for areas that may be affected by tropical cyclone winds and related hazards. The system is designed to inform the public about the expected strength of winds, the timeframe within which they may occur, and the potential impact, helping communities prepare and respond accordingly.

The tropical cyclone wind signals consist of five numbered levels, from Signal No. 1 to Signal No. 5, with higher numbers indicating stronger winds expected in a shorter lead time. Each signal corresponds to a range of wind speeds measured over a 10-minute average and is associated with increasing levels of threat to life and property (Table S2.1).

Table S2.1

Philippines' tropical cyclone wind signals

Symbol Display	Signals	Lead Time (hours)	Winds	Potential Impacts of The Wind
	1	36	30 to 60 km/h	No damage to very light damage
	2	24	61 to 120 km/h	Light to moderate damage
	3	18	121 to 170 km/h	Moderate to heavy damage
	4	12	171 to 220 km/h	Heavy to very heavy damage
	5	12	More than 220 km/h	Very heavy to widespread damage

The tropical cyclone wind signals are activated when a tropical cyclone is inside or near the Philippine Area of Responsibility and is projected to affect the country, with signals issued at the city or provincial level. These signals are updated regularly, escalating or de-escalating based on the cyclone's intensity and movement to provide timely warnings and facilitate preparedness and evacuation measures where necessary.

This structured, clear, and tiered system helps the public gauge the severity of the impending storm and respond appropriately to protect lives and property. It reflects decades of evolution and improvements based on past experiences, including lessons learned from major typhoons affecting the Philippines.

B. Hong Kong

The tropical cyclone warning signals in Hong Kong are issued by the Hong Kong Observatory (HKO) to alert the public about the potential impact of tropical cyclones approaching or affecting the territory. The system uses numbered signals from No. 1 up to No. 10, indicating increasing severity and likelihood of strong winds and hazardous weather conditions. Each level of signal carries specific meanings about the wind intensity expected and recommended public actions to ensure safety (Table S2.2).

Table S2.2

Hong Kong's tropical cyclone warning signals

Symbol Display	Signals		Meaning of Signals
T 1	Standby	1	A tropical cyclone is centred within about 800 kilometres of Hong Kong and may affect the territory.
L 3	Strong Wind	3	Strong wind is expected or blowing generally in Hong Kong near sea level, with a sustained speed of 41-62 km/h, and gusts which may exceed 110 km/h, and the wind condition is expected to persist.
▲ 8 NW 西北	Gale or Storm	8 NW	Gale or storm force wind is expected or blowing generally in Hong Kong near sea level, with a sustained wind speed of 63-117 km/h from the quarter indicated and gusts which may exceed 180 kilometres per hour, and the wind condition is expected to persist.
▼ 8 SW 西南		8 SW	
▲ 8 NE 東北		8 NE	
▼ 8 SE 東南		8 SE	
X 9	Increasing Gale or Storm	9	Gale or storm force wind is increasing or expected to increase significantly in strength.

Symbol Display	Signals		Meaning of Signals
	Hurricane	10	Hurricane force wind is expected or blowing with sustained speed reaching upwards from 118 km/h and gusts that may exceed 220 km/h.

Throughout the tropical cyclone event, the Hong Kong Observatory updates these signals in accordance with the storm's intensity and path, providing the public with timely warnings. The system is designed not only to warn people about the imminence of dangerous winds but also to guide government and community responses, ensuring safety and minimising disruption during severe weather. The signals also help coordinate closure of schools, businesses, and transport to safeguard the population.

C. China

The tropical cyclone warning signals system in China is operated by the CMA, which uses a standardised color-coded alert system to communicate the threat level posed by tropical cyclones. The system primarily focuses on average wind speeds and expected arrival times to help the public and authorities prepare and respond effectively (Table S2.3).

Table S2.3

China's tropical cyclone warning signals

Symbol Display	Signals	Meaning of Signals
	White	A tropical cyclone may affect the area within 48 hours. It serves as an early notice for communities to start monitoring the weather situation closely.
	Blue	When the area may be affected within 24 hours by winds averaging above force 6 (on the Beaufort scale), with gusts possibly exceeding force 7. This alert signals potential wind impacts and encourages readiness measures.
	Yellow	With tropical cyclone effects expected within 24 hours and average wind powers above force 8 or gusts above force 9. The public is advised to take precautions seriously as the risk of wind damage increases.
	Orange	The tropical cyclone effects are forecast within 12 hours, with average wind speeds exceeding force 10 and gusts above force 11. Strong winds and associated hazards are likely, necessitating more urgent protective actions.

Symbol Display	Signals	Meaning of Signals
 RED TYPHOON	Red	A signalling that tropical cyclone conditions have arrived or are imminent within 6 hours, with sustained winds above force 12 or stronger gusts. This alert represents a severe threat, requesting immediate safety measures and high public vigilance.

These warning signals are accompanied by guidance on protective actions and are designed to escalate or downgrade based on the tropical cyclone's intensity and proximity. The system is widely used along China's coastal areas and island regions, where tropical cyclones pose the greatest risk. It integrates meteorological observations from satellites, radar, and weather stations to provide timely and accurate warnings.

In addition to the typhoon alerts, China also employs more specific local or provincial signal practices, but the CMA's color-coded system forms the national standard for tropical cyclone warnings. This approach helps unify disaster risk communication and enhances public preparedness across the country.

This tiered warning system aids the government and public in responding proactively to tropical cyclone threats, minimising damage and protecting lives by ensuring timely dissemination of critical information and instructions.

Appendix III: Rainstorm Warning Signals

A. Philippines

The rainstorm warning signals in the Philippines are part of the country's weather alert system managed by the PAGASA. These warnings are issued to inform the public and local authorities of the likelihood of heavy rainfall and the possible impacts such as flooding and landslides. The system aims to enhance preparedness and prompt timely response to minimise damage and loss of life.

PAGASA issues different levels of rainstorm warnings depending on the intensity and expected duration of rainfall (Table S3.1). These warnings are usually categorised based on rainfall thresholds measured over specific periods (such as 1-hour, 3-hour, or 24-hour accumulations) and the severity of their impact in particular areas. The signals indicate the probability of flash floods, river flooding, and landslides, which are common hazards during heavy rain events in the Philippines' mountainous and low-lying regions.

Table S3.1

Philippines' rainstorm warning signals

Symbol Display	Description	Forecast
	Advisory (Community Awareness)	Flooding is possible in low-lying areas and near river channels.
	Alert (Community Preparedness)	Flooding is threatening in low-lying areas and near river channels.
	Emergency (Community Response)	SEVERE Flooding is expected. Take necessary precautionary measures.

When a rainstorm warning is issued, it alerts the public of probable flooding in vulnerable areas and encourages them to take precautionary measures. Local disaster risk reduction and management offices also use these warnings to implement evacuation and other safety protocols. The warnings are often accompanied by advisories that specify which regions or communities are expected to be affected.

In addition to rainstorm warnings, PAGASA issues thunderstorm advisories and flash flood alerts to provide more detailed information as conditions evolve. These advisories describe the

ongoing weather conditions, potential risks, and recommended safety measures. The warnings communicate the urgency of the situation, helping to reduce vulnerability especially in flood-prone and landslide-prone communities.

B. Hong Kong

The rainstorm warning signals in Hong Kong are issued by the HKO to alert the public and authorities about significant rainfall that could lead to major disruptions such as flooding, traffic congestion, and potential threats to life and property. The system is independent of other weather warnings like tropical cyclone or landslip warnings, focusing specifically on the intensity and impact of rainfall. The rainstorm warning system consists of three color-coded levels—Amber, Red, and Black—each indicating progressively severe levels of rainfall (Table S3.2).

Table S3.2

Hong Kong's rainstorm warning signals

Symbol Display	Signals	Meaning of Signals
	Amber	Heavy rain has fallen or is expected to fall generally over Hong Kong, exceeding 30 mm in an hour, and is likely to continue. This signal serves as an early alert that flooding may occur in low-lying and poorly drained areas. Key government departments and utility operators are put on alert to prepare for potential emergencies, and the public is advised to exercise caution but can generally continue with normal activities while staying informed.
	Red	Heavy rain has fallen or is expected to fall generally over Hong Kong, exceeding 50 mm in an hour, and is likely to continue. This level of warning signals a greater risk of serious road flooding and more widespread traffic disruption. The public is advised to stay alert, school classes may be suspended, and employers might arrange for flexible working hours. Emergency services begin to actively respond to the increased risk of flooding and other rain-induced hazards.
	Black	Very heavy rain has fallen or is expected to fall generally over Hong Kong, exceeding 70 mm in an hour, and is likely to continue. When this signal is raised, severe flooding, landslips, and road blockages are expected, leading to significant disruption. Schools are closed unless the school premises are deemed unsafe, and public transport services may be suspended to ensure public safety. The Observatory strongly advises everyone to seek shelter indoors and avoid unnecessary travel until conditions improve.

These rainstorm warning signals are broadcast widely via radio, television, and digital platforms to ensure timely dissemination of information. They play a crucial role in safeguarding residents by encouraging preparedness and enabling coordinated response efforts from government agencies, transport operators, and emergency services. The tiered system helps the public understand the level

of risk and fosters proactive measures to reduce casualties and damage during Hong Kong's rainy season, typically from April to September.

C. China

China's rainstorm warning signals are based on a standardised, color-coded system designed to inform the public and government agencies about the severity and expected impacts of heavy rainfall. Managed nationally by the CMA, this system uses four key alert levels: Blue, Yellow, Orange, and Red, each indicating increasing urgency and severity associated with rainstorms (Table S3.3).

Table S3.3

China's rainstorm warning signals

Symbol Display	Signals	Meaning of Signals
	Blue	The rainfall has reached or is expected to reach 50 mm within a 12-hour period and may continue. This signals the beginning of a rainstorm event and prompts government departments, schools, and the public to prepare for possible flooding and disruptions. Precautionary measures include securing drainage systems, alerting vulnerable areas, and advising motorists to be cautious of road waterlogging.
	Yellow	The rainfall is more intense, expected to reach 50 mm within 6 hours or has already reached that level and continues. This elevation in warning level means that the risk and potential impact of the rainstorm have increased. Government agencies begin heightened preparedness, including traffic control in affected areas, suspension of some school activities, and mobilisation of emergency response units.
	Orange	This is a critical stage called the "rainstorm defence state." It corresponds to rainfall intensities that threaten serious flooding, landslides, and other hazards. At this level, schools may be closed, non-essential government work suspended, traffic diversions implemented, and evacuation of high-risk areas undertaken to protect lives and property. Emergency departments are placed on high alert to respond swiftly to incidents.
	Red	The highest alert signifies the "emergency rainstorm defence state." This indicates extreme rainstorm conditions with severe impacts expected or already occurring, including widespread flooding, significant landslides, and disruption of transportation networks and utilities. All non-essential activities are typically halted, and full-scale emergency operations are initiated. The public is urged to stay indoors and avoid travel except in cases of absolute necessity.

In practice, this color-coded alert system ensures a clear, standardised communication framework across China's vast territory. While local governments may refine enforcement measures based on regional conditions, the signal colours and their meanings remain consistent nationwide.

Regions prone to typhoons and intense monsoonal rainfall, particularly in southeastern coastal areas like Guangdong and Shenzhen, apply these signals rigorously to safeguard communities through timely warnings, evacuation procedures, and resource mobilisation.

This system helps China enhance its disaster preparedness and minimise the adverse effects of heavy rainfall, ensuring the public and authorities respond proactively to protect lives and infrastructure. It works in coordination with other weather and hazard warning systems managed at regional and local levels for comprehensive risk management.

Appendix IV: Other Adverse Weather Warnings

A. Philippines

In the Philippines, thunderstorm and flood warnings are vital components of the country's disaster risk reduction strategy, managed by the PAGASA. These warnings help protect communities from the hazards associated with severe weather such as lightning, strong winds, heavy rainfall, flash floods, and riverine flooding, all of which are common during the rainy and typhoon seasons.

PAGASA regularly issues thunderstorm advisories and warnings to alert the public about weather conditions likely to produce significant hazards within the next few hours. A thunderstorm advisory is issued when moderate to heavy rain showers, lightning, and strong winds are detected or expected to develop within affected provinces or regions, usually within a two to three-hour period. These advisories are highly localised and regularly updated, with affected areas urged to take precautionary measures. The dangers highlighted in these alerts include potential flash floods, landslides, and damage due to strong winds and lightning. Residents are encouraged to remain vigilant, avoid outdoor activities, secure loose objects, and seek safe shelter, especially in flood-prone and mountainous areas.

Furthermore, PAGASA's flood warning system uses both rainfall intensity and river basin monitoring to provide timely alerts. Flood Advisories and Flood Warnings are categorised according to the severity and imminence of flooding (Table S4.1). When river levels or rainfall cross certain thresholds, an Alert status is given if water levels are rising but still below critical limits, warning communities that flooding is possible. When levels rise above the critical threshold, a Flood Warning is issued, indicating that flooding is occurring or imminent and immediate response is required. For worsening or persisting situations, a Severe Flood Warning may be issued, often accompanied by recommendations for forced evacuation, particularly if intense or torrential rains continue. Conversely, a Final Advisory signals the recession of water levels and the reduction of flood risk.

These warning systems are disseminated to the public through various means such as radio, television, short message service (SMS), digital platforms, and local government units. They aim to improve preparedness, facilitate timely evacuations, prevent loss of life, and minimise property damage. The dynamic and area-specific nature of these advisories ensures that residents in vulnerable and high-risk areas receive early and actionable information to help protect themselves and their communities.

Table S4.1*Philippines' flood warnings*

Symbol Display	Warnings	Description	Forecast	Action / Response
	Flood Monitoring	<ul style="list-style-type: none"> • Telemetered: Slow rise in water level but still below alarm level • Non-Telemetered: Monitor for possible flooding area 	<ul style="list-style-type: none"> • Telemetered: Flood is possible • Non-Telemetered: Light to Moderate Rainfall 	<ul style="list-style-type: none"> • Non-Telemetered: Advised to take Precautionary Measures
	Flood Alert	<ul style="list-style-type: none"> • Telemetered: Water level is continuously rising but still below critical level • Non-Telemetered: Alert for possible flash floods and landslides 	<ul style="list-style-type: none"> • Telemetered: Flood is threatening • Non-Telemetered: Moderate to Heavy Rainfall 	<ul style="list-style-type: none"> • Non-Telemetered: Advised to be alert for possible flood, flash flood and landslides
	Flood Warning	<ul style="list-style-type: none"> • Telemetered: Water level is above critical level • Non-Telemetered: Flood is occurring immediate action is recommended 	<ul style="list-style-type: none"> • Telemetered: Flood is occurring • Non-Telemetered: Heavy to Intense Rainfall 	<ul style="list-style-type: none"> • Non-Telemetered: Advised to take appropriate action
	Severe Flood Warning	<ul style="list-style-type: none"> • Telemetered: Water level is continuously rising above critical level • Non-Telemetered: Flood is persisting force evacuation is recommended 	<ul style="list-style-type: none"> • Telemetered: Flood is persisting • Non-Telemetered: Intense to Torrential Rainfall 	<ul style="list-style-type: none"> • Non-Telemetered: Advised to force evacuation
	Final	<ul style="list-style-type: none"> • Telemetered: Slow recession of water level • Non-Telemetered: Light rains 	<ul style="list-style-type: none"> • Flood is no longer possible 	

B. Hong Kong

The HKO issues Thunderstorm Warnings to provide short-term alerts, typically within a few hours, about the likelihood of thunderstorms affecting any part of Hong Kong (Figure S1.1(a)). These warnings are broadcast via radio, television, the HKO website, and mobile apps. When issued, the warning highlights the specific regions expected to be affected, especially when thunderstorms are isolated. The warnings may also include information on severe squally thunderstorms accompanied by

violent gusts, hail, waterspouts, or even tornadoes. This system is designed to inform the public quickly so they can take appropriate safety precautions, as thunderstorms in Hong Kong can develop rapidly and be highly localised. Lightning location networks support these warnings by displaying real-time lightning activity, helping the public identify affected areas and respond accordingly.

For flooding, the HKO provides Special Announcements on Flooding in the Northern New Territories when heavy rainfall causes significant water accumulation and flood risk in that region (Figure S1.1(b)). These announcements alert residents and local authorities about potential or ongoing flooding, especially in vulnerable low-lying and urban areas. The alerts aim to promote public awareness and encourage timely protective actions. The Northern New Territories, with its unique topography and urban development, can be prone to flooding when intense rainstorms hit, necessitating heightened vigilance and responses such as traffic management and emergency service deployment.

Regarding the Landslip Warning, HKO issues this alert when heavy rainfall triggers the risk of landslides or slope failures, particularly in Hong Kong's hilly and mountainous terrain (Figure S1.1(c)). The warning signals that soil saturation and rainfall intensity have reached a level where slope stability is compromised, posing danger to property and life. When a landslip warning is in force, residents in susceptible areas are advised to stay vigilant and prepare for possible evacuations. Government departments and emergency services heighten monitoring and readiness to respond swiftly to incidents. The landslip warning system helps prevent casualties by shifting from passive observation to proactive risk management during adverse weather conditions.

Figure S1.1

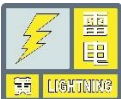
Hong Kong's weather warnings



C. China

China's thunderstorm warning system is part of a comprehensive, tiered weather alert framework operated by the CMA. The warning system is designed to quickly inform the public and authorities about the presence or imminent development of severe convective weather, including thunderstorms with associated hazards such as lightning, strong gusty winds, hail, and heavy rainfall (Table S4.2).

Table S4.2*China's thunderstorm warnings*

Symbol Display	Warnings	Meaning of Warnings
	Yellow	A higher risk with more intense thunderstorm activity expected or occurring within about two hours, including stronger winds and frequent lightning. People are advised to avoid outdoor activities and secure loose objects to minimise risk.
	Orange	The thunderstorms with severe weather effects such as very strong winds, heavy hail, and potentially damaging lightning are imminent or occurring, prompting authorities to implement safety protocols including suspension of outdoor operations and heightened emergency preparedness.
	Red	The thunderstorms bringing extreme conditions such as intense wind gusts, large hail, and dangerous lightning posing significant threats to life and property. During a red warning, the public is urged to stay indoors and follow official instructions closely, while emergency services enter full readiness to respond to any incidents.

This hierarchical warning system, supported by a sophisticated national meteorological monitoring network, including radar, lightning detection, and satellite imagery, enables timely dissemination of information and coordinated emergency responses. It plays a crucial role in minimizing casualties and material damage caused by severe thunderstorms across China's diverse geographical regions.